

**CLOSED-LOOP OPTIMIZATION OF  
EXTRACELLULAR ELECTRICAL STIMULATION FOR TARGETED  
NEURONAL ACTIVATION**

A Dissertation  
Presented to  
The Academic Faculty

by

Michelle Lea Kuykendal

In Partial Fulfillment  
of the Requirements for the Degree  
Bioengineering in the  
School of Electrical and Computer Engineering

Georgia Institute of Technology  
August 2014

Copyright © 2014 by Michelle L. Kuykendal

**CLOSED-LOOP OPTIMIZATION OF  
EXTRACELLULAR ELECTRICAL STIMULATION FOR TARGETED  
NEURONAL ACTIVATION**

Approved by:

Dr. Stephen P DeWeerth, Advisor  
School of Biomedical Engineering  
*Georgia Institute of Technology*

Dr. Martha A. Grover  
School of Chemical and Biomolecular  
Engineering  
*Georgia Institute of Technology*

Dr. Steve M. Potter  
School of Biomedical Engineering  
*Georgia Institute of Technology*

Dr. Cameron C. McIntyre  
Neural Engineering Center  
*Case Western Reserve University*

Dr. Garrett B. Stanley  
School of Biomedical Engineering  
*Georgia Institute of Technology*

Date Approved: August, 2014

## ACKNOWLEDGEMENTS

I would like to thank the many people who supported me in my journey. My committee helped me to find, understand and explore this dissertation work. My primary advisor, Prof. Stephen P. DeWeerth, has given me guidance and perspective to help me find my way along this complicated and interesting path. I also thank my co-advisors, Prof. Steve M. Potter and Prof. Martha A. Grover. I am inspired by Steve's vision for the future and his breadth of knowledge. I felt supported by Martha at every turn, both intellectually and emotionally, and I cannot tell her enough how important the contribution was that she made to my life. I greatly appreciate the advice of my committee members, Prof. Cameron C. McIntyre and Prof. Garrett B. Stanley to consider my work in the larger context of the world. I am thankful to my colleagues in all of my advisors' research groups. Everyone dedicated their time and energy to help me produce the best work that I could. Thank you to all of you. Additionally, I would like to thank my funding sources, including the National Institutes of Health and National Science Foundation; in particular, I thank the NSF Graduate Research Fellowship Program and NSF Integrative Graduate Education Research Trainee fellowships.

I thank my family most of all. My husband, Michael, is everything to me always and has supported me through every trial and tribulation, challenge and success. My parents, Janet and Robert, are the reason that I have come this far. They never once doubted my potential and always gave me the strength to persevere through everything. Much love goes out to my sister, Stephanie and the rest of my family. They have all stood by me over the years. Thank you to everyone.

# TABLE OF CONTENTS

	Page
ACKNOWLEDGEMENTS	iii
LIST OF TABLES	v
LIST OF FIGURES	vi
LIST OF SYMBOLS AND ABBREVIATIONS	xi
SUMMARY	xii
CHAPTER	
1 Introduction	1
2 Closed-loop extracellular electrical stimulation for determining the stimulus-evoked response of a neuron	5
3 Targeted stimulation using differences in activation probability across the strength–duration waveform space	50
4 Optimization of stimulation parameters for targeted neuronal activation	85
5 Conclusions and future direction	113
APPENDIX A: Software development	127
APPENDIX B: Biological and chemical protocols	134
REFERENCES	141

## LIST OF TABLES

	Page
Table 3.1: Characterization of activation curves for Neurons Y1 and Y2 according to the threshold and the span of the transition region	82

## LIST OF FIGURES

	Page
Figure 2.1: The closed-loop system of electrical stimulation, optical recording, automated image analysis and activation curve modeling	10
Figure 2.2: The closed-loop system of electrical stimulation, optical recording, automated image analysis and activation curve modeling	11
Figure 2.3: Dissociated neuronal culture	12
Figure 2.4: Stimulus-evoked fluorescence traces	15
Figure 2.5: Evoked fluorescence decays due to photobleaching	17
Figure 2.6: Automated image processing for locating cell somata.	19
Figure 2.7: Strength–duration curve fitting from neuronal activation data	24
Figure 2.8: Convergence of the closed-loop algorithm on the sigmoid model parameters	27
Figure 2.9: Shifting sigmoids are used to generate the strength–duration curve	30
Figure 2.10: Closed loop versus open loop experiments	33
Figure 2.11: The power spectrum for the blue LED and white LED	39
Figure 2.12: The imaging system comprises an upright microscope for epifluorescence microscopy	39

Figure 2.13: Time traces of the average fluorescence intensity from a cell and an empty area within a neuronal culture	41
Figure 2.14: The model sigmoid is shown	42
Figure 2.15: From the previous simulation study, the measured responses at each stimulus current were averaged and overlaid on the sigmoid models	43
Figure 2.16: To expand on previous studies, the progression of the CL was demonstrated to search for various probability levels in the sigmoid	44
Figure 2.17: Four model neuronal activation curves were created with varying levels of Gaussian noise added to them to simulate the noise in a stimulus-evoked neuronal response	45
Figure 2.18: All stimuli delivered for each of the three studies are plotted	46
Figure 2.19: Six sigmoid activation models, for the same neuron, were overlaid	47
Figure 2.20: The progression of the curve fit of the sigmoid model to activation data	48
Figure 2.21: Two neuronal strength-duration curves were constructed and an OL sweep was performed afterwards to evaluate the selectivity between them	49
Figure 3.1: The closed-loop routine was used to measure neuronal activation curves for Population A	64
Figure 3.2: Strength–duration curves for Population B	67
Figure 3.3: The physical locations of the two neurons of interest on the MEA	70

Figure 3.4: Two sets of shifting sigmoids produced from fixed-pulse-width, variable-current searches and fixed-current, variable-pulse-width searches	78
Figure 3.5: Example time traces of the evoked fluorescence	79
Figure 3.6: The progression of $\Delta F/F$ , or the evoked change in fluorescence over the baseline, is depicted for six neurons across 1140 stimulus iterations	80
Figure 3.7: For the N1 neuron previously shown, the progression of $\Delta F/F$ is plotted for each individual pixel within a 12 X 12 pixel grid around the soma	81
Figure 3.8: For the N6 neuron previously shown, the progression of $\Delta F/F$ is plotted for each individual pixel within a 12 X 12 pixel grid around the soma	81
Figure 3.9: The physical location of the two neurons of interest on the MEA are as show	83
Figure 4.1: Phase contrast micrograph of the high-density electrode array, on which healthy neurons are growing	90
Figure 4.2: Cartoon depiction of negatively-sloped cross sections through the strength-duration waveform space	95
Figure 4.3: Depiction of the first four searches in Powell's method	99
Figure 4.4: Implementation of the Powell search routine in the strength-duration waveform space	103
Figure 4.5: A map of selectivity regions accessible using one stimulating electrode	106

Figure 4.6: Two simulation studies were performed to find the selective region for the subpopulation of neurons including Neuron N2, N3 and N5	109
Figure 4.7: The strength–duration curves are plotted for five neurons using the experimental data collected during the Powell search routine.	111
Figure 4.8: The Powell Method was implemented in a simulation study	116
Figure 4.9: Simultaneous two electrode stimulation	117
Figure 4.10: The activation curves for one neuron across four stimulation directions for two different stimulus pulse-widths	118
Figure A.1: GUI for controlling the automated stage movement	135
Figure A.2: GUI for controlling the stimulation channels	136
Figure A.3: Automated image processing for locating cell somata	138
Figure A.4: A heat map representation of the background activity that was subtracted in the previous figure	139
Figure A.5: Two views of the Hough voting accumulation array	139
Figure A.6: The movalyze GUI to evaluate the stimulus-evoked activity	140
Figure B.1: Integrated spontaneous activity	142
Figure B.2: A cartoon depiction of a rectangular cathodic stimulus pulse	143

Figure B.3: Phase contrast image of dissociated neurons atop a hemacytometer for counting	145
Figure B.4: Dissociated neuronal culture	145
Figure B.5: Phase contrast image of a PDMS stencil atop a MEA	146
Figure B.6: Neurons were plated at an extremely high density atop an MEA	146
Figure B.7: The next generation of PDMS stencils was developed using a spin coating technique for higher precision control of the stencil thickness and opening	147

## LIST OF SYMBOLS AND ABBREVIATIONS

CL	Closed-loop
OL	Open-loop
SD	Strength–duration
MEA	Micro-electrode array
APV	(2R)-amino-5-phosphonopentanoate
BMI	Bicuculline methiodide
CNQX	6-cyano-7-nitroquinoxaline-2,3-dione
DBS	Deep brain stimulation
DIV	Days in vitro
FITC	fluorescein isothiocyanate
aCSF	Artificial cerebral spinal fluid
LED	Light emitting diode

## SUMMARY

We have developed a high-throughput system of closed-loop electrical stimulation and optical recording that facilitates the rapid characterization of extracellular stimulus-evoked neural activity. The ability to selectively stimulate a neuron is a defining characteristic of next-generation neural prostheses. Greater stimulus control and differential activation of specific neuronal populations allows for prostheses that better mimic their biological counterparts.

In our system, we deliver square current pulses using a microelectrode array; automated real-time image processing of high-speed digital video identifies the neuronal response; and a feedback controller alters the applied stimulus to achieve a targeted response. The system controller performs directed searches within the strength–duration (SD) stimulus parameter space to build probabilistic neuronal activation curves. An important feature of this closed-loop system is a reduction in the number of stimuli needed to derive the activation curves when compared to the more commonly used open-loop system: this allows the closed-loop system to spend more time probing stimulus regions of interest in the multi-parameter waveform space, facilitating high resolution analysis.

The stimulus-evoked activation data were well-fit to a sigmoid model in both the stimulus strength (current) and duration (pulse width) slices through the waveform space. The 2-D analysis produced a set of probability isoclines corresponding to each neuron-electrode pairing, which were fit to the SD threshold model described by Lapique (1907). We show that stimulus selectivity within a given neuron pair is possible in the one-

parameter search space by using multiple stimulation electrodes. Additionally, by applying simultaneous stimuli to adjacent electrodes, the interaction between stimuli alters the neuronal activation threshold. The interaction between simultaneous multi-electrode multi-parameter stimulus waveforms creates an opportunity for increased stimulus selectivity within a population.

We demonstrated that closed-loop imaging and micro-stimulation technology enable the study of neuronal excitation across a large parameter space, which is requisite for controlling neuronal activation in next generation clinical solutions.

# CHAPTER 1

## INTRODUCTION

Closed-loop experimentation has opened the door for researchers to study scientific realms that were previously inaccessible. Because of limited experimentation time and vast input parameter spaces, the sheer number of trials required to explore a space using open-loop methods is large enough to make manual exploration infeasible. Automation is essential to fully capture the advantages of closed-loop techniques. For example, online image analysis enabled researchers to develop novel techniques for fast 3-dimension two-photon imaging (Katona et al. 2012; Yasuda et al. 2003), leading to a vast improvement in imaging of dendritic spines. Understanding the integration of stimuli in the retina (Bölinger & Gollisch 2012) has benefitted greatly by adopting closed-loop methods. Brain-machine interfaces comprise an exciting up-and-coming research interest area for clinical and research applications, and this field is dependent on closed-loop sensory-motor integration (Koralek et al. 2012; Rutishauser et al. 2013). The heart of cochlear prostheses is closed-loop systems (O'Connor et al. 2005; Machens et al. 2005); these readily allow the device to make improvements to itself, online. At another end of the spectrum, robotic embodiment of neuronal networks guided by closed-loop control has enhanced researchers' ability to quantify and study learning in vitro (Potter et al. 2006) and closed-loop suppression of unwanted bursting in culture has enabled researchers to study network plasticity in vitro (Wagenaar et al. 2005). For studying single cell processes, the enhancement of the dynamic clamp method was enabled by closed-loop technology (Chamorro et al. 2012).

In all neuroscience research applications, it is essential to collect as much data from each experiment as is possible. To accomplish this goal, researchers require faster and more consistent experiment execution and improved online decision-making regarding the design of each experimental trial. These challenges motivate the use model-driven techniques for experiment execution (Zrenner et al. 2010). By updating the model online, experimental stimuli can be adapted to changing goals and experimental conditions such that the most relevant data from a system is extracted on each iteration. These techniques are especially useful in studying and using microstimulation, which has become ubiquitous in developing sensory prostheses; (Clark et al. 2011; Sekirnjak et al. 2006; Jensen et al. 2009; Bruce et al. 1999 ; Hatsopoulos & Donoghue 2009; Nicolelis et al. 2003; Fitzsimmons et al. 2007) and for improving clinical treatments for brain disorders (Rolston & Gross 2008; Foutz & McIntyre 2010). In a parallel vein, microstimulation techniques are essential for cortical mapping, understanding cortical processing and uncovering functional brain regions tied to specific behaviors (Clark et al. 2011; Buonomano & Maass 2009; Borchers et al. 2012). All of these applications are improved with a better understanding of the way in which extracellular electrical stimuli directly affect neural tissue (Basser & Roth 2000) and why some stimuli work better than others at evoking activity (Wagenaar et al. 2004). A more complete understanding of the way in which our stimuli excite neurons is needed to advance the field.

In this dissertation we present an automated closed-loop system for rapid exploration of the extracellular electrical stimulus waveform space. This technology enables us to characterize the probabilistic activation of a neuron in response to a stimulus. By performing automated closed-loop optical imaging in vitro, with single cell

resolution, we have the capability to improve the mapping from stimulus to excitation to help address the questions above. With a more efficient characterization of the large stimulus parameter space, we can rapidly extract single-parameter activation curves and two-parameter strength-duration curves for many cells within a population. As more parameters are added to the stimulation space, closed-loop experimentation becomes essential because the multitude of stimulus parameter combinations becomes too large to explore blindly. We use online data analysis for stimulus optimization to create "smarter" goal-directed stimuli, and additionally, by reducing the number of stimuli needed for understanding a particular neurons' activation curve, we are able to characterize the activation of many more neurons within population. We show that by exploiting the shape of the neuronal strength-duration curve, we can selectively activate neurons within a population using only a single stimulating electrode. For those pairs of neurons in which stimulus selectivity is only achievable for a single neuron, we show that the use of an alternate electrode within an array enables selective stimulation of the other neuron.

## **1.1 Dissertation Structure**

The following dissertation is divided into five body chapters and three appendices. Chapters 2, 3 and 4 comprise journal articles that are either in review or are undergoing preparation for submission at the time of this dissertation's preparation. We have created the first appendix for supplemental data that were not included in the journal manuscripts. The following two appendices describe the software that was developed for this project, and the experimental protocols that were implemented.

**Chapter 1:** Here, we explain the motivation for our work and outline the dissertation.

**Chapter 2:** In this chapter, we present a manuscript, which has been submitted for publication, describing and characterizing the closed-loop system of electrical stimulation and optical recording for finding the stimulus-evoked activity of a neuron.

**Chapter 3:** In this chapter we present another journal manuscript. This chapter explores the distribution of activation curves within a population of neurons and the potential for selective neuronal activation.

**Chapter 4:** We have included in this chapter a manuscript, which uses the closed-loop (CL) system to implement an optimized search routine through the strength-duration stimulus waveform space. This routine was developed to target neuronal populations for selective activation.

**Chapter 5:** Finally, I conclude our story and look to the future. I explore the path that this work has lead us down and describe the next steps that can be taken to build on this work.

**Appendix A:** Here, we provide supplementary data that supports our findings in Chapters 2, 3 and 4.

**Appendix B:** We describe the software that was developed in this dissertation.

**Appendix C:** This section describes the protocols used throughout the dissertation

# CHAPTER 2

## CLOSED-LOOP EXTRACELLULAR ELECTRICAL STIMULATION FOR DETERMINING THE STIMULUS-EVOKED RESPONSE OF A NEURON

### 2.1 Abstract

We have developed a high-throughput system of closed-loop electrical stimulation and optical recording that facilitates the rapid characterization of extracellular stimulus-evoked neural activity. A better understanding of the stimulus-evoked neuronal response will enable improvements in stimulus selectivity for use in next-generation neural prostheses. Greater stimulus control and differential activation of specific neuronal populations allows for prostheses that better mimic their biological counterparts. In our system, we deliver square current pulses using a microelectrode array; automated real-time image processing of high-speed digital video identifies the neuronal response; and a feedback controller alters the applied stimulus to achieve a targeted response. Action potentials are detected by measuring the post-stimulus calcium-sensitive fluorescence at the soma. The system controller performs directed searches within the strength–duration (SD) stimulus parameter space to build probabilistic neuronal activation curves. An important feature of this closed-loop system is a reduction in the number of stimuli

---

This manuscript has been submitted for publication by:  
Michelle L. Kuykendal, Gareth S. Givanasen, Martha A. Grover, Steve M. Potter, and Stephen P. DeWeerth\*  
\*Corresponding author e-mail address: [steve.deweerth@gatech.edu](mailto:steve.deweerth@gatech.edu)

needed to estimate the activation curves when compared to the more commonly used open-loop system: this allows the closed-loop system to spend more time probing stimulus regions of interest in the multi-parameter waveform space, facilitating high resolution analysis. The stimulus-evoked activation data were well-fit to a sigmoid model in both the current (strength) and pulse width (duration) parameter slices through the waveform space. The 2-D analysis produces a set of probability isoclines corresponding to each neuron-electrode pair, which were fit to the SD threshold model described by Lapicque (1907). We demonstrate that closed-loop imaging and micro-stimulation technology enable the study of neuronal excitation across a large parameter space, which is requisite for controlling neuronal activation in next generation clinical solutions.

## **2.2 Introduction**

Electrical stimulation is a promising tool for addressing the challenges of understanding and augmenting brain function. For example, prostheses restore lost neural function due to trauma or disease (Loeb et al. 1983; Ryu & Shenoy 2013; Clark 2013; Fried et al. 2006; Sekirnjak et al. 2006; Hochberg et al. 2006) and deep brain stimulators use electrical stimulation to treat neural disorders (McIntyre et al. 2004; Rolston & Gross 2008; Schiff 2010; Perlmutter & Mink 2006; Chabardes et al. 2003). Although current clinical stimulation techniques show great potential, improvement in stimulus selectivity may increase the efficacy of stimulators to target neuronal populations. Prosthetic devices could encode and deliver more sophisticated sensory messages to the brain by differentially activating neurons (Konrad & Shanks 2010; Wilke et al. 2011; Carmena et al. 2003; Lebedev & Nicolelis 2006; Jepson et al. 2011). Furthermore, deep brain stimulators (DBS) could improve efficacy with a better understanding of the activated

tissue (Butson & McIntyre 2006; Rolston & Gross 2008). Selective neuronal activation is important for improving clinical solutions; a better understanding of how extracellular electrical stimuli affect neuronal tissue will facilitate the development of new stimulation approaches.

One technique for characterizing neuronal systems is to quantify stimulus-evoked activity. This approach has a long history, dating back to the 19th century when it was first used by Fritsch and Hitzig (1870) to identify functional areas of the brain. Electrical stimulation is ubiquitous in research applications such as mapping cortical regions associated with behavioral outputs and uncovering cortical processing mechanisms (Cohen & Newsome 2004; Clark et al. 2011; Borchers et al. 2012; Mandonnet et al. 2010). Clinical applications of electrical stimulation include DBS to treat diseases such as depression, epilepsy and Parkinson's disease (Kringelbach et al. 2007; Foutz & McIntyre 2010; Cleary et al. 2000; Levy 2003; Rolston & Gross 2008) cochlear and retinal prostheses to restore the ability of damaged sensory organs to deliver messages to the brain (Loeb et al. 1983; Ryu & Shenoy 2013; Clark 2013; Fried et al. 2006; Sekirnjak et al. 2006; Hochberg et al. 2006); and brain-machine interfaces (BMIs) to directly record and augment cognitive function (Clark et al. 2011; Sekirnjak et al. 2006; Jensen et al. 2009; Bruce et al. 1999; Hatsopoulos & Donoghue 2009; Nicolelis et al. 2003; Fitzsimmons et al. 2007; Pais-Vieira et al. 2013; Lebedev et al. 2011). Further advancement in these stimulation technologies requires more precise control of the stimulus-evoked activity.

The delivery of multidimensional stimulus waveforms offers new approaches for the improvement of stimulus control. Specifically, for cathodic extracellular stimulus

pulses comprising a stimulus current, or strength, and a stimulus pulse width, or duration, there is a threshold of activation described by the strength–duration (SD) curve (Weiss 1901; Lapique 1907). These two parameters are ubiquitous in the electrical stimulation literature. The SD formulas see use in both experimental and modeling studies of neuronal activation (Gustafsson & Jankowska 1976; Holsheimer et al. 2000; Mogyoros et al. 1996; Rattay et al. 2012; Nowak & Bullier 1998; Lee et al. 2013). The applicability of the SD curve to a probabilistic model of neuronal activation is less prevalent due to the assumption that the SD curve describes a single activation threshold. There is a gradation in the activation probability of a neuron, and a single threshold is insufficient to describe stimulus-evoked behavior. For this reason, a different SD curve can be used to describe each probability level, which requires estimation of a large number of activation parameters.

The complexity of characterizing a multidimensional parameter space—even a 2-D space—invites closed loop (CL), smarter approaches to stimulus design. Automated CL methodologies are inherently more efficient in collecting the most informative data from each stimulus trial, resulting in faster characterization of neuronal activation (Arsiero et al. 2007; Benda et al. 2007; Zrenner et al. 2010; DiMattina & Zhang 2013). The use of CL stimulation techniques is especially vital for the aforementioned clinical applications, including neural prostheses and deep brain stimulators. The physical and electrical response properties of tissue surrounding electrodes can change over time, and the use of feedback to measure stimulus efficacy will enable real-time adjustment to a stimulus routine. In our experimental setting, we have chosen to use optical imaging of calcium signals to directly measure stimulus-evoked activity. One constraint is that

photobleaching of the fluorophore occurs with each light exposure, which inherently limits the number of stimulus trials that can be delivered during an experiment. Because experimentation time is limited, it is essential that each delivered stimulus be designed to more efficiently collect data on the system that it is designed to characterize. We use a model-driven CL approach which fits a sigmoid curve to probabilistic neuronal activation data. Our stimuli target the transition region, which enables the routine to converge on the model parameters more quickly when compared to open-loop approaches. Closed-loop optimization for determining the stimulus at each iteration allows for the characterization of the stimulus pulse space by rapidly homing in on the relevant parameters.

We present an automated, real-time, closed-loop system that combines electrical stimulation and optical imaging for rapid exploration of the extracellular electrical stimulus waveform space. This technology enables us to describe the probabilistic activation of a neuron in response to a stimulus. Stimulus response is measured through optical imaging of molecular probes, and the intermediate result of this imaging is used to calculate the next stimulus. Automated closed-loop stimulation, with optical imaging in vitro, allows the capability to improve the mapping from stimulus to excitation to help address the questions above. By developing a more efficient characterization of the large parameter space, we can then rapidly extract single-parameter activation curves and two-parameter strength—duration curves for an arbitrary neuron. We use online data analysis for stimulus optimization to create smarter goal-directed stimuli, and additionally, by reducing the number of stimuli needed for understanding a particular neurons' activation curve, light exposure is minimized within an experiment to reduce phototoxicity and photobleaching.

## 2.3 Methods

We designed a closed-loop system (Figure 2.1) for optimizing stimulus pulse parameters based on a model of neuronal activation and an experimental goal. The system comprises hardware and software components that select and deliver stimuli, which are designed to evoke a particular neuronal response. Each measured response is used to refine the model and the next stimulus is automatically chosen. The modular design, which separates data collection from both data analysis and decision-making, enables the user to plug in a model function and a variety of experimental goals to ask and answer a multitude of questions (Figure 2.2). Each section of the system is described in more detail below.

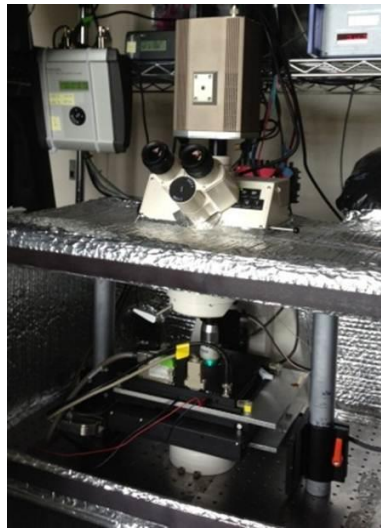


Figure 2.1. The closed-loop system of electrical stimulation, optical recording, automated image analysis and activation curve modeling. A photograph of the system apparatus is shown. The camera is mounted atop the microscope with an inline piezoelectric actuator connected to the 20X objective for high-precision focal plane adjustments. LED fluorescence excitation is digitally controlled using the TLC001 current controller eliminating the need for a shutter. The neuronal culture lives atop the microelectrode array (MEA), which is nested inside of the heated Multichannel Systems preamplifier. Imaging is carried out inside of an enclosure to eliminate ambient light exposure and reduce the effects of other environmental factors including the laboratory heating and ventilation. The preamplifier is housed inside of this “light tight” imaging chamber and interfaces with the external stimulator.

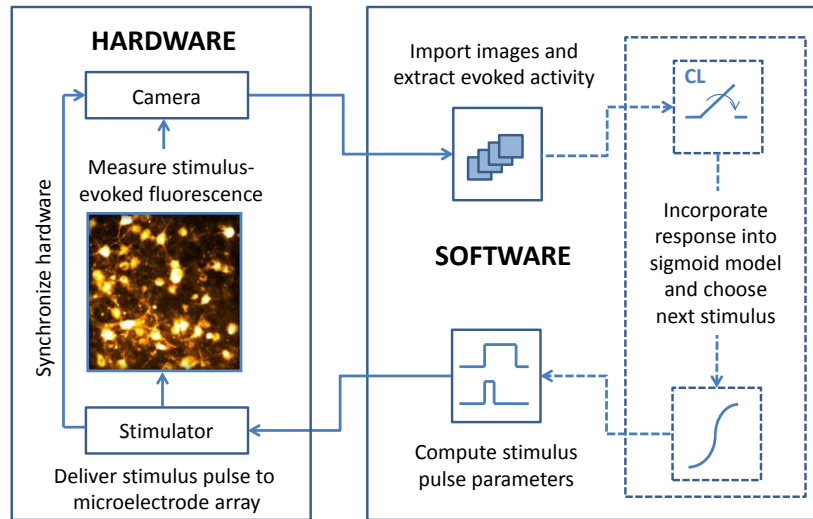


Figure 2.2. The closed-loop system of electrical stimulation, optical recording, automated image analysis and activation curve modeling. Hardware for delivering electrical stimuli and optically recording evoked responses (left half) interfaces directly with the MATLAB-based software system (right half). The open-loop experiment path is depicted with solid arrows. Predefined stimulus pulse parameters are sent to the stimulator for delivery to the MEA. The stimulator supplies synchronizing triggers to the camera, LED and preamplifier. Fluorescence is evoked at cell somata that fire action potentials in response to the stimulus. This fluorescence signal is captured by the camera with a series of high-speed digital frames. The set of frames is imported into MATLAB and saved to the hard disk using the Micro-Manager library (Edelstein et al. 2010). In the closed-loop configuration (dotted lines) the neuronal response is used to inform the calculation of the next iteration of stimulus pulse parameters. Digital images are analyzed using custom software to extract stimulus-evoked action potentials. This newly acquired response data is compiled with previous stimulus iterations and the sigmoid activation model is updated to reflect all measured responses. The next stimulus pulse is then automatically chosen to increase the measurement resolution along the slope of the response curve.

### 2.3.1 Cortical Cell Culture

A phase contrast image of a typical neuronal culture at 14 days in vitro (DIV) is shown in Figure 2.3. Neurite outgrowth can be observed in between the cell bodies indicating that the cell culture is healthy.

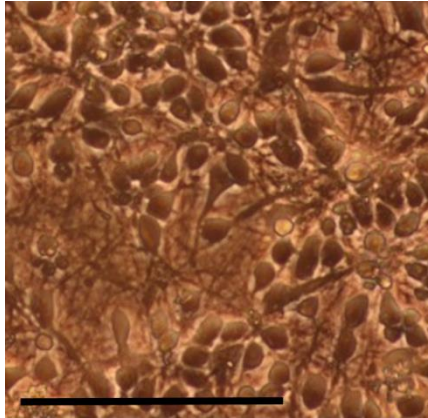


Figure 2.3. Dissociated neuronal culture. A phase contrast micrograph of a dissociated rat cortical culture at 14 days in vitro (DIV) illustrates the extent to which the culture has developed. Neurites (axons and dendrites) can be seen in the space between the somata. Scale bar: 100  $\mu$ m.

Embryonic Day 18 (E18) rat cortices were enzymatically and mechanically dissociated according to (Potter & DeMarse 2001). Cortices were digested with trypsin (0.25% w/EDTA) for 10-12 minutes, strained through a 40  $\mu$ m cell strainer to remove clumps and centrifuged to remove cellular debris. Neurons were re-suspended in culture medium [90 mL Dulbecco's Modified Eagle's Medium (Irvine Scientific 9024), 10 mL horse serum (Life Technologies 16050-122), 250  $\mu$ L GlutaMAX (200 mM; Life Technologies 35050-061), 1 mL sodium pyruvate (100 mM; Life Technologies 11360-070) and insulin (Sigma-Aldrich I5500; final concentration 2.5  $\mu$ g/mL)] and diluted to 3000 cells/ $\mu$ L. Microelectrode arrays (MEAs; Multi Channel Systems 60MEA200/30iR-Ti) were sterilized by soaking in 70% ethanol for 15 minutes followed by UV exposure

overnight. MEAs were treated with polyethylenimine to hydrophilize the surface, followed by three water washes and 30 minutes of drying. Laminin (10  $\mu$ L; 0.02 mg/mL; Sigma-Aldrich L2020) was applied to the MEA for 20 minutes, half of the volume was removed, and 30,000 neurons were plated into the remaining laminin atop the MEA. Cultures were protected using gas-permeable lids (Potter & DeMarse 2001) and incubated at 35°C in 5% carbon dioxide and 95% relative humidity. The culture medium was fully replaced on the first DIV and then once every four DIV afterwards.

### 2.3.2 Electrical Stimulation

Extracellular electrical stimuli were used to elicit neuronal activity. Stimuli were delivered to the neurons using a STG-2004 stimulator and MEA-1060-Up-BC amplifier (Multi Channel Systems). MATLAB (Natick, MA) was used to control all hardware devices, which were synchronized by TTL pulses sent from the stimulator at the beginning of each stimulation loop. In all stimulus iterations, a trigger pulse was first delivered to the camera to begin recording so that background fluorescence levels could be measured. An enable pulse was then delivered to the amplifier, which connected the stimulus channel to a pre-programmed electrode. A single cathodic square current pulse was then delivered to a single electrode centered under the camera field of view. Cathodic pulses were chosen because they have been shown to be most effective at evoking a neuronal response (Wagenaar et al. 2004).

### 2.3.3 Optical Imaging

Automated optical imaging was used to measure the stimulus-evoked neuronal response. All preparation procedures were conducted in the dark to lengthen experiments by minimizing photobleaching and phototoxicity. First, culture media was removed and

neurons were loaded with Fluo-5F AM (Life Technologies F-14222), a calcium-sensitive fluorescent dye with relatively low binding affinity (2.3  $\mu\text{M}$ ) at a concentration of 9.1  $\mu\text{M}$  in DMSO (Sigma-Aldrich D2650), Pluronic F-127 (Life Technologies P3000MP) and artificial cerebral spinal fluid (aCSF; 126 mM NaCl, 3 mM KCl, 1 mM  $\text{NaH}_2\text{PO}_4$ , 1.5 mM  $\text{MgSO}_4$ , 2 mM  $\text{CaCl}_2$ , 25 mM D-glucose) with 15 mM HEPES buffer for 30 minutes at ambient 25°C and atmospheric carbon dioxide. Before imaging, cultures were rinsed two times with aCSF to remove free dye. Cultures were bathed in a mixture of synaptic blockers in aCSF (15 mM HEPES buffer). This included (2R)-amino-5-phosphonopentanoate (AP5; 50  $\mu\text{M}$ ; Sigma-Aldrich A5282), an NMDA receptor antagonist; bicuculline methiodide (BMI; 20  $\mu\text{M}$ ; Sigma-Aldrich 14343), a GABAA receptor antagonist; and 6-cyano-7-nitroquinoxaline-2,3-dione (CNQX; 20  $\mu\text{M}$ ; Sigma-Aldrich C239), an AMPA receptor antagonist. This mixture was shown to suppress neuronal communication (Bakkum et al. 2008) to ensure that the recorded neuronal activity was directly evoked by the stimulus. The culture was then kept in the heated amplifier (Multichannel systems TC02, 37C) within the imaging chamber. The stage position was calibrated with respect to the desired field of view (FOV) using the electrodes as fiducial markers. A MATLAB GUI was used to automatically position the FOV over the stimulation electrode. During an experiment neurons were illuminated using a light-emitting diode (LED; center wavelength of 500 nm) and LED current source (TLCC-01-Triple LED, relative power = 30; Prizmatix) through a 20X water-immersion objective, NA = 1.0, and a fluorescein isothiocyanate (FITC) filter cube. Evoked activity was optically recorded using a high-speed electron multiplication CCD camera (30 fps; QuantEM 512S; Photometrics), which has a 512 X 512 pixel grid covering a 400  $\mu\text{m}$  X

400  $\mu\text{m}$  area. After an experiment concluded, three aCSF washouts were performed at three minute intervals, the culture media was replaced, and the culture was returned to the incubator.

#### 2.3.4 Detecting Action Potentials

For each neuron, the measured intensity of 16 X 16 pixels (12.5  $\mu\text{m}$  X 12.5  $\mu\text{m}$ ) surrounding the soma center was spatially averaged. The relative change in fluorescence,  $\Delta F/F$ , was calculated by subtracting the baseline (an average of four pre-stimulus frames) from the peak (an average of four post-stimulus frames) and dividing the difference by the baseline. Two fluorescence traces are shown across time in Figure 2.4.

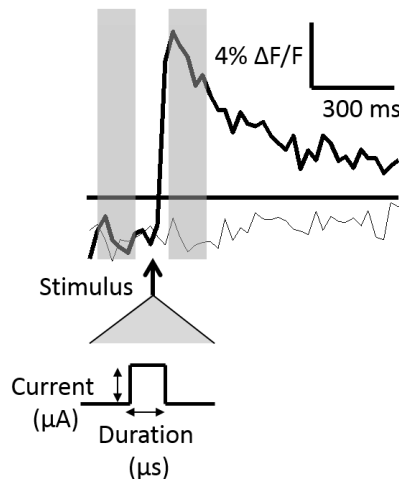


Figure 2.4. Stimulus-evoked fluorescence traces. Two traces are shown in which an action potential was evoked in response to the stimulus (bold line) and no action potential was evoked (light line). The stimulus timing with respect to the evoked signal is denoted by the bold arrow and is expanded below to show the two stimulus pulse control variables, the current ( $\mu\text{A}$ ) and the pulse width ( $\mu\text{s}$ ). The fluorescence traces are generated by spatially averaging 16 pixels at a neuron soma. Action potentials were detected by thresholding (threshold shown as a horizontal bar) the measured change in fluorescence of four time-averaged post-stimulus frames over four pre-stimulus baseline frames,  $\Delta F/F$ . The pre-and-post-stimulus frames are represented with transparent gray bars.

An action potential was evoked in one trace (bold) and no action potential was evoked in the other. The traces were generated from the average of sixteen pixels that overlay the neuron soma. The peak and baseline frames are highlighted with gray bars, and the stimulation time is marked with an arrow. The standard deviation of the baseline frames was calculated in initial stimulus iterations and used as a measure of the fluorescence noise level. An action potential was said to have occurred if the  $\Delta F/F$  was greater than three times the noise level within a particular neuron. The average decay time constant of a stimulus-evoked fluorescence curve was 1.5 seconds. Because of this relatively slow signal decay, the experiment loop time was chosen to be 4.5 seconds, which is three decay constants long, to give the signal sufficient time to return to baseline. The progression of  $\Delta F/F$  for one neuron over the course of 1140 open-loop stimulus iterations is plotted in Figure 2.5, which illustrates the evoked signal decay with increasing light exposure. Stimuli were randomly presented from a range of stimulus pulse widths and currents, and so the neuronal response (whether an action potential occurred) is mixed throughout the experiment. For the first 200 stimuli, the change in fluorescence resulting from an evoked action potential is unchanging. The signal then subsequently decays with each light exposure. After 1000 stimulus iterations, action potential detection is unreliable. Therefore, further experiments were limited to 1000 stimulus iterations to ensure that action potentials could be detected.

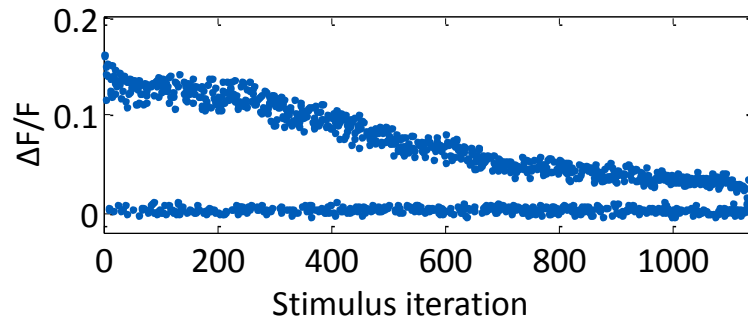


Figure 2.5. Evoked fluorescence decays due to photobleaching. The progression of the relative fluorescence change,  $\Delta F/F$ , is shown across an experiment. A set of 1140 stimuli was applied in random order that spanned the stimulus pulse parameter space. Some of the stimuli evoked action potentials and others did not. The measured  $\Delta F/F$  is plotted at each stimulus iteration, which decays with each light exposure. Experiments were limited to 1000 stimulus iterations.

### 2.3.5 Automated Location of Neuronal Somata

The automated process for locating cell bodies is outlined in Figure 2.6. A single raw image is shown from a series along with the evoked difference image, the processed image gradient and the cells overlaid on the gradient image. In order to first define the population of neurons an automated strategy was employed to locate all cell somata in which activity was evoked in response to a relatively large stimulus. A relatively large current amplitude, which varied depending on the electrode impedance, was chosen to evoke as much activity as possible without creating voltages at the electrode that would electrolyze water or current densities that could be harmful to those neurons located nearest to the electrode. The first step in the image processing routine was to average the four post-stimulus *peak* frames and four pre-stimulus *baseline* frames, as was described above. The averaged baseline frame was subtracted from the averaged peak frame to create a difference image. A smoothing Gaussian filter with a large standard deviation of 100 pixels was applied to measure the general activity throughout the image, and this activity was subtracted from the difference image. This technique was used to eliminate

the fluorescence signal originating from neurites that span the culture because each axon and dendrite contributes to the image fluorescence, making detection of cell soma boundaries more difficult. A sharp Gaussian filter with a standard deviation of 10 pixels was then applied to smooth the image, and a gradient image was calculated to highlight soma boundaries. A circular Hough filter was applied to the gradient image, which looks for circle centroids belonging to cell borders, over a range of diameters (adapted from Peng (2005)). “Gradient pixels” were found as pixels having gradients surpassing a threshold, which designated the border between soma fluorescence and background. Gradient pixels then “voted” on possible soma centers; each pixel located at a given radius from a gradient pixel was counted as a potential soma center for that particular radius. The votes were weighted by the gradient of the pixels that contributed each vote. All of the possible votes for the image area were tallied in the “accumulation array,” to which a threshold was applied to find the most common votes, or circle centers. Five standard deviations of the image intensity was used as a measure of the noise and as a threshold for the voting accumulation array.

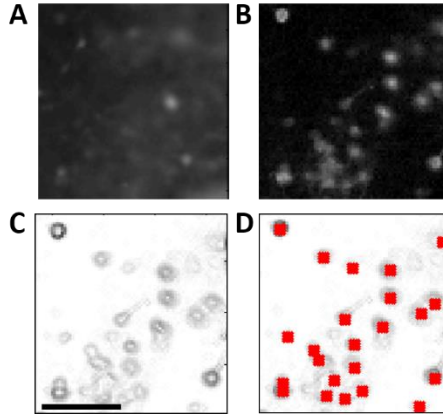


Figure 2.6. Automated image processing for locating cell somata. (A) A raw single post-stimulus frame (512 X 512 pixels) is displayed from a series of frames (30 fps). (B) Image subtraction is performed to highlight the fluorescence difference post-stimulus from pre-stimulus. (C) The background is subtracted, and a gradient of the difference image is used to highlight the somata boundaries. (D) A circular Hough filter is applied to the gradient image to locate neuronal somata. Grid of 16 X 16 pixels (shown with dark squares) mark the soma centers. Scale bar: 100  $\mu\text{m}$ .

### 2.3.6 The sigmoid activation model

A saturating nonlinear curve was used to fit to the neuronal probability of firing an action potential in response to a varying stimulus current or pulse width. Specifically, a two-parameter sigmoid (Equation 2.1) was used to describe this 1-D activation curve for cathodic square-pulse stimuli.

$$p = \frac{1}{1 + b_2 e^{-(x-b_1)}} \quad \text{Equation 2.1}$$

The sigmoid model provides an approximation for the stimulus needed to activate a particular neuron with any given probability. The input activation parameter,  $x$ , is either the stimulus current or pulse width, and the output is the probability,  $p$ , of a neuron to fire an action potential. The two parameters describing the sigmoid are  $b_1$ , the midpoint of the sigmoid, and  $b_2$ , the slope of the curve at the midpoint. Because the sigmoid describes a probability of activation, it spans from zero to one.

### 2.3.7 The closed-loop search algorithm

The closed-loop search procedure began with five open-loop stimuli that divided the stimulation space evenly and bracketed the activation region. After the fifth iteration, the sigmoid model was analytically linearized, and a linear least-squares fit of the midpoint and slope parameters was performed. All measured stimulus-evoked responses were equally weighted. The output of the linear regression was used as an initial guess for a nonlinear least squares curve fit using the MATLAB Optimization Toolbox, which generated the best-fit sigmoid parameters. The measured response was a binomial distribution describing the evoked action potential probability, which was calculated as a mean of all responses at a particular stimulus value. In order to gain information about the midpoint and slope, a probability goal was randomly chosen from the set of 0.25, 0.50 and 0.75, which spans the transition region of the sigmoid. The stimulus that was predicted to produce the target firing probability was calculated analytically by inverting the sigmoid model. The probability goals span the linear region of the transition region of the sigmoid curve, and an accurate measurement of the stimulus values at these probabilities provided an estimate of the slope of the curve at the midpoint. In the case that the next stimulus chosen was the same as the previously delivered stimulus, a random jitter was added to the stimulus up to 20% in either direction so that more data would be collected over the full range of the transition region of the activation curve. After every stimulus iteration, the linear and nonlinear curve-fits were run to update the model.

### 2.3.8 The strength–duration activation model

Neuronal activation in the 2-D strength–duration waveform space was described according to Lapique (1907, Equation 2.2).

$$I = r \left( 1 + \frac{c}{PW} \right) \quad \text{Equation 2.2}$$

The stimulus pulse width,  $PW$ , is the input; the stimulus current,  $I$ , is the output, and the two model parameters are the rheobase,  $r$ , and the chronaxie,  $c$ , which describes the knee of the curve. The rheobase describes the stimulus current below which a stimulus with infinite pulse width will not evoke an action potential, and the chronaxie describes the stimulus pulse width that corresponds to a stimulus current of twice the rheobase.

## 2.4 Results

The automated system for optically measuring stimulus-evoked neuronal activation was used to characterize the response to a single extracellular stimulus pulse. In the 1-D stimulus pulse parameter space, neurons activate in a probabilistic manner that is well described by the sigmoid activation model (Equation 2.1). We show that our closed-loop (CL) approach is effective and efficient at constructing the activation model. As compared to open-loop (OL) stimulation techniques, the CL approach quickly converges on the activation curve. The faster convergence rate of the CL approach is particularly important as the dimensionality of the parameter space increases. We analyze two particular stimulus parameters: the current (strength) and the width of the pulse (duration).

### 2.4.1 Open-loop characterization of the strength–duration waveform space

The stimulus-evoked neuronal response is a stochastic process. It can be defined by the probability of a given neuron firing with an action potential in response to an input stimulus. We characterized the stimulus-evoked activation of a neuron using open-loop methodologies, using a sigmoidal activation model (Equation 2.1) to define the probability of a neuron to fire an action potential when one of the stimulation parameters (current or pulse width) is varied (Figure 2.7A). A randomized set of 1140 stimuli was delivered to the MEA spanning currents from 2  $\mu\text{A}$  to 20  $\mu\text{A}$  in 1  $\mu\text{A}$  increments and pulse widths from 300  $\mu\text{s}$  to 800  $\mu\text{s}$  in 100  $\mu\text{s}$  increments. One pulse was presented per stimulus iteration, and ten repetitions of each pulse were delivered in the experiment. Action potentials were extracted after each stimulus iteration using our fluorescence thresholding routine. We calculated stimulus-evoked neuronal response probabilities by

averaging the ten responses delivered at each stimulus point. It was unknown, a priori, where the activation curve would lie within the pulse parameter space. The activation curve generated from the 700  $\mu\text{s}$  stimulus pulses spans the full range of stimulus currents from 2  $\mu\text{A}$  to 20  $\mu\text{A}$  (Figure 2.7A). The best-fit midpoint and slope parameters were 9.3  $\mu\text{A}$  and 1.1, and the 0.25 to 0.75 probability range spans 2.0  $\mu\text{A}$ . The sigmoid model, which was fit to the 700  $\mu\text{s}$  data, was used to extract the predicted stimulus currents that would produce probability estimates ranging from 0.1 to 0.9 in steps of 0.2 (highlighted with a box, Figure 2.7B). Similar to the 700  $\mu\text{s}$  data analysis, we generated 1-D sigmoidal curves for each of the other stimulus pulse widths (300  $\mu\text{s}$ , 400  $\mu\text{s}$ , 500  $\mu\text{s}$ , 600  $\mu\text{s}$  and 800  $\mu\text{s}$ ).

We generated a set of strength–duration probability isoclines in the 2-D stimulus–pulse parameter space from the 1-D sigmoids. These SD curves describe the probabilistic neuronal activation across the strength–duration pulse space (Figure 2.7B). As was described above, each sigmoid model was used to predict stimulus currents that would produce probability estimates from 0.1 to 0.9. These sets comprise a range of stimulus currents for each pulse width. A separate SD curve was calculated for each probability level, which was done by fitting Equation 2.2 to each set of model-predicted stimulus currents. It was necessary to use the model-predicted currents from the sigmoid curve fits because it was unlikely that probability estimates were available at all probability levels of interest. The chronaxie and rheobase parameters for the 0.5 probability level were 535  $\mu\text{s}$  and 5.2  $\mu\text{A}$ .

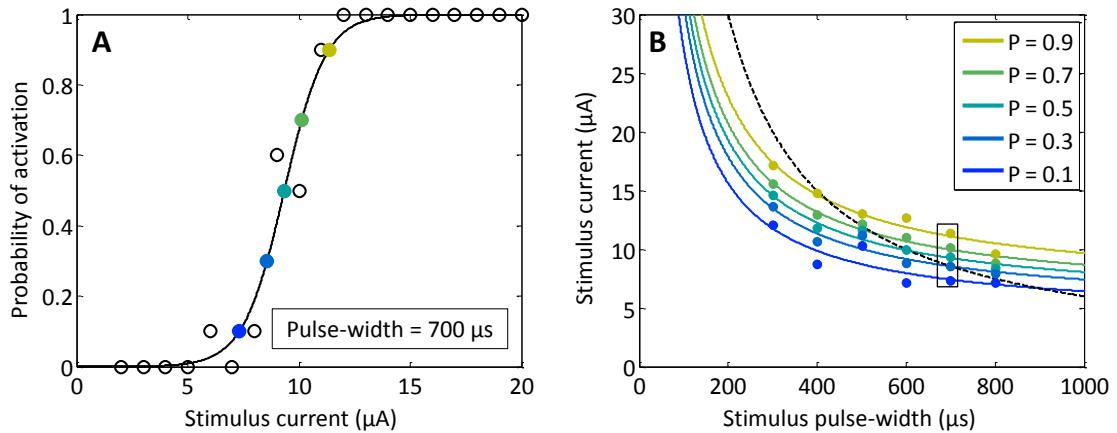


Figure 2.7. Strength–duration curve fitting from neuronal activation data. A randomized set of 1140 stimuli was delivered to the MEA spanning currents from 2  $\mu\text{A}$  to 20  $\mu\text{A}$  in 1  $\mu\text{A}$  increments and pulse widths from 300  $\mu\text{s}$  to 800  $\mu\text{s}$  in 100  $\mu\text{s}$  increments. Each stimulus was randomly repeated ten times to measure the activation probability with 0.1 resolution. (A) Averaged responses from the ten repetitions of each stimulus with 700  $\mu\text{s}$  pulse width are plotted with open circles. Below 6  $\mu\text{A}$ , no action potentials were detected, and above 11  $\mu\text{A}$  action potentials were detected 10 out of 10 times. A non-linear least squares curve-fit of the sigmoid in Equation 2.1 was performed on the 700  $\mu\text{s}$  data. The best fit is shown by the solid line. The sigmoid model was used to predict the stimuli that would produce activation probabilities ranging from 0.1 to 0.9 in 0.2 steps (closed circles, increasing probability from dark to light). (B) Model-predicted stimuli from (A), corresponding to activation probabilities ranging from 0.1 to 0.9, were plotted with solid circles and are outlined with a box. In the same manner as (A), sigmoid models were built for each of the sets of stimulus pulse-width data from 300  $\mu\text{s}$  to 800  $\mu\text{s}$ . These models were again used to predict a set of stimulus currents for the range of probability levels (vertical sets of solid circles). Strength–duration curves (solid lines) for each of the probability levels were created from a non-linear least squares curve-fit of the predicted points to the model in Equation 2.2. The shade of each curve corresponds to the equivalent probability level in (A). Probability steps of 0.2 were chosen for clarity. A constant-charge curve (6 nC) is shown as a reference (dotted line).

### 2.4.2 Closed-loop analysis of neuronal 1-D activation curves

We utilized the closed-loop routine to rapidly extract activation curves for a neuron in the search space of both the stimulus current and stimulus pulse width (Figure 2.8). We performed two sets of experiments in which we held one of the pulse parameters constant and varied the other parameter. The best-fit sigmoid model (Equation 2.1), which is defined for probabilities spanning from zero to one, was constructed for each of the stimulus current and pulse-width searches (Figure 2.8A-B). We calculated the averaged responses to each of the stimulus points. The 0.25 to 0.75 probability ranges span  $2.2 \mu\text{A}$ , from  $12.3 \mu\text{A}$  to  $14.5 \mu\text{A}$ , for the constant pulse-width search, and  $66 \mu\text{s}$ , from  $366 \mu\text{s}$  to  $432 \mu\text{s}$ , for the constant current search. We calculated the best fit of each of the two sigmoid parameters, midpoint and slope, from the nonlinear least squares curve fit, after each stimulus iteration (Figure 2.8E-H). The shaded region marks the 95% confidence interval on those fit parameters. After the last iteration, the sigmoid midpoint and slope for the constant pulse-width search were  $13.4 \mu\text{A}$  and  $1.0 \mu\text{A}^{-1}$ , and for the constant current search the fit parameters were  $399 \mu\text{s}$  and  $0.03 \mu\text{s}^{-1}$ . The convergence of the sigmoid midpoint and slope had three phases. In the first 20 stimulus iterations, the slopes are nearly infinite because stimulus repetitions were not likely to be present until the algorithm had converged on the sigmoid midpoint. In this phase, the midpoint is fluctuating and the slope is infinite. For the next 20 stimulus iterations, the midpoints are relatively constant, and as the search routine selected the stimulus values predicted to produce firing probabilities of 0.25, 0.50 and 0.75, repetitions began to emerge. After 40 stimulus iterations, the algorithm has produced a good measurement of the sigmoid midpoint and slope and time is spent refining those parameters. It is important to note that

even after 100 stimulus iterations, the confidence interval, while stable, does not converge to zero. It will always be non-zero because the data comprise a binomial set, in which the least squares fitting algorithm will always fit zeroes and ones to a smooth probability curve. The experimental measurements taken along the slope of the curve, will therefore, never overlay the actual curve, causing the confidence interval remain non-zero (Cox 1959).

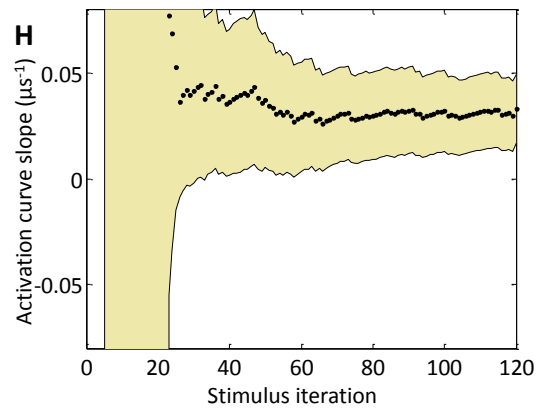
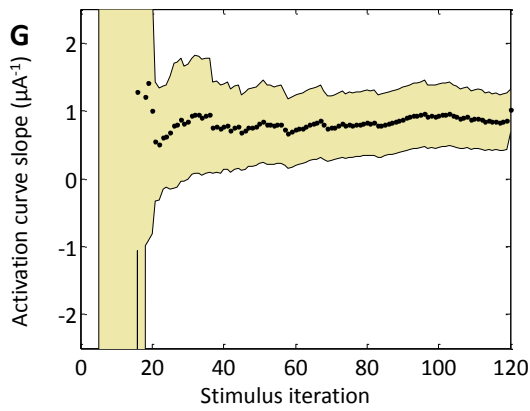
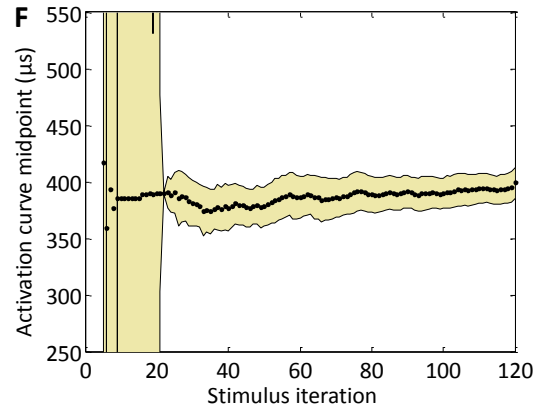
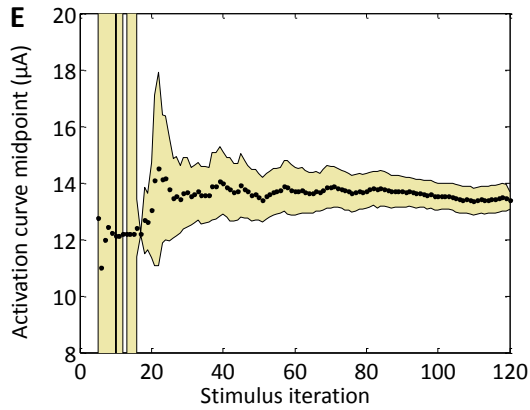
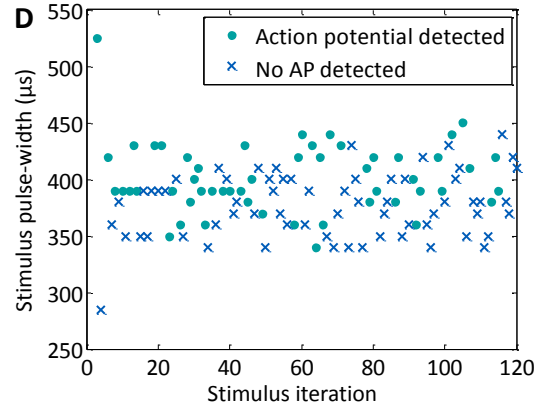
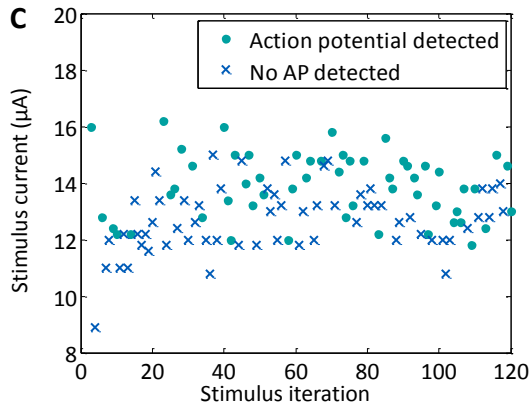
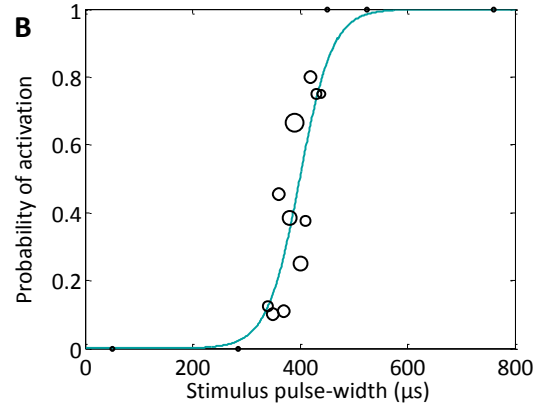
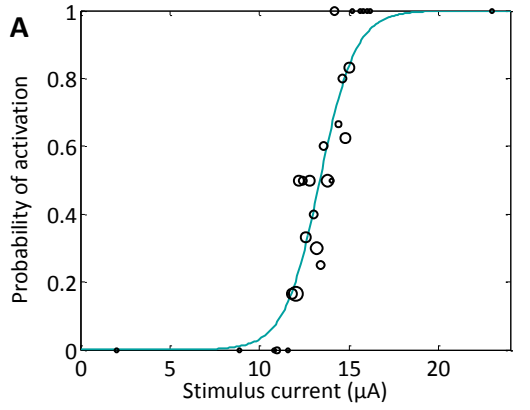


Figure 2.8. Convergence of the closed-loop algorithm on the sigmoid model parameters. During an experiment, one stimulus parameter (current or pulse width) is fixed while the other is allowed to vary according to the closed-loop algorithm in order to find the neuronal activation curve. In one set of CL stimuli the pulse width was fixed and the current was varied (A,C,E,G), and in another set of stimuli the current was fixed and the pulse width was varied (B,D,F,H). (A-B) The best-fit sigmoid from Equation 2.1 is plotted after the final stimulus iteration for each of the stimulus current and pulse-width searches. The activation curve is defined for probabilities spanning from zero to one. The averaged response to each of the stimulus values is depicted with open circles, which are proportional in size to the number of stimuli that were delivered at that value. The 10% to 90% probability regions span  $4.3 \mu\text{A}$  and  $130 \mu\text{s}$ . (C-D) The individual measured response to each stimulus is plotted as a dot to denote that an action potential was detected or an “X” to denote that no action potential was detected. The stimuli span the range of probabilities from the sigmoid activation curve. Two points were excluded in both plots from the extremes of the stimulus range, for clarity at the region of interest. The excluded stimuli at maximum intensity produced an action potential, and those at minimum intensity did not. (E-F, G-H) The convergence of the sigmoid midpoint and slope is shown with stimulus iteration. The black circles record the best fit of each of the two sigmoid parameters, midpoint and slope, from the nonlinear least squares curve fit of Equation 2.1, after each stimulus iteration. The shaded region marks the 95% confidence interval on the fit parameters.

#### 2.4.3 Derivation of probabilistic strength–duration curves

The automated routine performed searches that were 1-D slices through the 2-D strength–duration waveform space in order to derive probabilistic strength–duration curves (Figure 2.9). We constructed these curves using two search directions in which one stimulus pulse parameter, the current or pulse width, was fixed while the other was allowed to vary. Each search yielded a sigmoid response curve in the horizontal, constant current, search direction or the vertical, constant pulse width, search direction. For each new search, the fixed parameter was then incremented, and the resulting sigmoid shifted. This produced two sets of shifting sigmoids where the activation threshold increased as the fixed parameter value decreased (Figure 2.9A-B). For the fixed pulse-width searches ranging from  $400 \mu\text{s}$  to  $2000 \mu\text{s}$ , the sigmoids shift from  $66.3 \mu\text{A}$  down to  $23.0 \mu\text{A}$ , and for the fixed current searches ranging from  $40 \mu\text{A}$  to  $150 \mu\text{A}$ , the sigmoids shift from  $665 \mu\text{s}$  down to  $140 \mu\text{s}$ . Although the curves appear to be nearly vertical, it is an artifact of the

large stimulus range. When we zoom in on two of the sigmoids (Figure 2.9C-D), it becomes apparent that the slopes are finite. For the constant current search (Figure 2.9D), the midpoint and slope were  $421 \mu\text{s}$  and  $0.1 \mu\text{s}^{-1}$  and for the constant pulse-width search (Figure 2.9C), the midpoint and slope were  $34.7 \mu\text{A}$  and  $1.1 \mu\text{A}^{-1}$ . The 0.25 to 0.75 probability ranges span  $2.0 \mu\text{A}$  and  $25 \mu\text{s}$ . The midpoints of each sigmoid (markers in Figure 2.9E), or 50% thresholds, were used as inputs into the SD non-linear curve-fitting routine using the model in Equation .22. These curves, which define the square pulse shapes that will produce a firing probability of 0.5 through SD space, were overlaid for the two data sets, and both search techniques produce similar output curves. The chronaxie and rheobase parameters for the constant current set of searches were  $315 \mu\text{s}$  and  $6.5 \mu\text{A}$  and were  $360 \mu\text{s}$  and  $5.9 \mu\text{A}$  for the constant pulse-width searches. The two sets of search data were combined, and the SD best-fit chronaxie and rheobase parameters were  $316 \mu\text{s}$  and  $6.5 \mu\text{A}$  for the 0.5 probability level. SD curves were calculated from the shifting sigmoids for the probability levels ranging from 0.1 to 0.9 in 0.2 steps (Figure 2.9F).

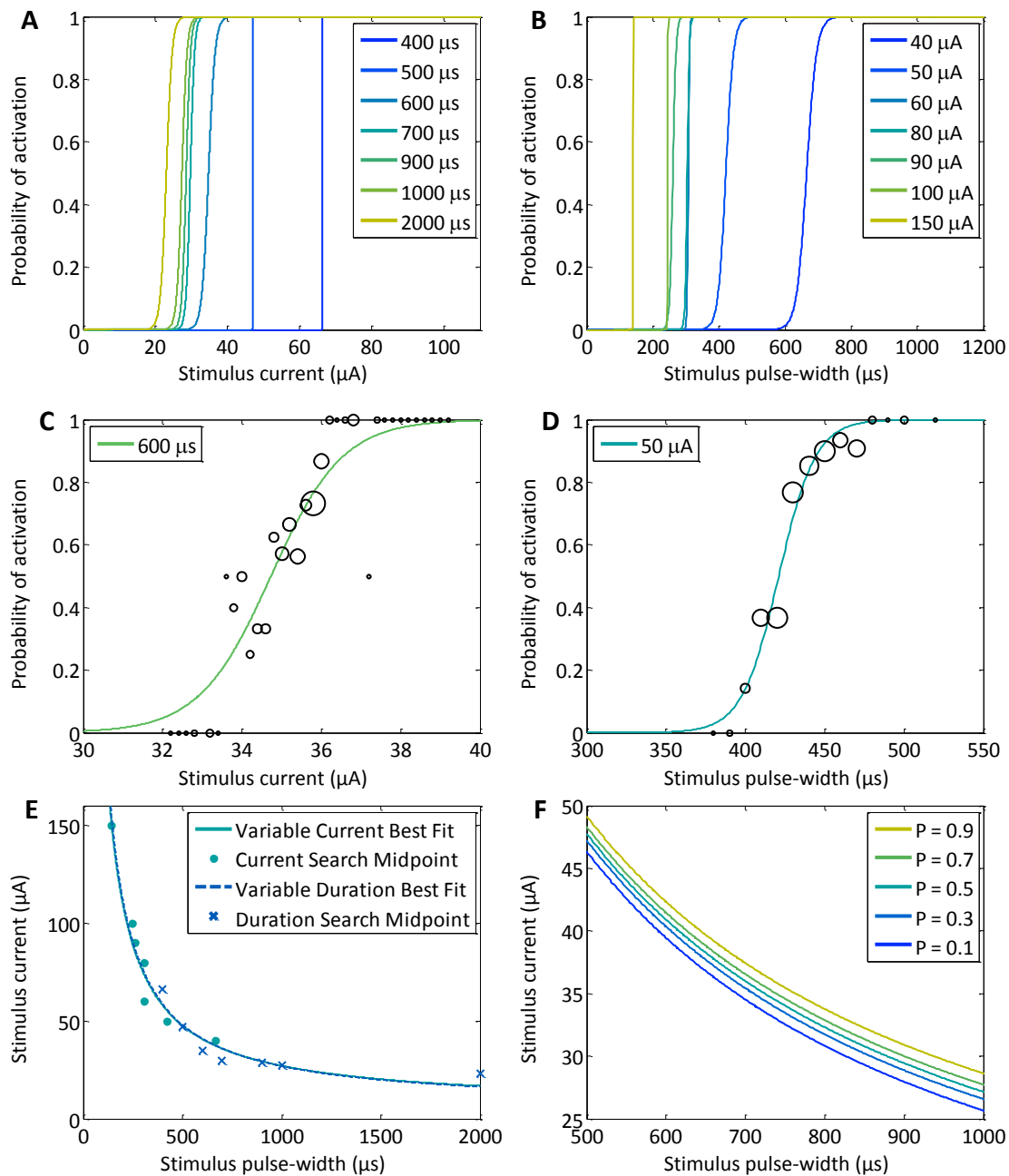


Figure 2.9. Shifting sigmoids are used to generate the strength–duration curve. Closed-loop experiments were performed to generate two sets of sigmoid activation curves corresponding to various constant pulse width and constant current searches. (A-B) The *pulse-width* parameter was fixed in (A), and the *current* pulse parameter was fixed in (B). CL searches yielded sigmoid activation curves, which shifted to lower currents with increasing stimulus pulse width and shorter pulse widths with increasing stimulus pulse currents. The sigmoids appear to be extremely steep because the stimulus space is large. (C-D) Two sigmoid activation curves are blown up to demonstrate that the slopes span a significant stimulus range of 4  $\mu\text{A}$  and 500  $\mu\text{s}$ . The shade of the activation curve

corresponds to the same shade in (A) and (B). The open circles overlaying the activation curves are a measure of the activation probability at a given stimulus level and are proportional in size to the number of stimuli that were applied at that stimulus. (E) The strength–duration curve, for a probability of 0.5, was built two ways. Each of the sigmoid models were used to predict the stimulus that would produce an activation probability of 0.5 for the constant pulse-width (dots) and constant current (“X’s”) searches. The best fit of the strength–duration curve for both sets of searches was calculated using a nonlinear least squares curve fit of Equation 2.2 is shown with solid lines. (F) Strength–duration curves were constructed using Equation 2.2 for probability levels spanning from 0.1 to 0.9 in 0.2 increments (increasing probability, from dark to light).

#### 2.4.4 Comparison of closed-loop and open-loop techniques

An experimental study was performed in order to compare closed-loop to open-loop stimulation methods (Figure 2.10). A set of 250 stimuli were delivered using the CL approach and, subsequently, 250 stimuli were delivered using an OL approach. The OL stimuli were chosen at random from the stimulus current space, and the pulse width was held constant. The stimulus current space spanned 0 to 40  $\mu\text{A}$  with 0.2  $\mu\text{A}$  steps. The OL study did not converge within the 250 trials, however, the CL study converged by the 100<sup>th</sup> stimulus iteration. The CL sigmoid slope was 2.8  $\mu\text{A}^{-1}$  and the midpoint was 13.6  $\mu\text{A}$ . Because the stimulator resolution was 0.2  $\mu\text{A}$ , the maximum slope that could be estimated was about five. When the convergence of the fit parameters for the CL search was analyzed, we found that there were again three phases: In the first 20 stimulus iterations the algorithm finds the sigmoid midpoint. It requires the next 80 iterations to find the slope. During these trials, the best-fit slope was near infinite (off of the chart in Figure 2.10E). In all subsequent stimulus iterations, the stimuli presented served to refine the fit parameters (Figure 2.10E). The best-fit sigmoid found after the final iteration (Figure 2.10A) has a probability range of 0.25 to 0.75 that spans 0.8  $\mu\text{A}$ , and the stimulus values along the slope of the curve, 13.0  $\mu\text{A}$ , 13.2  $\mu\text{A}$ , 13.4  $\mu\text{A}$ , 13.6  $\mu\text{A}$ , 13.8  $\mu\text{A}$ , and 14.0  $\mu\text{A}$ , were measured 19, 27, 27, 35, 62 and 13 times, respectively. Whenever a

stimulus to be delivered was equal in magnitude to the previous stimulus, a uniformly distributed jitter, up to 20% in either direction, was added to the stimulus. Because the sigmoid slope was steep, many of the stimuli that were delivered with jitter were beyond either knee of the curve and provided little additional information to the curve fit. Those stimuli can be seen in the clusters where the sigmoid curve saturates, either at probabilities of 0 or 1 (Figure 2.10A) and in the spread of the stimulus points in Figure 2.10C.

In the OL experiment, neither sigmoid fit parameter stabilized. Because most of the stimuli delivered were below the probability level of 0.1, or above 0.9, on the sigmoidal activation curve, they contributed little to improving the fit. This made the sigmoidal model fit highly sensitive to additional measurements lying within the 0.1 to 0.9 probability range. The model sensitivity is exemplified by the sudden drop in the midpoint parameter after the last stimulus and the multiple times that the slope parameter flips from under one to near infinite. The midpoint and slope were 16.9  $\mu\text{A}$  and 0.4  $\mu\text{A}^{-1}$  after iteration 249 and jumped to 13.9  $\mu\text{A}$  and 114  $\mu\text{A}^{-1}$  after the final iteration (Figure 2.10F).

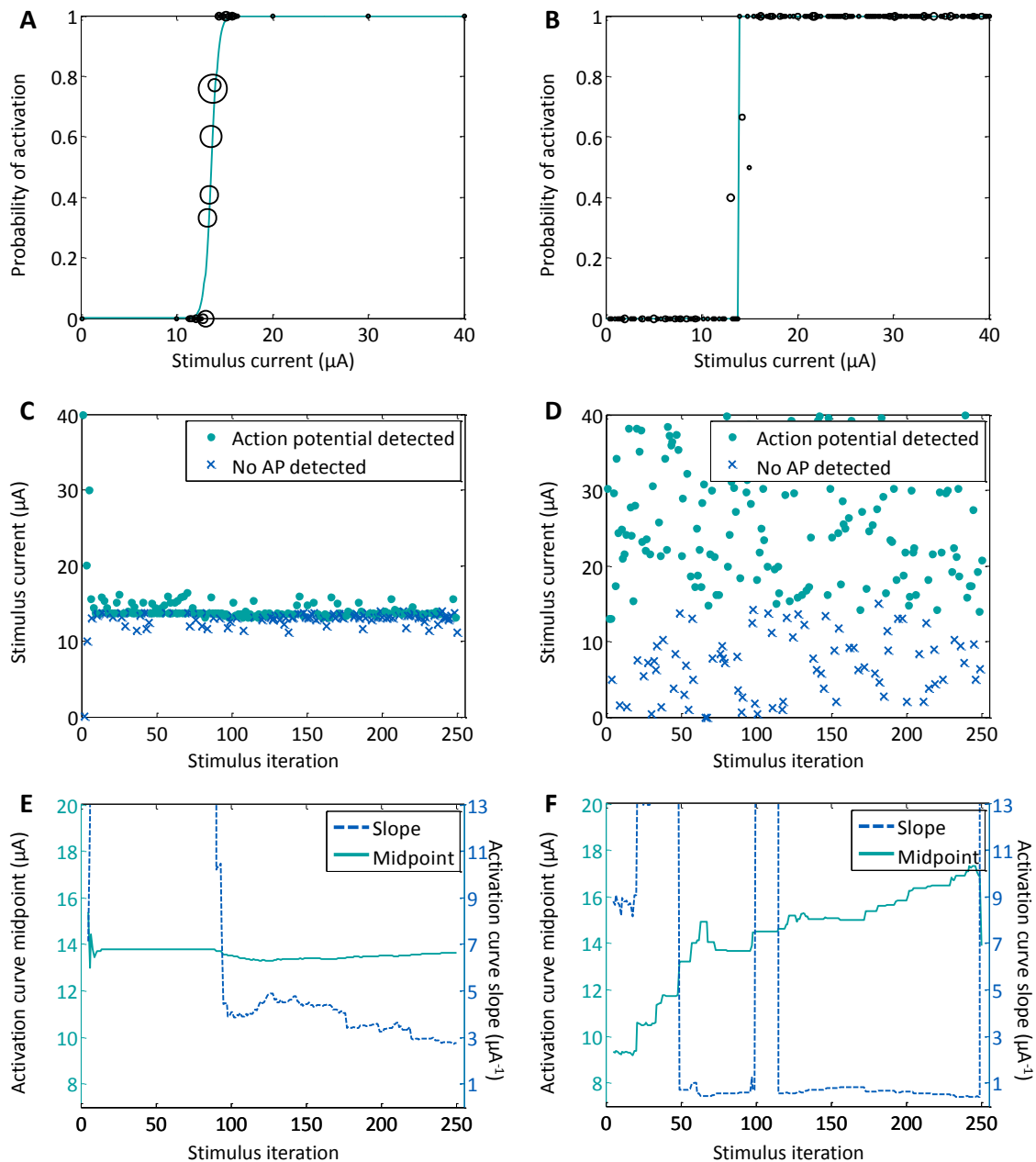


Figure 2.10. Closed loop versus open loop experiments. Two sets of 250 stimuli were delivered to the culture via one electrode. In the closed-loop experiment, the model-based algorithm selected the stimuli in real-time (A,C,E), and in the open-loop experiment a random set of stimuli were chosen from the stimulus pulse parameter space (B,D,F). (A-B) The best fit of a sigmoid from Equation 2.1 is plotted after the 250<sup>th</sup> stimulus iteration. The averaged response to each of the stimulus currents is depicted with open circles, which are proportional in size to the number of stimuli that were delivered. (C-D) The individual measured response to each stimulus is plotted as a dot to denote that an action potential was detected or an “X” to denote that no action potential was detected. (E-F) The convergence of the sigmoid midpoint (solid line, left *y-axis*) and slope (dotted line,

right *y-axis*) is shown with stimulus iteration. The sigmoid activation model was calculated in real-time after each stimulus iteration for the CL experiment and was calculated post-hoc for the OL experiment. The OL fit parameters did not converge.

## 2.5 Discussion

Furthering the understanding of the way in which electrical stimuli directly affect neuronal activity is necessary in order to design stimuli that can selectively activate a neuron. The stimulus space, however, is sufficiently large to require optimized search approaches for characterization, even when varying only the aspect ratio of the pulse. Performing an open-loop sweep of a stimulus parameter space is inefficient because the activation of a neuron in response to an extracellular square current pulse is probabilistic, which requires multiple repetitions of any given stimulus value to measure that activation probability. In the pulse parameter space, there is a trade-off between probability resolution and stimulus resolution: repeated measurements at each stimulus point increase probability resolution, at the expense of limiting the number of stimulus points that may be explored. Above the upper knee of the sigmoid activation curve the neuronal response is near unity, and below the lower knee, the neuronal response is near zero; probing these stimulus regions is unnecessary. To better explore the stimulus parameter space, it is essential that experiment time is spent primarily in the stimulus regions that lie within the transition region, near the activation threshold, so that each additional measurement contributes significantly to improve the activation model. The closed-loop search routine featured here illustrates one technique to rapidly characterize neuronal activation by extensively probing the transition region of the sigmoid curve.

The convergence of the sigmoid fit parameters was used to evaluate the iteration at which the CL search routine could have exited. In the experiments presented here, there were many more stimuli delivered than were needed and future experiments would

benefit from optimizing stimulus delivery. If a slope estimate along the sigmoid transition region is not needed, then the search routine could have been terminated after only 20 stimulus iterations with a relatively accurate measure of the activation threshold. However, if information is needed to describe the slope, then more stimuli are required. In the case that the sigmoid has a relatively shallow slope at the midpoint (Figure 2.8), an additional 20 stimulus iterations were sufficient to measure the slope. However, in the CL/OL comparison, 100 stimuli were required to measure the slope (Figure 2.10) because the slope at the transition region was steep. We would argue that in practical terms, the difference between a slope of  $3 \mu\text{A}^{-1}$  and infinity is negligible. In that case, like in the case of a shallower slope, 20 additional stimulus iterations after the midpoint was determined to be sufficient to approximate the slope. Furthermore, it would be beneficial to develop an algorithm that adds adaptive jitter to the stimulus depending on the estimate of the slope at the sigmoid midpoint. When the sigmoid slope was steep, the uniform distribution of jitter up to 20% in either direction produced stimuli that often fell beyond the transition region of the activation curve. These stimuli, therefore, were less useful than if they had been limited to a smaller range, such as a 5% jitter, around the sigmoid midpoint.

There are limitations in the CL approach when it is applied to many neurons in the same experiment. The experiments conducted in this study were focused on a single neuron per experiment. While the system simultaneously collected activation data for all neurons within the imaging area, the CL feedback was focused on one specific neuron. Therefore, the activation data collected for other neurons within the imaging area were not assured to lie in the stimulus range where the other neurons' activation curves

transition from zero to one. The OL approach has an advantage for measuring the activation of a large population of neurons within an experiment. Although the resolution along the slope of all curves will be low, many more neuronal activation curves can be built. However, some closed-loop adaptation of the stimuli based on the observed population dynamics might still be beneficial.

Future approaches that incorporate optimized search strategies can address the inefficiencies of CL stimulation applied to a population of neurons, which we explore in chapters three and four. Different search directions can be used for different regions of the SD parameter space because the activation of a neuron is sigmoidal for both vertical and horizontal slices through the space. For example, in 2.9E, a 10  $\mu\text{A}$  constant current, horizontal search would not have converged because 10  $\mu\text{A}$  falls below the asymptotic rheobase of the curve. Instead, a constant pulse-width, vertical search will converge for long pulse widths. Conversely, a constant current search should be used for the high-current, short-pulse-width parameter region. For these reasons, the constant pulse-width searches better fit the right-hand portion of the strength–duration curve and the constant current searches better fit the left-hand portion of the curve. When mapping multiple neuronal activation curves in a single experiment, it may become more efficient to expand the search strategy to include many directions within the SD space (e.g. diagonally, at  $45^\circ$ ).

The probabilistic nature of stimulus-evoked neuronal activation can be exploited to improve the selectivity of stimulation techniques. For example, two square pulses delivering the same charge, but with different aspect ratios, activate neurons with differing probabilities. The product of the stimulus strength and duration is the charge

delivered at the electrode, but the charge alone is insufficient to predict activation. The shape of the strength–duration curve does not follow a constant-charge curve in part because of the asymptotic feature, the rheobase. As an example, a constant charge curve is plotted in Figure 2.7B. Two square pulses of equal charge lie along this 6 nC line, one of 400  $\mu\text{s}$  pulse width (15  $\mu\text{A}$ ) and one with 800  $\mu\text{s}$  pulse width (7.5  $\mu\text{A}$ ). The 400  $\mu\text{s}$  pulse has a high activation probability of 0.91, while the 800  $\mu\text{s}$  pulse is only 0.17. This demonstrates that stimuli of the same total charge can activate a neuron with very different probabilities. Clinical applications will benefit from improved selectivity and efficacy when activating a desired population of neurons because it will enable stimuli to activate neurons while simultaneously avoiding off-target neuronal activation. By better characterizing the stimulus-evoked neuronal response, we will improve our ability to deliver those stimuli that will most efficaciously activate a neuronal population.

## **2.6 Conclusions**

We demonstrated that closed-loop electrical stimulation is superior to open-loop techniques for measuring and controlling neuronal activation across a large parameter space. Our CL routine quickly homed in on the relevant activation curve features so that they could be more thoroughly probed to increase our measurement confidence. We showed that the stimulus-evoked neuronal response is probabilistic, and by using our CL imaging system and micro-stimulation technology, we were able to stimulate a neuron with an arbitrary probability. By exploiting the shape of the strength–duration curve we could activate a neuron with different probabilities by varying the aspect ratio of a constant-charge stimulus pulse. Closed-loop strategies are indispensable for developing techniques to selectively activate neurons, which is critical for the advancement of next-generation clinical stimulation solutions.

## 2.7 Supplemental data relating to Chapter 2

### 2.7.1 LED Illumination

During experimentation neurons were illuminated using a light-emitting diode (LED; center wavelength of 500) and current source (TLCC-01-Triple LED, relative power = 30; Prizmatix) through a 20X water-immersion objective, NA = 1.0, and a FITC filter cube. The FITC filter has a peak excitation wavelength of 494 nm and peak emission wavelength of 520 nm.

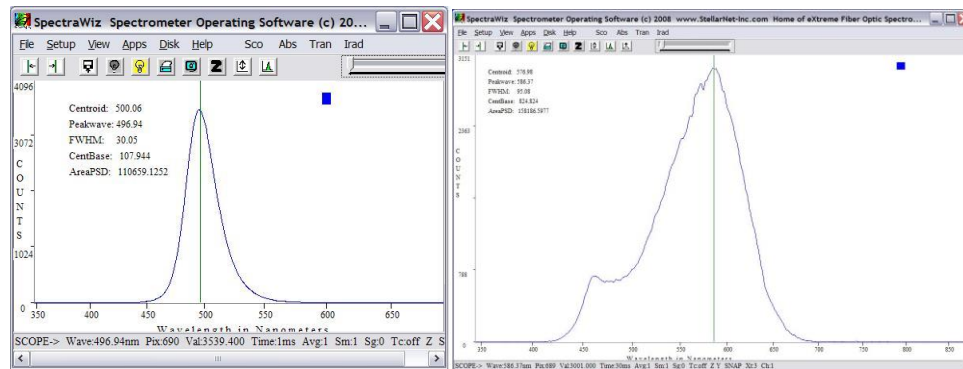


Figure 2.11. The power spectrum for the blue LED (left) and white LED (right).

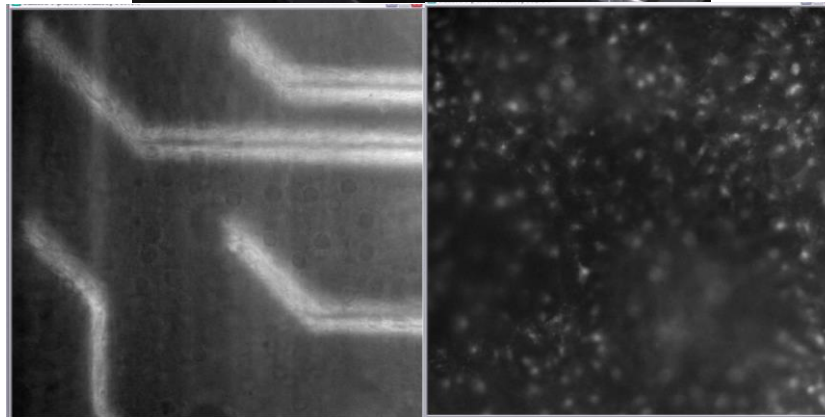
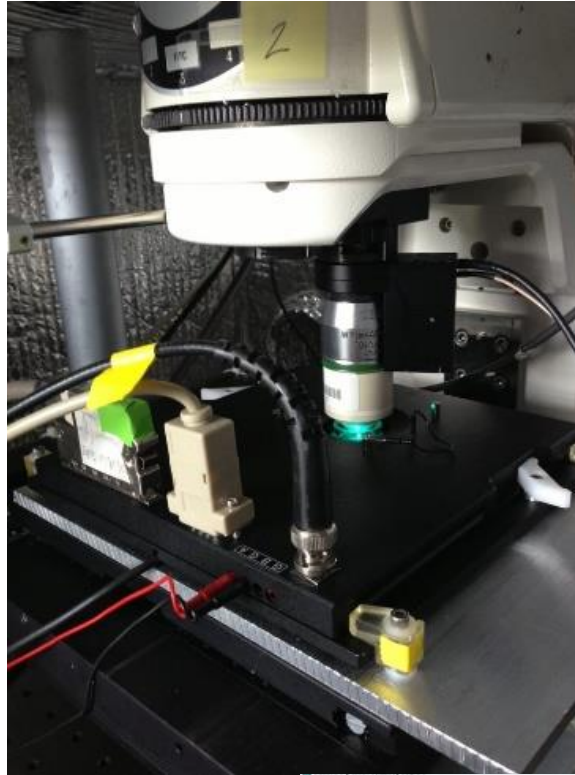


Figure 2.12. The imaging system comprises an upright microscope for epifluorescence microscopy. In the top frame is a photograph of the setup. An immersion objective is inserted into the cell culture well for imaging. One LED is a pseudo-white light for positioning the stage with respect to the objective so that the electrode areas of interest are within view. The bottom left panel shows an image collected using the white LED. The imaging plane is focused at the level of the neuron cell bodies, just above the electrode array. In the bottom right panel, the blue/green, 500 nm LED is used to excite the Fluo-5F fluorophore, and the resulting fluorescence is imaged through a FITC filter. As the cell culture ages, glia continue to divide, and the density of the culture increases. Eventually, glia begin to migrate and form 3-D groups, which can be observed where the culture is no longer in focus.

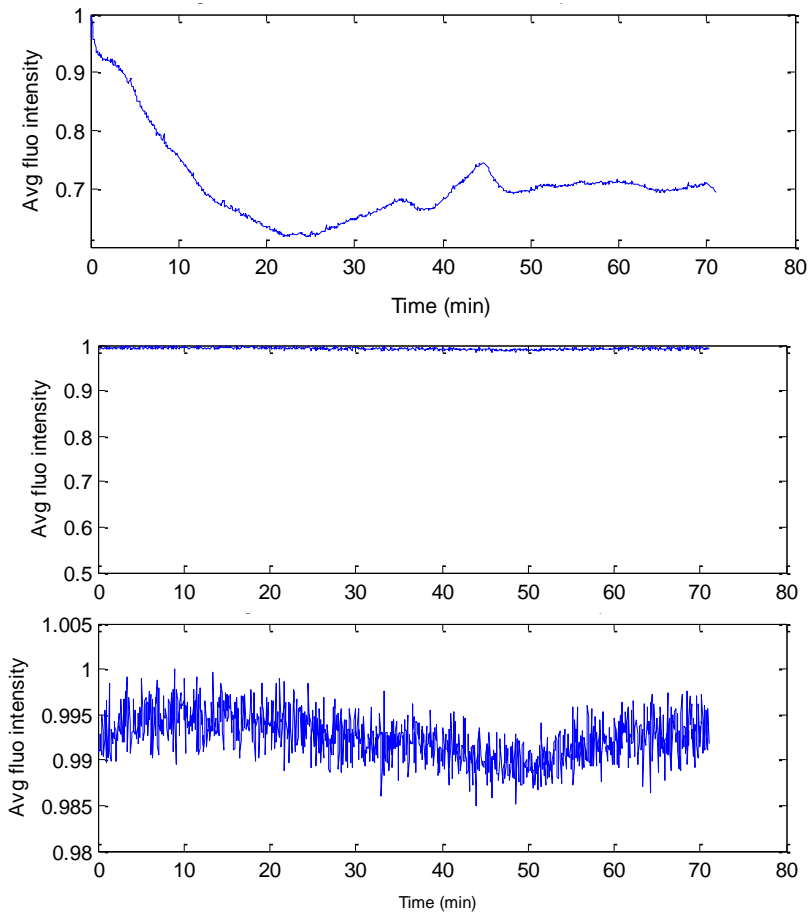


Figure 2.13. Time traces of the average fluorescence intensity from a cell (top panel) and an empty area (bottom two panels) within a neuronal culture. Baseline frames were collected pre-stimulus before every stimulus iteration for over 70 minutes of experimentation. Stimuli were presented every 4.5 seconds. The cell shows a drifting fluorescence baseline over the course of the experiment, which is not always decreasing due to photobleaching. This drift could be explained the normal variation in the cell's calcium regulation. In the bottom two panels, it can be seen that in the absence of a neuron, the baseline fluorescence is unchanging. The bottom panel is a zoomed in view of the middle panel.

### 2.7.2 Open-loop simulations

An open-loop simulation study was conducted in which a 1000-stimulus experiment was repeated 100 times and the measurement of the model neuron activation sigmoid was measured. The neuron was modeled by a sigmoid from Equation 2.1 with a midpoint of 10  $\mu\text{A}$  and a slope of 1.0 at the midpoint

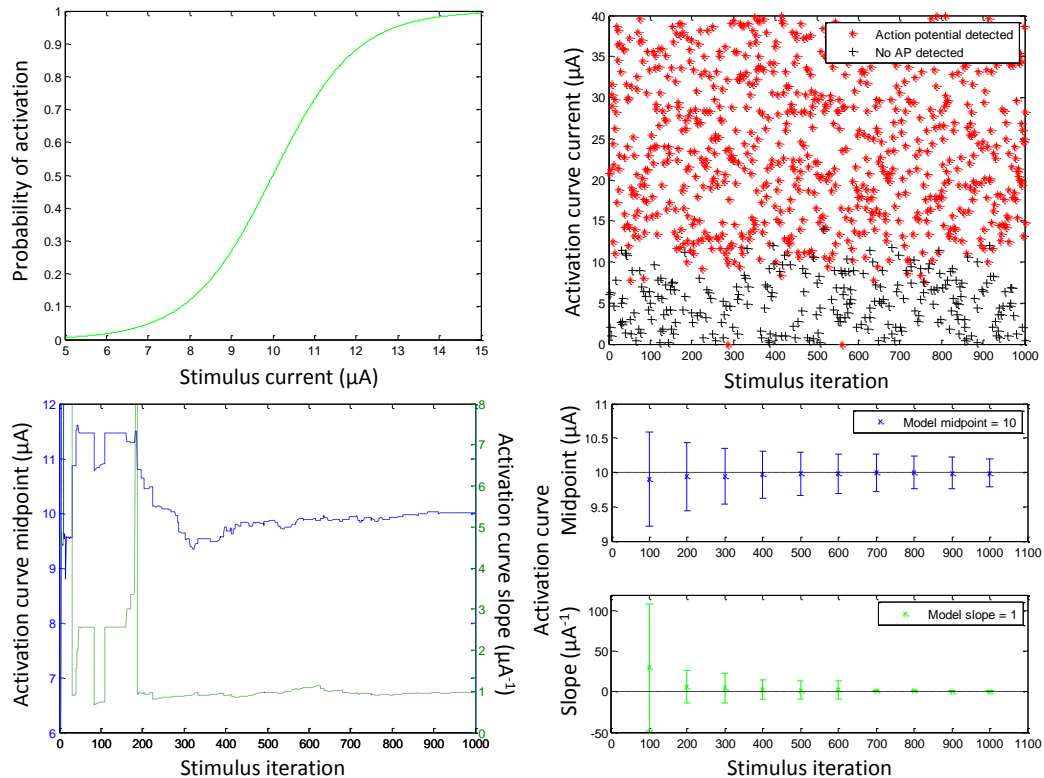


Figure 2.14. The model sigmoid is shown (top, left, the stimulus axis is zoomed in for clarity). An example set of 1000 stimuli and the neuronal output is shown in the top, right. The stimulus chosen at each iteration was chosen randomly from the stimulus current space, which spanned 0 to 40  $\mu\text{A}$  in 0.2  $\mu\text{A}$ . The step size was chosen based on the output resolution of the stimulator. A stimulus was tested by randomly choosing a number using the MATLAB rand function, and the output of the neuron model was evaluated by determining if the number fell above or below the sigmoid curve. In the bottom left panel, the convergence of the sigmoid fit parameters is shown for a sample experiment simulation. After approximately 200 stimuli were presented, there was sufficient measurement resolution to along the transition region of the sigmoid to measure the slope. For the 100 repetitions of the experiment, the estimate of the model parameters, along with 95% confidence intervals, is plotted every 100 stimulus iterations (bottom, right).

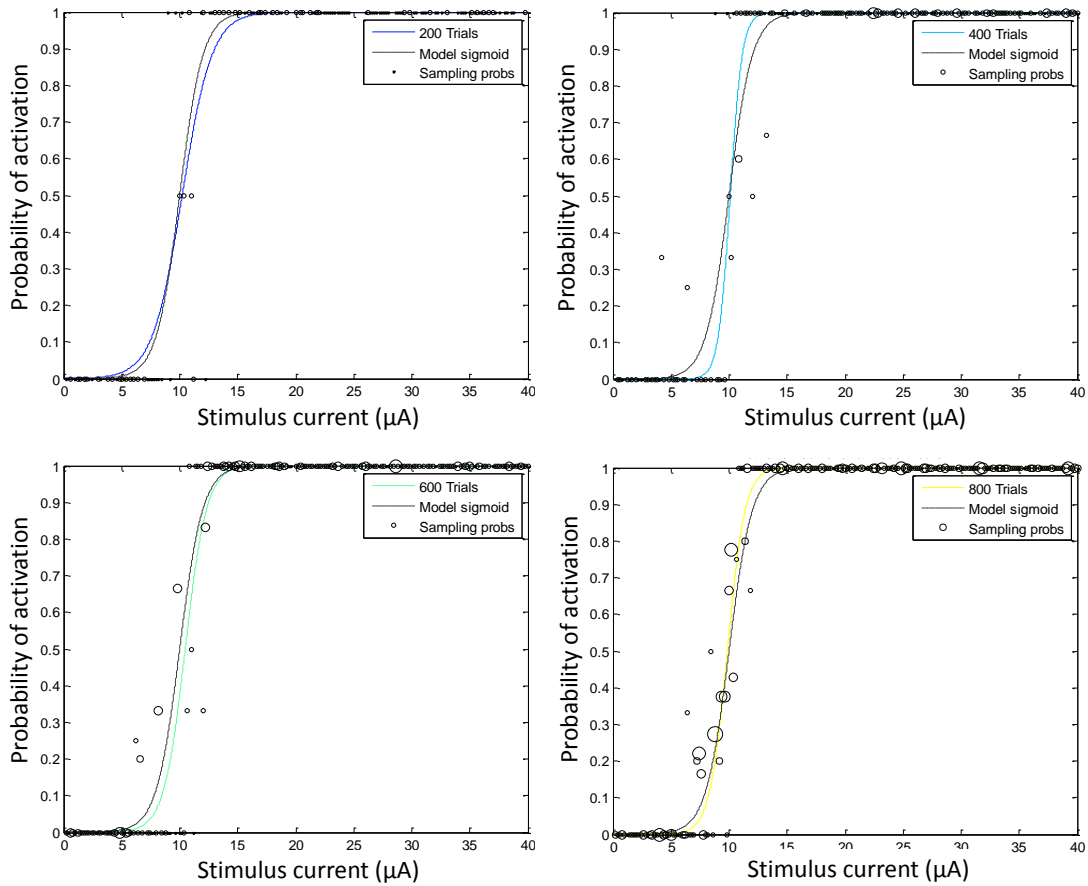


Figure 2.15. From the previous simulation study, the measured responses at each stimulus current were averaged and overlaid on the sigmoid models. The dotted black line depicts the model neuron. The lighter colored line depicts the sigmoid model built after 200 (top, left), 400 (top, right), 600 (bottom, left) and 800 (bottom, right) measurement iterations. The open black circles are proportional in size to the average of the response at each stimulus value, such that more stimuli were collected where larger circles reside, and so the confidence in the measurement at those points is higher.

### 2.7.3 Closed-loop simulations

To develop and test the closed-loop system, we modeled four neurons with sigmoid activation models. We added noise to each of the neurons to test if the system would have trouble converging on a model with a high level of noise. We found that all four converged on the sigmoid midpoint, although the simulations on the neuron with only a signal-to-noise ratio of 5 required more stimulus iterations.

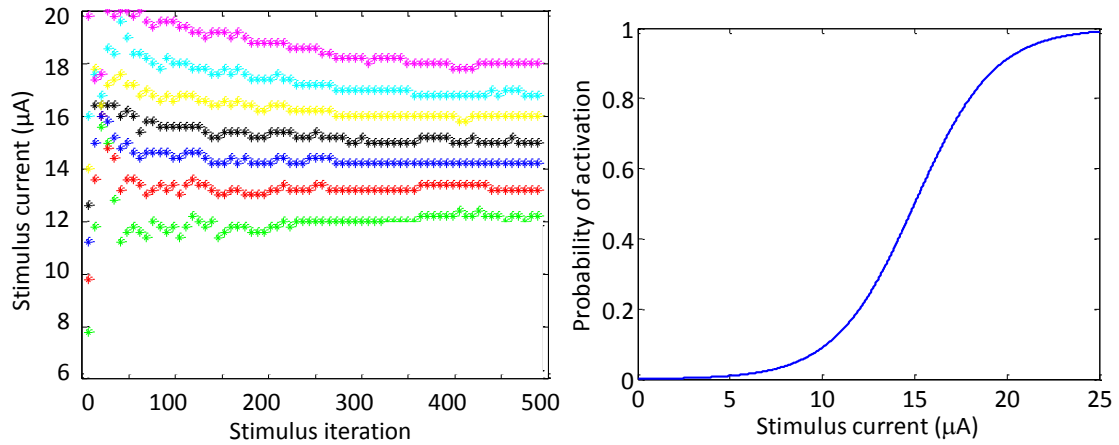


Figure 2.16. To expand on previous studies, the progression of the CL was demonstrated to search for various probability levels in the sigmoid.

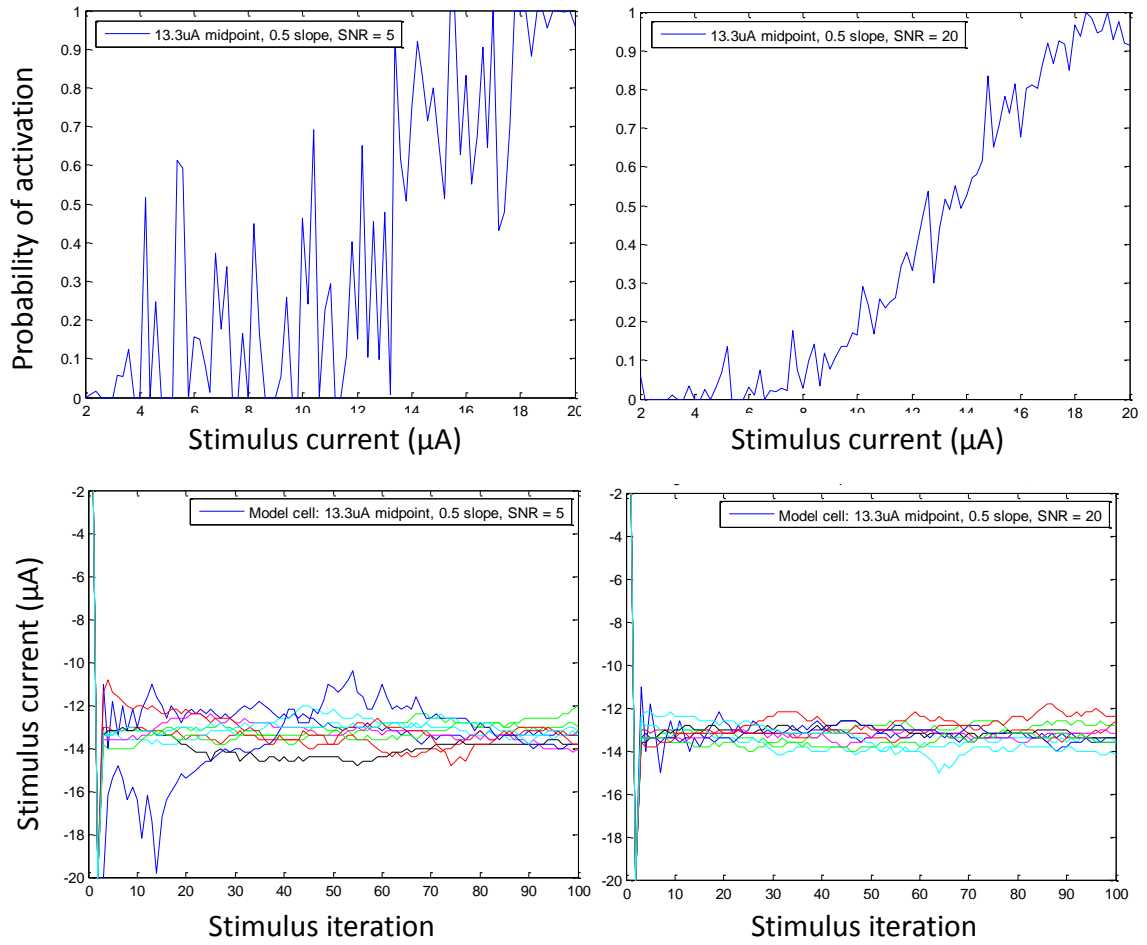


Figure 2.17. Four model neuronal activation curves were created with varying levels of Gaussian noise added to them to simulate the noise in a stimulus-evoked neuronal response. All four neurons had a midpoint of 13.3  $\mu\text{A}$  and a slope of  $0.5 \mu\text{A}^{-1}$ .

### 2.7.4 Experimental comparison of open-loop vs. closed-loop

Two neuronal activation curves were measured in the OL vs CL experiment from Chapter 2. For both neurons, the CL routine produced a narrow band of stimuli through the 250 iterations. The OL stimuli were distributed randomly throughout the range of currents. After the conclusion of the experiment, the sigmoid model was built for each of the neurons after each OL and CL stimulus iteration. The progression of the model parameters showed that the CL searches quickly converged on the sigmoid midpoint, however, the OL routine does not.

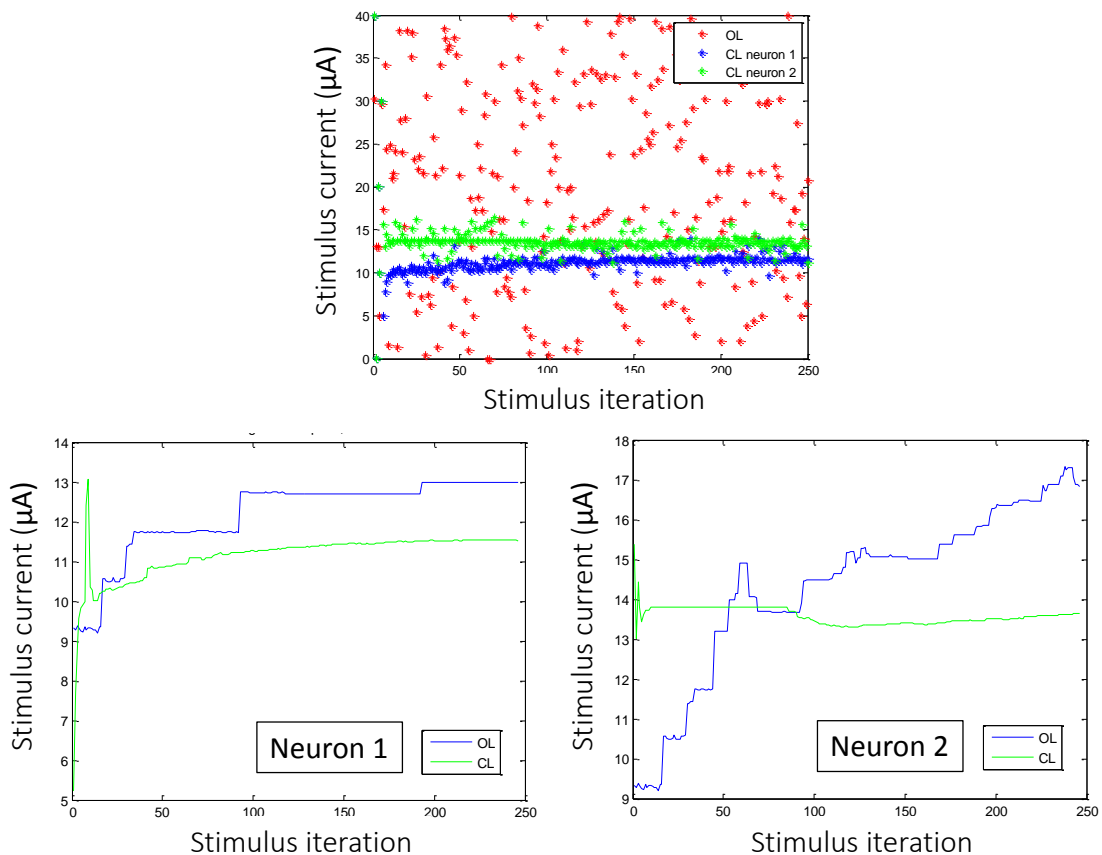


Figure 2.18. All stimuli delivered for each of the three studies (1 OL, 1 CL Neuron 1 and 1 CL Neuron 2) are plotted (top). The CL stimuli form tight bands around the activation curves and OL stimuli are spread throughout the entire stimulus space. Bottom: The progression of the sigmoid midpoint model parameter for both neurons with each stimulus.

### 2.7.5 Stationarity of the sigmoid activation curve

Six studies were conducted to evaluate the stationarity of a neuronal activation curve in the presence of synaptic blockers. Five sets of 50 stimuli and one set of 250 stimuli were delivered to measure the activation curve. The sixth set (250 stimuli) was run to provide a higher probability resolution on the measurement. Stimuli spanned a range of currents from 0 to 40  $\mu\text{A}$ . The total range in variability between the curves was less than 1  $\mu\text{A}$ , which can be attributed to noise in the measurement. The activation curve resulting from the sixth set of stimuli (250 stimuli) fell in the middle of all other curves.

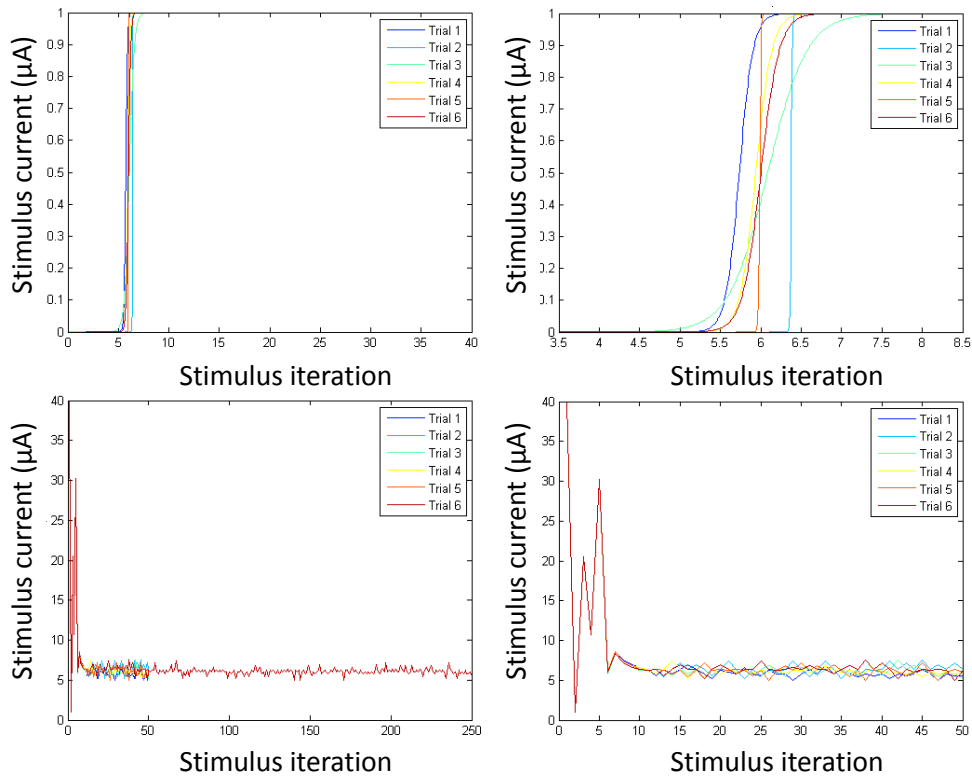


Figure 2.19. Six sigmoid activation models, for the same neuron, were overlaid in (A). The stimulus current axis was zoomed in to span only 5  $\mu\text{A}$  in (B). The stimuli delivered are highlighted in (C) and zoomed in on only the first 50 stimulus iteration in (D).

### 2.7.6 The progression of the sigmoid fit

A sigmoid model was calculated and plotted after every 10 stimulus iterations for a closed-loop search in both the variable-pulse-width and variable-current space. The sigmoid models approximate a step function in the beginning of the search. Once the stimuli overlap one another to measure the transition region of the sigmoid, the model begins to have a non-infinite slope. This study demonstrates that a CL search can very rapidly find the midpoint of an activation curve, but it requires at least 20 iterations before the slope can be calculated.

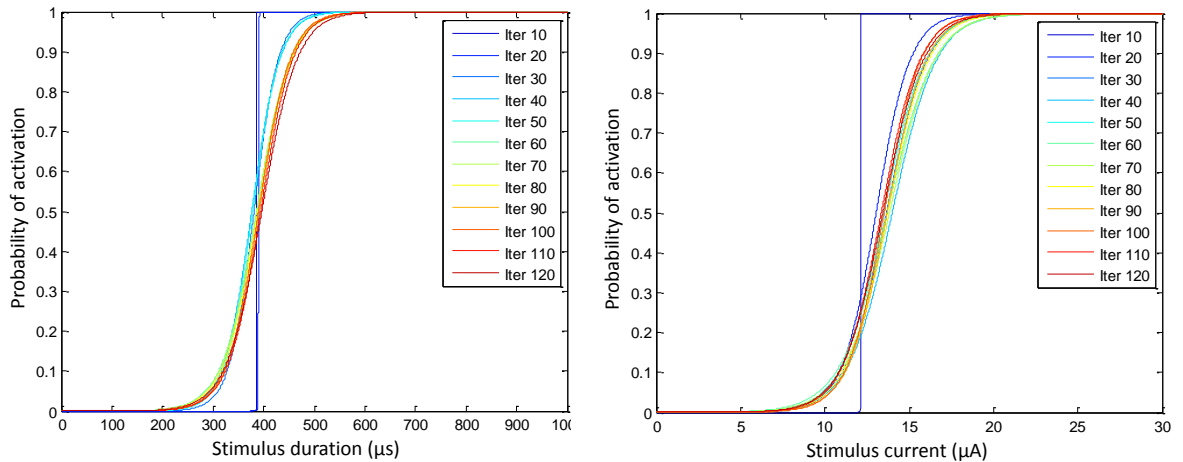


Figure 2.20. The progression of the curve fit of the sigmoid model to activation data. The initial model was nearly a step function.

### 2.7.7 Experimentally building strength-duration curves

We constructed strength-duration curves from variable-current searches for two neurons.

Following the CL searches to build the SD curves, an open-loop sweep of the waveform space near the activation curves was probed.

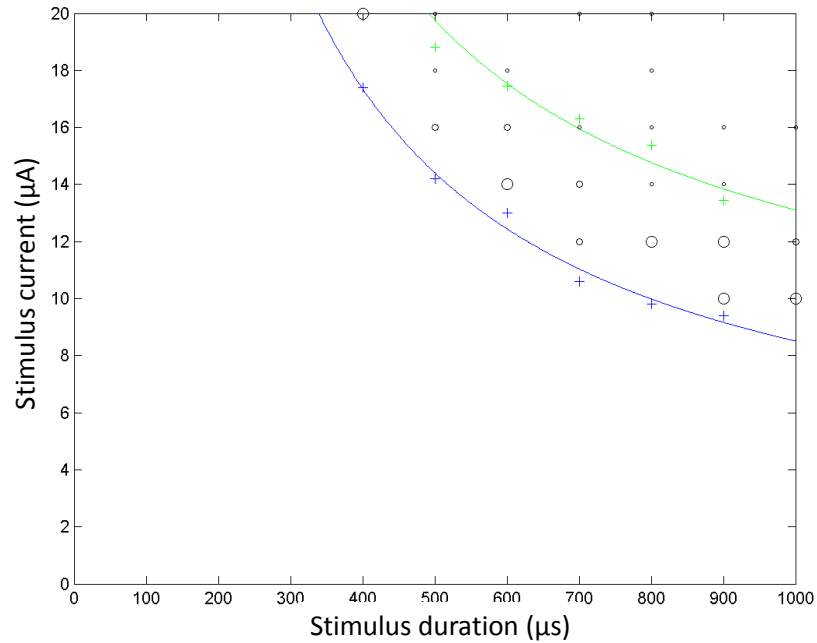


Figure 2.21. Two neuronal strength-duration curves were constructed and an OL sweep was performed afterwards to evaluate the selectivity between them. The difference in activation at the OL points was used as a measure of selectivity. Open circles were plotted, sized in proportion to that difference.

# CHAPTER 3

## TARGETED STIMULATION USING DIFFERENCES IN ACTIVATION PROBABILITY ACROSS THE STRENGTH- DURATION WAVEFORM SPACE

### 3.1 Abstract

New methods for targeted neuronal activation would improve on existing activation technology by offering the ability to selectively activate a single neuron or a subpopulation of neurons. This improvement allows devices to reduce off-target neuronal activation that causes unwanted side effects, while permitting greater functionality and therapeutic efficacy. Electrical stimulation is ubiquitous as a method for activating neuronal tissue. There is still significant room for advancement in the ability of these electrical devices to implement smart stimulus waveform design to more selectively target populations of neurons. The capability of a device to encode more complicated and precise messages to a neuronal network greatly increases if the stimulus input space is broadened to include variable shaped waveforms and multiple stimulating electrodes. The relationship between a stimulating electrode and the activated population is unknown, a priori. For that reason, the population of excitable neurons must be characterized in real-

---

This manuscript is being prepared for publication:  
Michelle L. Kuykendal, Martha A. Grover, Steve M. Potter, and Stephen P. DeWeerth\*  
\*Corresponding author e-mail address: [steve.deweerth@gatech.edu](mailto:steve.deweerth@gatech.edu)

time and for every combination of stimulating electrodes and neuronal populations.

Our automated experimental system allows investigation into the stimulus-evoked neuronal response to a current pulse using dissociated neuronal cultures grown atop microelectrode arrays. The studies presented here demonstrate that differential activation is achievable between two neurons using either multiple stimulating electrodes or variable waveform shapes. By changing the aspect ratio of a rectangular current pulse, the stimulus activated neurons in the strength–duration (SD) waveform space with differing probabilities. Additionally, in the case when two neuronal activation curves intersect each other in the SD space, one neuron can be selectively activated with short-pulse-width, high-current stimuli while the other can be selectively activated with long-pulse-width, low-current stimuli. Exploring the capabilities and limitations of electrical stimulation allows for improvements to the delivery of stimulus pulses to activate neuronal populations. Many state-of-the-art clinical stimulation solutions, including those using a single microelectrode, can benefit from waveform design methods to improve stimulus efficacy. These findings have even greater import into multi-electrode systems because spatially distributed electrodes further enhance accessibility to differential neuronal activation.

### **3.2 Introduction**

Artificial neuronal stimulation has been used for many decades to activate neuronal tissue in order to learn how the brain works and to alleviate symptoms due to neurological disease. However, the efficacy of neuronal stimulation is dependent on its ability to target specific neuronal populations. To target populations, stimuli must be designed to evoke activity in particular neurons and brain regions while simultaneously

preventing the activation of off-target neurons. Selective activation of individual neurons can improve stimulus efficacy by enabling therapeutic devices to better control their direct effects on activated tissue. Improvements in selective stimulation are applicable to a variety of techniques for activating neuronal tissue. Widely used stimulation modalities include deep brain stimulation (DBS), optogenetics, transcranial magnetic stimulation (TMS), intracellular electrical stimulation, and extracellular electrical stimulation. Some activation modalities are inherently selective, such as optogenetics or intracellular activation, but these techniques are limited in their clinical application due to excessive invasiveness and complexity.

The most broadly used neuronal activation technique is extracellular electrical stimulation, which is inherently nonselective. Improvements in selective activation carry forward into selective modulation of neuronal population activity, which enables clinicians to treat symptoms from neural pathologies. An example target application for selective techniques is DBS, which is used in treating Parkinson's Disease and epilepsy. During DBS, stimuli must be designed to specifically target a baseline activity level such that the stimulus evokes sufficient activity to provide a therapeutic effect, while not excessively activating tissue leading to side effects. (Freeman et al. 2010; Twyford et al. 2014; Lee et al. 2013; McIntyre et al. 2011). In addition to the previous example of DBS, extracellular electrical stimulation has found widespread clinical application for the development of cortical and peripheral prostheses to restore lost function due to trauma or disease. In bypassing damaged tissue, prostheses can encode motor intentions or sensory interpretations of the environment by delivering stimuli to the remaining intact population of neurons. One of the primary challenges to a perfect prosthesis is in the

development of stimulation strategies that enable it to encode a large range of stimuli with a finite number of electrodes. Highly selective stimulation methods are required to differentially target populations of neurons in order to deliver the necessarily complex messages. (Sekirnjak et al. 2006; Lebedev et al. 2011; Jepson et al. 2011; Kipke et al. 2008; Fried et al. 2006; Guggenmos et al. 2013; Carmena et al. 2003; Fitzsimmons et al. 2007; Freeman et al. 2010; Twyford et al. 2014; Lee et al. 2013; McIntyre et al. 2011).

Exploiting the probabilistic nature of neuronal activation in response to extracellular electrical stimulation can offer access to selectivity that is otherwise unobtainable with classic methods. There is a well-defined strength–duration (SD) stimulus space that describes the changing probability of a neuron to fire an action potential in response to a variable stimulus current and pulse width (Jankowska & Roberts 1972; Jensen et al. 2009; Sekirnjak et al. 2006; Yoemans et al. 1988; Bostock 1983; Nowak and Bullier 1998; McIntyre & Grill 2002; Boinagrov et al. 2010). In this two-parameter stimulus space even the smallest differences in SD curves can be used to differentially deliver messages into the nervous system. For example, stimuli are traditionally delivered in an on/off modality using relatively large stimulus currents. By changing the shape of the stimulus pulse while delivering the same total charge, a typically excitatory pulse can activate a particular neuron with significantly lower probability. This differences in susceptibility of neurons within a population to activate preferentially to different stimulus pulse widths, which can be understood by their SD curves, offers access opportunities for selectivity using this more complex activation space.

We have created a test bed for delivering electrical stimuli and assessing the efficacy of the stimulus waveforms to selectively activate a single neuron or a neuronal population. The value of the in vitro test bed is that it facilitates the testing of a wide variety of selective stimulation techniques in a controlled setting. Stimulation modalities vary greatly in their spatial and temporal scope but what is learned in studies of extracellular electrical stimulation can inform other stimulation techniques including clinical applications. Our in vitro system delivers electrical stimuli to a culture via a microelectrode array, and neuronal activation is measured using bulk loaded calcium fluorescent dyes. In this work, we show while using a single stimulating electrode that specific neurons in a population can be selectively activated by stimulating along different regions of the SD curve. Many state-of-the-art clinical stimulation solutions, including those using a single microelectrode, can benefit from waveform design methods to improve stimulus efficacy. These findings have even greater import into multi-electrode systems because spatially distributed electrodes further enhance accessibility to differential neuronal activation.

### **3.3 Methods**

We designed a closed-loop system, as was described in Chapter 2, for optimizing stimulus pulse parameters based on a model of neuronal activation and an experimental goal. The system comprises hardware and software components that select and deliver stimuli, which are designed to evoke a particular neuronal response. Each measured response is used to refine the model and the next stimulus is automatically chosen. The modular design, which separates data collection from both data analysis and decision-making, enables the user to plug in a model function and a variety of experimental goals to ask and answer a multitude of questions. Each section of the system is described in more detail below.

#### 3.3.1 Cortical cell culture

Embryonic Day 18 (E18) rat cortices were enzymatically and mechanically dissociated according to (Potter & DeMarse, 2001). Cortices were digested with trypsin (0.25% w/EDTA) for 10-12 minutes, strained through a 40  $\mu\text{m}$  cell strainer to remove clumps and centrifuged to remove cellular debris. Neurons were re-suspended in culture medium [90 mL Dulbecco's Modified Eagle's Medium (Irvine Scientific 9024), 10 mL horse serum (Life Technologies 16050-122), 250  $\mu\text{L}$  GlutaMAX (200 mM; Life Technologies 35050-061), 1 mL sodium pyruvate (100 mM; Life Technologies 11360-070) and insulin (Sigma-Aldrich I5500; final concentration 2.5  $\mu\text{g}/\text{mL}$ )] and diluted to 3000 cells/ $\mu\text{L}$ . Microelectrode arrays (MEAs; Multi Channel Systems 60MEA200/30iR-Ti) were sterilized by soaking in 70% ethanol for 15 minutes followed by UV exposure overnight. MEAs were treated with polyethylenimine to hydrophilize the surface, followed by three water washes and 30 minutes of drying. Laminin (10  $\mu\text{L}$ ; 0.02 mg/mL; Sigma-Aldrich

L2020) was applied to the MEA for 20 minutes, half of the volume was removed, and 30,000 neurons were plated into the remaining laminin atop the MEA. Cultures were protected using gas-permeable lids (Potter & DeMarse, 2001) and incubated at 35°C in 5% carbon dioxide and 95% relative humidity. The culture medium was fully replaced on the first DIV and then once every four DIV afterwards.

### 3.3.2 Electrical stimulation

Extracellular electrical stimuli were used to elicit neuronal activity. Stimuli were delivered to the neurons using a STG-2004 stimulator and MEA-1060-Up-BC amplifier (Multi Channel Systems). MATLAB (Natick, MA) was used to control all hardware devices, which were synchronized by TTL pulses sent from the stimulator at the beginning of each stimulation loop. In all stimulus iterations, a trigger pulse was first delivered to the camera to begin recording so that background fluorescence levels could be measured. An enable pulse was then delivered to the amplifier, which connected the stimulus channel to a pre-programmed electrode. A single cathodic square current pulse was then delivered to a single electrode centered under the camera field of view. Cathodic pulses were chosen because they have been shown to be most effective at evoking a neuronal response (Wagenaar, 2004).

### 3.3.3 Optical imaging

As was described in Chapter 2, automated optical imaging was used to measure the stimulus-evoked neuronal response. All preparation procedures were conducted in the dark to lengthen experiments by minimizing photobleaching and phototoxicity. First, culture media was removed and neurons were loaded with Fluo-5F AM (Life Technologies F-14222), a calcium-sensitive fluorescent dye with relatively low binding

affinity at a concentration of 9.1  $\mu\text{M}$  in in DMSO (Sigma-Aldrich D2650), Pluronic F-127 (Life Technologies P3000MP) and artificial cerebral spinal fluid (aCSF; 126 mM NaCl, 3 mM KCl, 1 mM  $\text{NaH}_2\text{PO}_4$ , 1.5 mM  $\text{MgSO}_4$ , 2 mM  $\text{CaCl}_2$ , 25 mM D-glucose) with 15 mM HEPES buffer for 30 minutes at ambient 25°C and atmospheric carbon dioxide. Before imaging, cultures were rinsed two times with aCSF to remove free dye. Cultures were bathed in a mixture of synaptic blockers in aCSF (15 mM HEPES buffer). This included (2R)-amino-5-phosphonopentanoate (AP5; 50  $\mu\text{M}$ ; Sigma-Aldrich A5282), a NMDA receptor antagonist; bicuculline methiodide (BMI; 20  $\mu\text{M}$ ; Sigma-Aldrich 14343), a GABAA receptor antagonist; and 6-cyano-7-nitroquinoxaline-2,3-dione (CNQX; 20  $\mu\text{M}$ ; Sigma-Aldrich C239), an AMPA receptor antagonist. This mixture was shown to suppress neuronal communication (Bakkum, Chao, & Potter, 2008) to ensure that the recorded neuronal activity was directly evoked by the stimulus. The culture was then kept in the heated amplifier (Multichannel systems TC02, 37C) within the imaging chamber. The stage position was calibrated with respect to the desired field of view (FOV) using the electrodes as fiducial markers. A MATLAB GUI was used to automatically position the FOV over the stimulation electrode. During an experiment neurons were illuminated using a light-emitting diode (LED; center wavelength of 500 nm) and LED current source (TLCC-01-Triple LED, relative power = 30; Prizmatix) through a 20X water-immersion objective, NA = 1.0, and a fluorescein isothiocyanate (FITC) filter cube. Evoked activity was optically recorded using a high-speed electron multiplication CCD camera (30 fps; QuantEM 512S; Photometrics), which has a 512 X 512 pixel grid covering a 400  $\mu\text{m}$  X 400  $\mu\text{m}$  area. After an experiment concluded, three

aCSF washouts were performed at three minute intervals, the culture media was replaced, and the culture was returned to the incubator.

#### 3.3.4 Detecting action potentials

For each neuron, the measured intensity of 16 X 16 pixels (12.5  $\mu\text{m}$  X 12.5  $\mu\text{m}$ ) surrounding the soma center was spatially averaged. The relative change in fluorescence,  $\Delta F/F$ , was calculated by subtracting the baseline (an average of four pre-stimulus frames) from the peak (an average of four post-stimulus frames) and dividing the difference by the baseline. An action potential was evoked in one trace (bold) and no action potential was evoked in the other. The traces were generated from the average of sixteen pixels that overlay the neuron soma. The peak and baseline frames are highlighted with gray bars, and the stimulation time is marked with an arrow. The standard deviation of the baseline frames was calculated in initial stimulus iterations and used as a measure of the fluorescence noise level. An action potential was said to have occurred if the  $\Delta F/F$  was greater than three times the noise level within a particular neuron. The average decay time constant of a stimulus-evoked fluorescence curve was 1.5 seconds. Because of this relatively slow signal decay, the experiment loop time was chosen to be 4.5 seconds, which is three decay constants long, to give the signal sufficient time to return to baseline.

### 3.3.5 The sigmoid activation model

A saturating nonlinear curve was used to fit to the neuronal probability of firing an action potential in response to a varying stimulus current or pulse width. Specifically, a two-parameter sigmoid (Equation 3.1) was used to describe this 1-D activation curve for cathodic square-pulse stimuli.

$$p = \frac{1}{1 + b_2 e^{-(x-b_1)}} \quad \text{Equation 3.1}$$

The sigmoid model provides an approximation for the stimulus needed to activate a particular neuron with any given probability. The input activation parameter,  $x$ , is either the stimulus current or pulse width, and the output is the probability,  $p$ , of a neuron to fire an action potential. The two parameters describing the sigmoid are  $b_1$ , the midpoint of the sigmoid, and  $b_2$ , the slope of the curve at the midpoint. Because the sigmoid describes a probability of activation, it spans from zero to one.

### 3.3.6 The closed-loop search algorithm

The closed-loop search procedure began with five open-loop stimuli that divided the stimulation space evenly and bracketed the activation region. After the fifth iteration, the sigmoid model was analytically linearized, and a linear least-squares fit of the midpoint and slope parameters was performed. All measured stimulus-evoked responses were equally weighted. The output of the linear regression was used as an initial guess for a nonlinear least squares curve fit using the MATLAB Optimization Toolbox, which generated the best-fit sigmoid parameters. The measured response was a binomial distribution describing the evoked action potential probability, which was calculated as a mean of all responses at a particular stimulus value. In order to gain information about

the midpoint and slope, a probability goal was randomly chosen from the set of 0.25, 0.50 and 0.75, which spans the transition region of the sigmoid. The stimulus that was predicted to produce the target firing probability was calculated analytically by inverting the sigmoid model. The probability goals span the linear region of the transition region of the sigmoid curve, and an accurate measurement of the stimulus values at these probabilities provided an estimate of the slope of the curve at the midpoint. In the case that the next stimulus chosen was the same as the previously delivered stimulus, a random jitter was added to the stimulus up to 20% in either direction so that more data would be collected over the full range of the transition region of the activation curve. After every stimulus iteration, the linear and nonlinear curve-fits were run to update the model.

### 3.3.7 The strength–duration activation model

Neuronal activation in the 2-D strength–duration waveform space was described according to Lapicque (1907, Equation 3.2).

$$I = r \left( 1 + \frac{c}{PW} \right) \quad \text{Equation 3.2}$$

The stimulus pulse width,  $PW$ , is the input; the stimulus current,  $I$ , is the output, and the two model parameters are the rheobase,  $r$ , and the chronaxie,  $c$ , which describes the knee of the curve. The rheobase describes the stimulus current below which a stimulus with infinite pulse width will not evoke an action potential, and the chronaxie describes the stimulus pulse width that corresponds to a stimulus current of twice the rheobase.

### 3.4 Results

We utilized the in vitro test bed to analyze the stimulus selectivity achievable using one- and two-parameter stimuli for multiple populations of neurons. In the first experiment, the stimulus selectivity achievable by varying a single input parameter was analyzed using Population A ( $n_A=12$  neurons). The one-parameter stimulus-evoked neuronal activation curves were uncovered using a closed-loop (CL) search strategy and the distance between the curves was measured. The second experiment was performed on Population B ( $n_B=30$  neurons) and focused first on understanding the spatial relationship between neuronal somata and the stimulating electrode. An open-loop (OL) stimulation strategy was used to simultaneously construct two-parameter strength–duration curves for Population B, and the achievable selectivity was measured by allowing both stimulus input parameters to be varied. In the final study, we analyzed an alternative method for variation on two input parameters by varying a single stimulus parameter and varying the stimulating electrode location. We used the CL routine to measure activation curves for two neurons from multiple stimulating electrodes (Population C,  $n_C=2$  neurons). In evaluating the stimulus selectivity between neurons, we found we were able to differentially target our stimulus to particular neurons by exploiting the distribution of neuronal activation curves within the strength–duration waveform space, on multiple electrodes.

#### 3.4.1 Analysis of selectivity with a one dimensional input space

The sigmoid activation curves for Population A were measured using the closed-loop search routine. The stimulus pulse width was held constant at 800  $\mu\text{s}$  during the searches. To improve the resolution of the model along the transition region of the activation curve,

for each iteration of the CL routine the measured stimulus-evoked response was used to update the neuronal activation curve and the model was used to choose the next stimulus that would be delivered. While searching for the activation response data for a specific neuron, the CL routine simultaneously recorded activation response data for all other neurons in view. For example, while the algorithm searched for the activation curve parameters for fifth neuron, it was continuously updating the model parameters for neurons A1 – A4 and A6 – A10. After each set of 30 stimuli, the CL system switched focus to a different neuron. Each neuronal activation curve was the target of the algorithm for an equal number of stimuli and a total of 360 stimuli were delivered equally across the twelve neurons. When neuronal activation curves were proximal in the stimulus space, the data collected for one neuron increased the measurement resolution for other neurons. Therefore, after the controller concluded its search for one neuronal activation curve, it already had a model built for the activation curves of all other neurons. The model built passively for neurons with activation curves similar to the previously targeted neuron had more stimuli delivered across the activation curve transition region, which increased the probability measurement for those curves. The lowest activation threshold, defined as the midpoint of the sigmoid model, was  $7.6 \mu\text{A}$  and the highest threshold was  $21.1 \mu\text{A}$ , although the maximum stimulus current reached  $30 \mu\text{A}$ . Of the twelve activation curves, seven curves lie within less than a  $5 \mu\text{A}$  range from  $10.6 \mu\text{A}$  to  $14.8 \mu\text{A}$  (Figure 3.1A).

We evaluated the stimulus selectivity that was achievable between neurons using the sigmoid activation curves. The selectivity range between a pair of neurons was defined as the stimulus distance between their thresholds, or sigmoid midpoints (Figure

3.1B). This metric was chosen because, at all points through the selectivity range, the neuron with a lower activation threshold will necessarily activate with probability greater than 0.5 and the neuron with the higher activation threshold will activate with probability less than 0.5. For neurons with vastly differing thresholds, there was a large stimulus range that was selective such that one neuron was exclusively activated. The largest selectivity range was between neurons A3 and A11 over a range of 13.7  $\mu\text{A}$ . The selectivity is non-zero for all pairs of neurons, even along the transition region of the neuronal activation curves. We characterize neuron pairs into three classes of selectivity: highly selective (not shown), moderately selective (Figure 3.1C), and minimally selective (Figure 3.1D). For example, between Neurons A1 and A7, there was a selectivity range of 8.0  $\mu\text{A}$  in which A7 activated while A1 was silent. Between Neurons A3 and A9, the selectivity range is more continuous—there is no discrete transition in selectivity between zero and one because A9 activated with a shallower activation curve slope along the transition region. This means that as the probability of activating A9 increases, it does so more slowly with increasing stimulus current, and even near the transition region of A9, there is still a non-zero probability of selectively activating A3 (Figure 3.1C). For neurons with relatively similar thresholds, as is the case of A5 and A8, selectivity remains non-zero. Even in this extreme example, despite minimal selectivity between the neurons, there is still selectivity achievable: at the point 13.8  $\mu\text{A}$ , A8 activated 100% of the time while A5 never activated. Even at stimuli surrounding that point, there was a non-zero level of selectivity (Figure 3.1D).

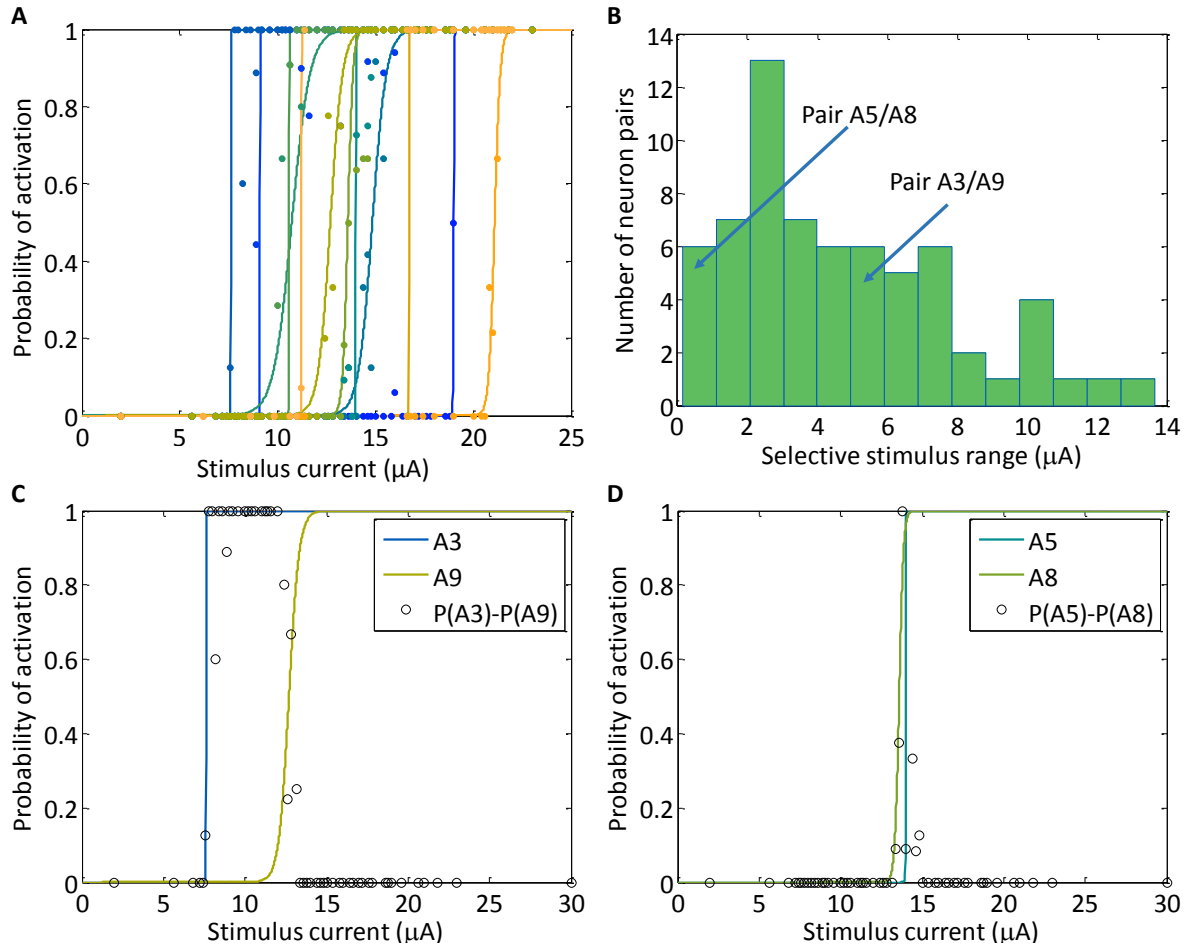


Figure 3.1. (A) The closed-loop routine was used to measure neuronal activation curves for Population A in the stimulus current space while the stimulus pulse width was fixed. Each activation curve describes the probability of a neuron to fire an action potential across a range of stimulus currents. The curves are arbitrarily shaded to aid in viewing the lines. For each curve there are similarly shaded probability points lying along the curve, which describe the average firing probability for a neuron at a particular stimulus current. (B) The selectivity achievable between all possible pairs within Population A is depicted in a histogram. The selective stimulus range is calculated as the absolute value of the difference in the  $P=0.5$  points for each pair of neurons. For all pairs of neurons the selectivity is non-zero. (C,D) Two pairs of neuronal activation curves (solid lines) are depicted. For each stimulus current, the difference in neuronal activation (open circles) was calculated by subtracting the two probabilities of firing. This difference in probabilities is a measure of the selectivity of the stimulus between the two neurons and was calculated directly from the data. (C) The selectivity achievable between A3 and A9 spanned 5  $\mu\text{A}$ . (D) For the pair of neurons, A5 and A8, although the activation curves lie close to one another, there is a stimulus point at 13.8  $\mu\text{A}$  where A8 is activated and A5 is not.

### 3.4.2 Analysis of selectivity with a two dimensional input space

To maximize the number of neurons that could be characterized in Population B, we used an open-loop stimulus routine to sweep a large range of stimulus currents and pulse-widths. This experiment delivered a randomized set of stimuli spanning currents from 2  $\mu\text{A}$  to 20  $\mu\text{A}$  in 1  $\mu\text{A}$  increments and pulse-widths from 300  $\mu\text{s}$  to 800  $\mu\text{s}$  in 100  $\mu\text{s}$  increments simultaneously to all neuron targets. One pulse was presented per stimulus iteration, and ten repetitions of each pulse were delivered in the experiment. Action potentials were extracted, post hoc, for each stimulus iteration according to the methods. The activation data corresponding to stimuli with similar pulse widths were grouped together, such that only the stimulus currents were variable within each group. An activation curve was constructed for each grouping, which was modeled by a sigmoid that spanned the entire current space. All of the sigmoid models, each corresponding to a different stimulus pulse width, were used to predict the stimulus currents that would produce a probability estimate of 0.5. A separate activation curve was constructed for each neuron. For each pulse width, there were then 30 measured threshold currents, at which the activation probability for each neuron was 0.5. This analysis resulted in six different pulse widths and six corresponding threshold currents for each neuron. Each set of these six points in the strength–duration stimulus space were used as inputs into the SD model from Equation 3.2 to create  $P=0.5$  threshold curves for each of the 30 neurons (Figure 3.2A). The two parameters used to describe the SD curve, chronaxie and rheobase, show a negative trend: the rheobase tends to increase, while the chronaxie tends to decrease (Figure 3.2D).

We examined the spatial distribution of neuronal cell bodies in Population B within a 400  $\mu\text{m}$  X 400  $\mu\text{m}$  area across a range of neurons and stimulus pulse widths. A sigmoid activation curve was built for each neuron using the 300  $\mu\text{s}$  and 800  $\mu\text{s}$  pulse-width data, and the radial distance of the cell body from the stimulating electrode was calculated. Because the imaging methods employed here provided direct access to the radial soma-to-electrode distance, it was compared to the sigmoid model midpoint measured for each neuron individually (Figure 3.2B-C). As was the case for Population A, there was no observable correlation between the threshold and soma-electrode distance.

Neuronal activation probabilities were compared between the shortest and longest pulse-width data points collected, 300  $\mu\text{s}$  and 800  $\mu\text{s}$ . Each of the 30 neurons of Population B is depicted by its 300  $\mu\text{s}$  and 800  $\mu\text{s}$  activation thresholds (Figure 3.2E), defined as the current levels at which a neuron fires an action potential with 0.5 probability. We manually selected two pairs of neurons with similar rheobase (B4, B21) or chronaxie (B19, B25) values. Because these neurons lie in the second and fourth quadrants around the cross hatch, they reverse order from 300  $\mu\text{s}$  to 800  $\mu\text{s}$ . Neuron B19 has a higher activation threshold than B25 for the 300  $\mu\text{s}$  pulse, but has a lower activation threshold for the 800  $\mu\text{s}$  pulse. Similarly, neuron B21 has a higher threshold than neuron B4 for the 300  $\mu\text{s}$  pulse and vice versa at 800  $\mu\text{s}$ . Graphically, this is seen as intersecting strength–duration activation curves (Figure 3.2F). When the SD curves intersect, the single stimulating electrode can be used to selectively activate neuron B4 over B21 and B25 over B19 at short stimulus pulse-widths and high stimulus currents. The opposite holds true for long stimulus pulse-widths and low currents.

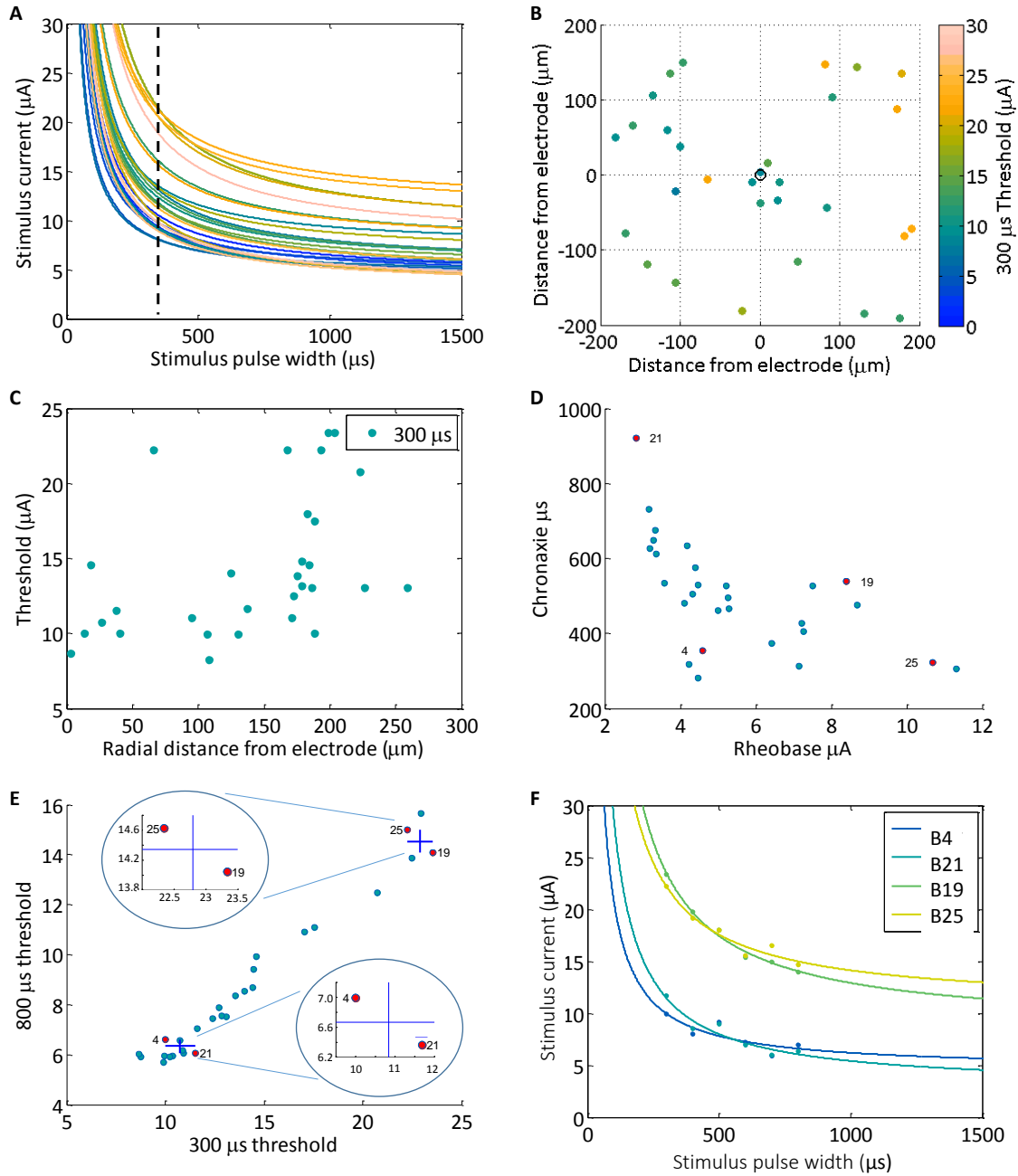


Figure 3.2. (A) Strength–duration curves for Population B span a large range of the stimulus-pulse parameter space. These curves are described by the rheobase, or the stimulus current threshold at infinite pulse-width, and the chronaxie, or the stimulus pulse-width at twice the rheobase current. Intuitively, these parameters define the horizontal asymptote and the knee of the curve. (B) The spatial location with respect to the stimulating electrode (open circle in the center) of all 30 neuronal somata is depicted within the imaging plane. Each soma is shaded according to its activation threshold for a  $300 \mu\text{s}$  stimulus pulse width. (C) For the same neurons, the radial distance of the soma to the electrode is shown versus the activation threshold for both  $300 \mu\text{s}$  and  $800 \mu\text{s}$  pulse

widths. Twelve neurons lie between 150  $\mu\text{m}$  and 200  $\mu\text{m}$  away from the electrode, radially, and have activation thresholds that span a 14  $\mu\text{A}$  ranges of currents for the 300  $\mu\text{s}$  pulse-width data and 10  $\mu\text{A}$  for the 800  $\mu\text{s}$  pulse-width data. (D) The distribution of rheobase and chronaxie parameters is shown for Population B. Four neurons are highlighted. (E) Each of the 30 neurons from Population B is depicted by its 300  $\mu\text{s}$  and 800  $\mu\text{s}$  activation thresholds, which are the current levels at which a neuron fires an action potential half of the time. The same four neurons are highlighted from the previous figure. A cross hatch is drawn for two pairs of neurons that evenly divides the space between them. Because these neurons lie in the second and fourth quadrants around the cross hatch, they reverse order from 300  $\mu\text{s}$  to 800  $\mu\text{s}$ . Neuron B19 has a higher threshold than B25 for the 300  $\mu\text{s}$  pulse, but has a lower threshold for the 800  $\mu\text{s}$  pulse. (F) The strength–duration activation curves are plotted for the four neurons highlighted in (E). Each pair of neurons (B19/B25 and B4/B21) has curves that cross one another. Because of this crossing, this single stimulating electrode can be used to selectively activate Neuron B4 over B21 and Neuron B25 over B19 at short stimulus pulse-widths and high stimulus currents. The opposite holds true for long stimulus pulse-widths and low currents.

### 3.4.3 Analysis of selectivity with multiple electrodes

We constructed sigmoidal activation curves for the two neurons in Population C for a neuronal culture grown on a high-density micro-electrode array (HD MEA) according to the closed-loop (CL) search routine. The CL search algorithm applied 50 stimuli to each neuron. After each iteration of the search was performed, probability measurements were calculated at each stimulus point, and the sigmoid model of Equation 2.1 was fit to the collected data for each neuron. The transition region of the sigmoid was defined as the stimulus range over which the activation probability transitioned from 0.25 to 0.75. The somata of Neurons C1 and C2 were at distances of 162  $\mu\text{m}$  and 26  $\mu\text{m}$ , respectively, from the center of the electrode array (Figure 3.3A). The activation curves for both neurons of interest were measured using Electrode 1. Neurons C1 and C2 had thresholds of 14.3  $\mu\text{A}$  and 14.2  $\mu\text{A}$ , and the transition regions spanned 0.4  $\mu\text{A}$  and 0.9  $\mu\text{A}$  (Figure 3.3B). Minimal selectivity is achievable for C2 at lower currents and for C1 and higher currents because these curves intersect. Nevertheless, the resulting selectivity is

minimal because the activation curves are nearly overlapping. Next, the sigmoid activation curve measurement was repeated from Electrode 2. Using Electrode 2, C1 and C2 had activation thresholds of 5.1  $\mu\text{A}$  and 9.2  $\mu\text{A}$  and transition regions spanning 0.2  $\mu\text{A}$  and 0.1  $\mu\text{A}$  respectively (Figure 3.3C). The stimulus current range that was selective for C1 was measured as the current distance between the midpoints of the activation curves and spanned 4.1  $\mu\text{A}$ . Finally, when Electrode 3 was used, the activation curves for Neurons C1 and C2 reversed order. C1 and C2 had activation thresholds of 18.8  $\mu\text{A}$  and 11.7  $\mu\text{A}$  (Figure 3.3D). The transition region for C1 was less than 0.2  $\mu\text{A}$  and for C2 was 0.8  $\mu\text{A}$ . The selective current range for C2 spanned 7.1  $\mu\text{A}$ .

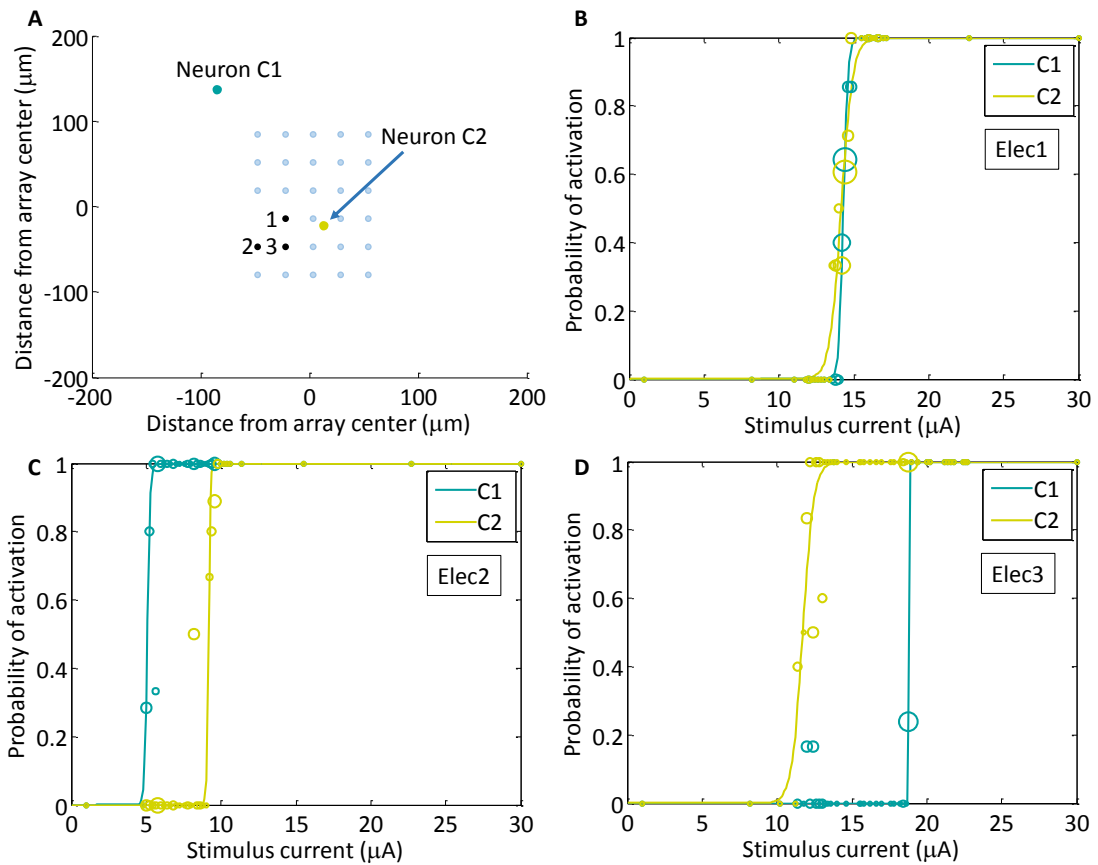


Figure 3.3. (A) The physical locations of the two neurons of interest on the MEA are as shown. The origin is set at the center of the array, and the three stimulating electrodes used (10  $\mu\text{m}$  diameter, 30  $\mu\text{m}$  spacing) are as numbered (black circles). Neurons C1 (dark circle) and C2 (light circle) are located 162  $\mu\text{m}$  and 26  $\mu\text{m}$ , radially, from the center of the array. (B–D) The activation curves found using the CL algorithm for two neurons, C1 (dark shade) and C2 (light shade), are depicted with solid lines. The measurement of the activation probability for each neuron in response to all stimuli delivered are shown with open circles, with the circle radius in proportion to the number of stimuli delivered at that point. (B) The activation curves for both neurons C1 and C2 found using Electrode Elec1. As the curves intersect, slight selectivity is achievable for C2 at lower currents and for C1 and higher currents; the selectivity is minimal however due to the small difference between curves. (C) The activation curves for both neurons C1 and C2 found using Electrode Elec2, and (D), the activation curves for both neurons C1 and C2 found using Electrode Elec3. Using either Elec1 or Elec2, good selectivity is achievable for neuron C1 over C2 (C, Elec2) or for neuron C2 over C1 (D, Elec3) due to the large difference in activation curves.

### **3.5 Discussion**

Effective waveform design is integral in improving the selectivity and control of neuronal stimulation systems. Altering the stimulus amplitude (current or voltage) is the most frequently used method for waveform modification; this approach is inherently limited in its selectivity as it typically activates many axons within a region (Nowak & Bullier 1998; Tehovnik et al. 2006). Control of the stimulus amplitude is an essential element but is insufficient for differential activation of neurons within a population using a single electrode. Expanding the one-dimensional approach to multidimensional waveforms applied to multiple neurons facilitates the development of targeted stimulation technologies.

#### 3.5.1 Adaptive targeted searches can find even a small window for selectivity

We have shown that even for similar neuronal activation curves, when the apparent selectivity achievable was minimal, such as between A5 and A8 (Figure 3.1D), it remained non-zero. The CL routine was used to measure each neuronal activation curve, however, it could be adapted to target specific selectivity regions between neuronal pairs. By searching for the maximum of the difference of sigmoids, the CL search routine could be used to find the 13.8  $\mu\text{A}$  stimulus current, which would enable the targeting of Neuron A8. The use of an optimized CL routine for searching the multi-parameter space additionally enhanced the ability to find stimuli enabling the reversal of selectivity between neurons (Figure 3.1B). Additionally, the CL routine could be optimized for many other stimulation goals, including finding the most selective stimulus range to divide the population or stimulate two neurons and not another. A combination of the two techniques, using closed-loop searches to find the optimal stimulus, and then searching in

a multi-parameter stimulus space, we can quickly locate the relevant stimulus waveform subspace. An array of stimulating electrodes could be used to further increase selectivity. The opportunity for reversing the activation curves between a pair of neurons expands when increasing the parameter space to include spatially distributed electrodes.

Other metrics could be used to describe the selectivity between neurons, depending on the end goal. As an example, if the target metric is to first minimize the activation of A5, the previous definition of selectivity, which finds the range over which the difference in the activation probabilities is greater than 0.5, could be sacrificed to ensure with higher probability that A5 did not activate. A lower stimulus current could be delivered in the range of 13.4 – 13.6  $\mu\text{A}$ , where although there is a limited probability of activating A8, the probability of activating A5 is significantly lower. The selectivity may also be defined as the integral of the area between the activation curves.

### 3.5.2 Probing of the population response is essential for targeted stimulation

From Figure 3.2B, it can be inferred that there is no apparent relationship between soma location and activation threshold. Numerous modeling and experimental studies focus on the activation of neurons and their elements in response to electrical stimulation. These studies show that axons are most susceptible to stimulation, which can explain the vast spatial distribution of activated neuronal somata in response to an extracellular stimulus (Nowak & Bullier 1998; Tehovnik et al. 2006; Ranck 1975; Histed et al. 2009; Rattay 1999). Knowledge of the location of neuronal somata within a tissue volume is insufficient to determine the threshold at which a particular population of neurons will activate. Due to the complex spatial organization of neuronal cultures and networks, implanted electrodes or planar electrode arrays will have access to many different

locations along many different axons. Additionally, electrode locations and neuronal populations are unique: what may work in one neuronal environment may fail in another environment. The natural variability in electrode locations and neuronal populations demands that for each application the stimulus-evoked response in the reachable populations is rapidly probed and characterized. The inability to precisely locate an electrode array in a neuronal culture requires that a BCI be functionally evaluated via targeted stimulation. If a functional map may be constructed, the practical need for precise spatial mapping of electrodes and axons is unnecessary.

In the experimental application, there is variability in the cell numbers, absolute cell position, and location of the cells relative to the micro-electrode arrays (MEA). This high variability will similarly apply to clinical applications, given natural patient-to-patient variability. It must therefore be assumed that each experimental or clinical application will have a unique response. It is the uniqueness of each application that requires that the accessible neuronal population be learned, and this accessible population be probed for response in the stimulus parameter space. Feedback is required in this system because, as is shown in this work and others (Histed et al. 2009), there is no apparent correlation between cell distance from the electrode and stimulus response. In our experimental system, we use widefield optical imaging as a measurement tool; it is likely that in a clinical application that non-optical methods will be used to record evoked activity. The findings in this work are independent of measurement method, and so also apply to non-optical recording methods. Ultimately, any stimulation routine needs to implement a technique to probe and characterize the population response in order to

design targeted stimuli that will enable more sophisticated control of the evoked response.

### 3.5.3 Using an array of spatially distributed electrodes

In a repetition of the multi-electrode experiment from Figure 3.3, we characterized neuronal activation for two neurons using seven stimulating electrodes. Six showed activation preference for one neuron, while the other one allowed access to selectively stimulate the second neuron. There is no guarantee that a pair of adjacent electrodes will enable selectivity between a pair of neurons, which emphasizes the need for a method that utilizes the full extent of the accessible electrodes within the array for finding the right stimulating electrode for a particular goal. More specifically, a fast closed-loop search routine is required because it is unknown, a priori, which electrodes will provide access to which neurons.

Based on the activation data in Figure 3.3, we hypothesize that the axon of C1 is directed downward and the axon of C2 is directed to the left (oriented as shown on Figure 3.3A). Due to the near identical activation thresholds for these two neurons from the stimulation location at Electrode Elec1, it is possible that both axons traverse the array such that the most excitable element passes equidistant from Elec1. The axon of Neuron C1 is then likely positioned closer to stimulating Electrode Elec2 and farther from Electrode Elec1, with respect to the position of the axon of Neuron C2. Conversely, the axon of Neuron C2 is likely closer to stimulating Electrode Elec1 and more distant from Electrode Elec2. The observations of this experiment underscore that an array of electrodes be used in selective stimulation so that multiple electrodes are available for stimulation and may be selected based on the stimulation goals. Access to multiple

electrode locations, with respect to the underlying tissue, provides greater access to selectivity between neurons.

#### 3.5.4 As the parameter space increases, CL systems behave more similarly to OL systems

There is a constraint on the number of stimulus trials that may be presented, due to the need for efficient alleviation of symptoms, in a clinical environment, and due to photobleaching and phototoxicity, in the experimental setting presented here. For this reason, if 30 stimuli per neuron are required and only the stimulus current or pulse-width is of experimental interest, a CL routine is preferred for up to approximately 20 neurons. The number of neurons for which this CL method is preferable quickly decreases to only a handful when the experimental interest expands to the 2-D strength–duration space. An OL stimulation approach becomes superior when a large population of neurons must be described, as in the case of the 30 neuron experiments of this work. It is also notable that even with a CL approach, for a sufficient number of neurons (ca. 10) the aggregation of all the CL searches becomes similar to an OL approach because the stimuli cover a similar area. The CL routine has a distinct advantage when the activation curves are close in proximity; in these cases, the stimuli delivered to uncover one activation curve is simultaneously increasing the resolution of the activation probability measurement for another neuron. As the stimulus space increases with more neurons, more waveform parameters, or more electrodes, the set of CL searches will eventually tend toward an OL sweep. Despite this tendency the CL approach reduces inefficiencies in the OL routine, including eliminating the delivery of stimuli at the lowest currents or shortest pulse-widths. Further improvements in efficiency can be made to make the CL routine more

adaptive by allowing the CL routine to terminate early if neuronal activation curves are similar to one another, reducing the number of stimuli necessary for subsequent neurons.

### **3.6 Conclusions**

Selectivity between two neurons is achievable using a single electrode. For a single stimulus parameter search, in either current or pulse-width, even for neurons with very similar activation transition regions, a CL technique can find the stimulus waveform that is able to selectively activate the lower threshold neuron. This selectivity is assured, however, only for the lower threshold neuron. For this reason, it is important that the full stimulus waveform space be exploited to differentially target neurons. Selectivity is achievable in many cases between pairs of neurons using only a single stimulating electrode, but it is limited to those pairs in which the strength–duration curves cross one another. The organization of the culture with respect to the stimulating electrode can be functionally measured in real-time to assess the achievable selectivity. Additionally, it is essential that the multi-parameter activation space be initially measured so that the delivered stimuli can then be optimized for improving the efficiency with which a population activation probability is measured. The techniques developed here can be used to improve the selectivity of a stimulus waveform by simultaneously stimulating on multiple electrodes.

In the next chapter, we explore the application of a closed-loop search routine, in experimental and simulation studies, to optimize stimulus parameters to find regions within the stimulus waveform space that can be utilized to selectively stimulate subpopulations of neurons.

### **3.7 Supplemental data relating to Chapter 3**

#### 3.7.1 Experimentally building strength-duration curves

We executed an experiment comprising 9 closed-loop searches in the vertical, variable-current stimulus space and 9 in the horizontal, variable-pulse-width space. The midpoints of each sigmoid activation curve for the two sets of 9 CL searches were plotted in the strength-duration space, and each set of points was fit separately to Equation 3.2. The two resulting strength-duration curves were overlaid to demonstrate the agreement between the outputs from the two search techniques. We first validated the shape of the strength-duration curve. Although typical stimuli lie in the middle range of stimulus durations and currents, it is important to understand neuronal activation along the entirety of the SD curve because it could provide stimulus waveform regions where neurons activate differentially.

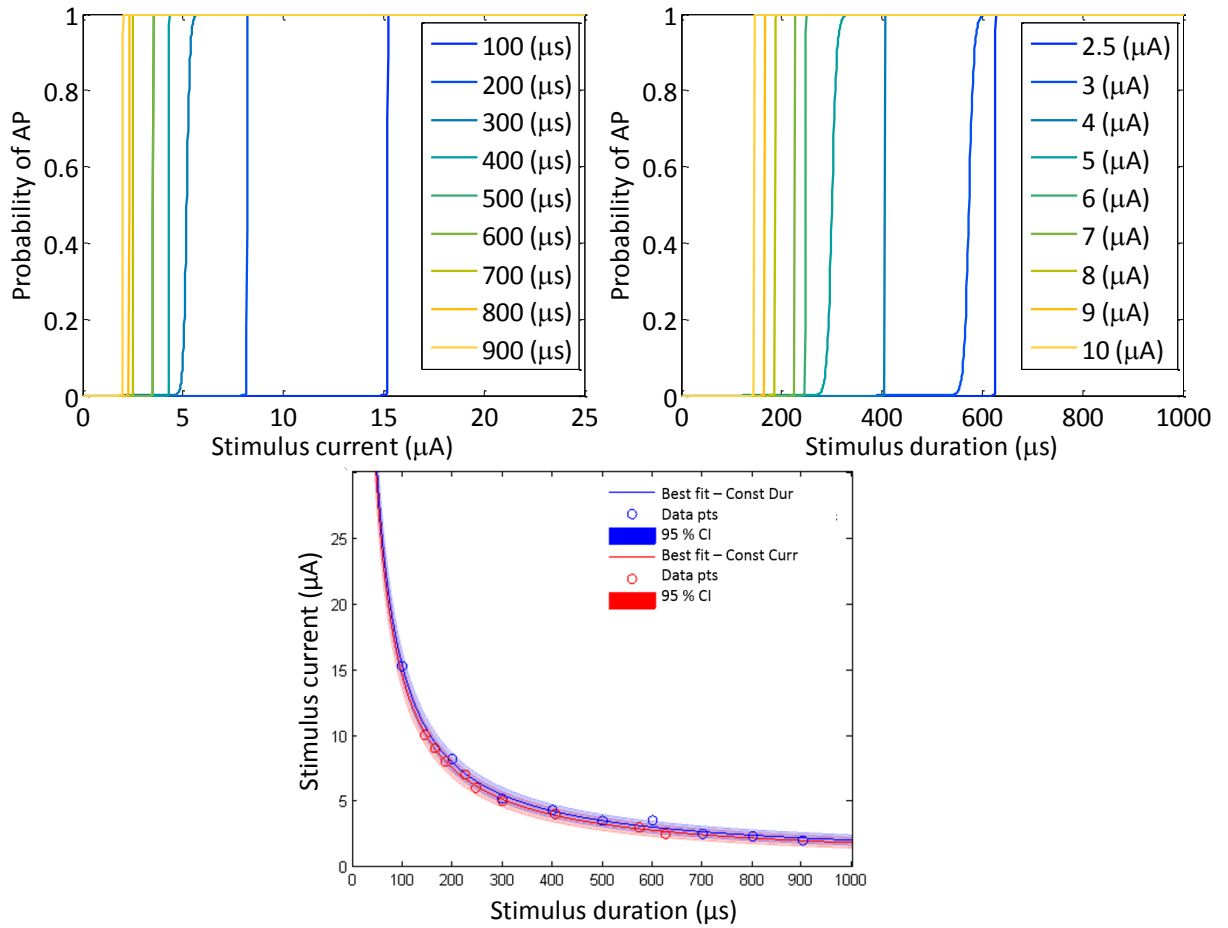


Figure 3.4. Top row: Two sets of shifting sigmoids produced from fixed-pulse-width, variable-current searches (left) and fixed-current, variable-pulse-width searches (right). Bottom panel: The  $P=0.5$  thresholds from each set of the shifting sigmoids in the top panel were used as inputs to build the strength–duration curve, two ways. The blue shade was built using the constant duration sigmoids (top, left), and the red shade was built using the constant current sigmoids (to, right). Both strength–duration curves are in good agreement.

### 3.7.2 Investigation into the stimulus-evoked fluorescence

There is always a tradeoff between imaging speed and spatial resolution. We have chosen to increase the imaging speed at the cost of spatial resolution. We found that we had some interesting fluorescence traces through time, which could be further investigated. There is a chance that there are axons overlapping some of the cell bodies, which could be causing a double fluorescence. We're not sure, but the point of the paper was to look at the somata for analysis. If there's something more on top of that, then it's worth future exploration.

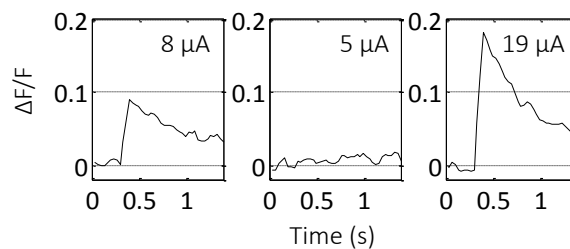


Figure 3.5. Example time traces of the evoked fluorescence are shown for neuron N5 from the previous figure. The stimulus was presented at 0.3 seconds into the recording. All three traces are for 300  $\mu s$  stimulus durations. In response to the 8  $\mu A$  stimulus, the  $\Delta F/F$  lies along the mid-level from the previous figure. No  $\Delta F/F$  is observed in response to the 5  $\mu A$  pulse and a large  $\Delta F/F$  is observed for the 19  $\mu A$  pulse. Although other duration pulses were presented in between these pulses, the three depicted here for 300  $\mu s$  durations were presented in order.

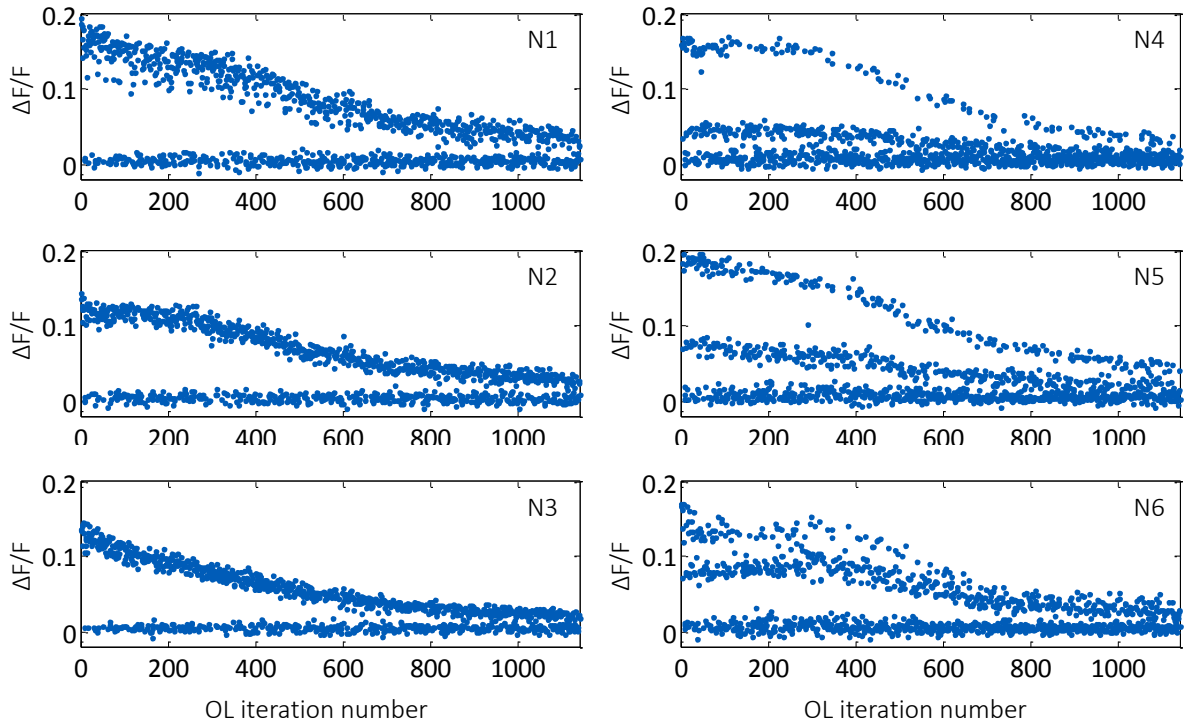


Figure 3.6. The progression of  $\Delta F/F$ , or the evoked change in fluorescence over the baseline, is depicted for six neurons across 1140 stimulus iterations. These stimuli were randomly presented and range from currents of  $2 \mu\text{A}$  to  $20 \mu\text{A}$  in  $1 \mu\text{A}$  steps and durations of  $300 \mu\text{s}$  to  $800 \mu\text{s}$  in  $100 \mu\text{s}$  steps. In the left column, the neurons appear to activate in a single mode; either there was no change in fluorescence, which indicates that no action potential occurred, or there was a change in fluorescence, indicating that an action potential was evoked. For the top two neurons, the  $\Delta F/F$  is relatively flat for the first 300 stimulus iterations and it then begins to decay, due to photobleaching. For the bottom neuron, the signal decays immediately from the start. In right column, the neurons appear to activate in two distinct modes. For each neuron, the larger  $\Delta F/F$  level occurs at higher currents and longer durations. The mid-level  $\Delta F/F$  occurs at stimulus currents, which are near the activation threshold for a given stimulus duration. It is important to note that the difference in  $\Delta F/F$  levels is variable across neurons. For neuron N4, the highest  $\Delta F/F$  level is greater than two times the mid-level  $\Delta F/F$ ; for the neuron N5, it is approximately twice as large; and for neuron N6, the top level is less than twice as large as the mid-level  $\Delta F/F$ .

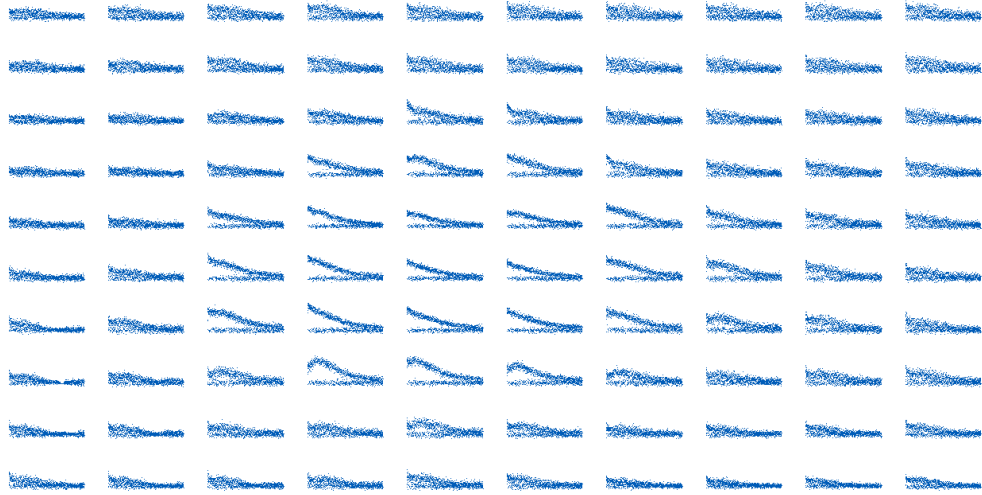


Figure 3.7. For the N1 neuron previously shown, the progression of  $\Delta F/F$  is plotted for each individual pixel within a 12 X 12 pixel grid around the soma. Only one “mode” is observable.



Figure 3.8. For the N6 neuron previously shown, the progression of  $\Delta F/F$  is plotted for each individual pixel within a 12 X 12 pixel grid around the soma.

### 3.7.3 Repetition of the HD multi-electrode searches

You can see the third fluorescence level show up around half way down the fifth column. This experiment was repeated with a different HD MEA culture, examining two different neurons. The somata of Neurons Y1 and Y2 were radially located 55  $\mu\text{m}$  and 72  $\mu\text{m}$ , respectively, from the center of the electrode array. Seven different stimulating electrodes were used to activate the two neurons and the resulting sigmoid activation curves were measured. We then determined activation thresholds (the midpoint of the sigmoid) and span of the transition region from probability of 0.25 to 0.75 (Table 3.1). We found that only Electrode 7 could be used to selectively activate Neuron Y1. There was a small difference in the activation curves using Electrode 3 that was preferential for Y1. For the other five electrodes, Neuron Y2 could be selectively activated over Neuron Y1.

This experiment underscores the importance of utilizing the full extent of the accessible electrodes within the array for finding the right stimulating electrode for a particular goal. Although we characterized the neuronal activation at seven electrodes, only one allowed access to selectively stimulate Neuron Y1. There is no guarantee that a pair of adjacent electrodes will enable selectivity between a pair of neurons.

**Table 3.1. Characterization of activation curves for Neurons Y1 and Y2 according to the threshold and the span of the transition region.**

	Elec1	Elec2	Elec3	Elec4	Elec5	Elec6	Elec7
Y1 threshold ( $\mu\text{A}$ )	11.0	17.2	9.7	12.4	9.2	13.2	8.6
Y1 span ( $\mu\text{A}$ )	0.5	< 0.2	0.4	2.2	< 0.2	< 0.2	0.3
Y2 threshold ( $\mu\text{A}$ )	8.6	8.2	9.9	7.1	7.4	7.5	10.7
Y2 span ( $\mu\text{A}$ )	< 0.2	0.2	0.3	0.3	< 0.2	0.4	1.4

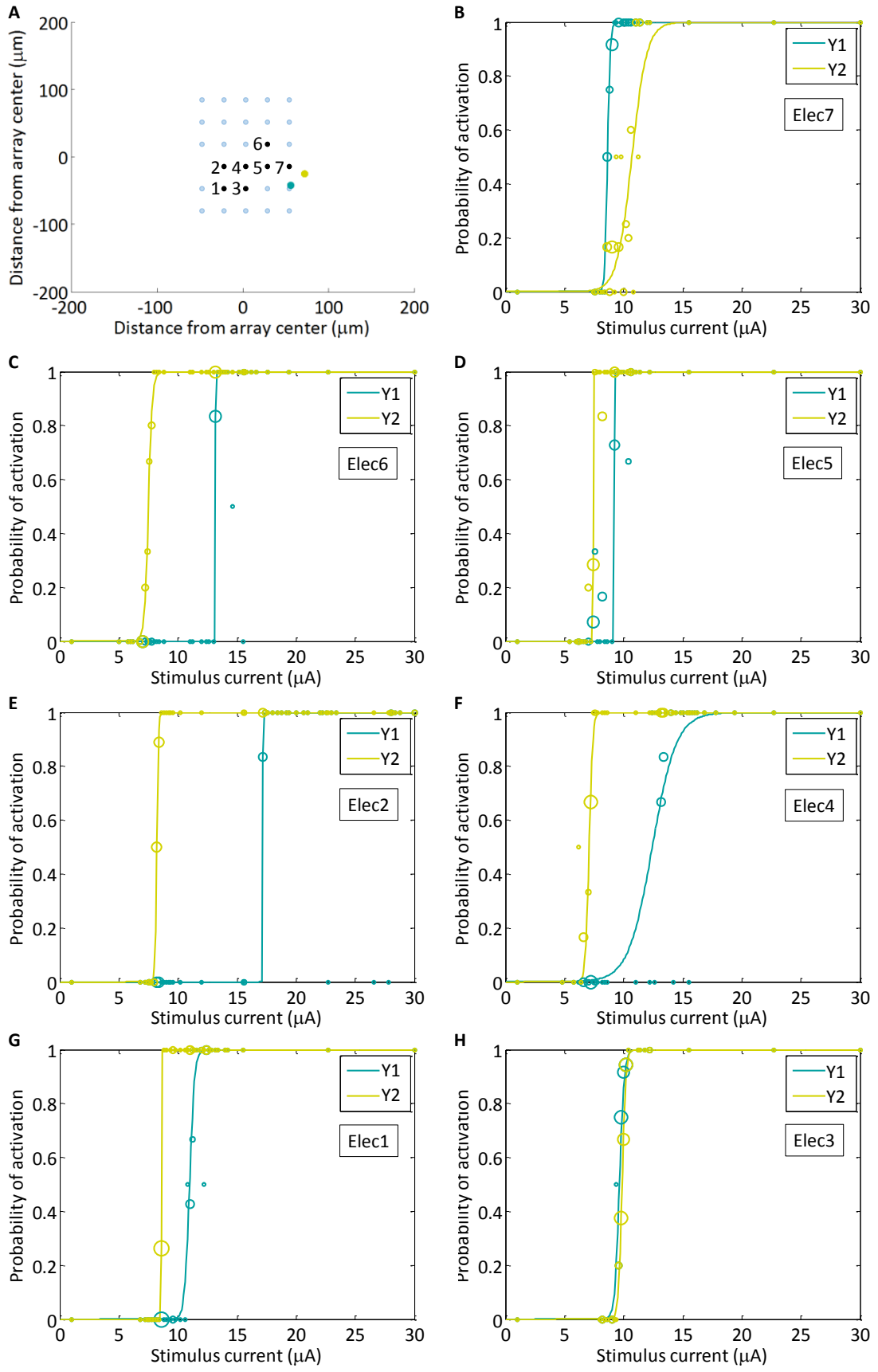


Figure 3.9. (A) The physical location of the two neurons of interest on the MEA are as shown. The center of the array is defined as (0,0), and the seven stimulating electrodes (10  $\mu\text{m}$  diameter, 30  $\mu\text{m}$  spacing) are as numbered (black circles). Neurons Y1 (dark circle) and Y2 (light circle) are located 55  $\mu\text{m}$  and 72  $\mu\text{m}$ , radially, from the center of the array. The triangle denotes that the electrode used as ground. (B-H) The activation curves found using the CL algorithm for two neurons, Y1 (dark shade) and Y2 (light shade), are depicted with solid lines. The measurement of the activation probability for each neuron in response to all stimuli delivered is shown with open circles, with the circle radius proportional to the number of stimuli delivered (taken as an average of all responses at that stimulus current).

# CHAPTER 4

## OPTIMIZATION OF CLOSED-LOOP SEARCHES FOR TARGETED STIMULATION OF MULTIPLE NEURONS

### 4.1 Abstract

Better electrical stimulation methods are needed to differentially activate neuronal populations to improve the efficacy of clinical devices such as sensory or cortical prostheses. Improving stimulus specificity will facilitate targeted neuronal activation to convey biologically realistic percepts. In order to deliver more complex stimuli to a neuronal population, new techniques must be developed that will enable a single electrode to activate subpopulations of neurons. However, determining the stimulus needed to evoke targeted neuronal activity is challenging. To find the most selective waveform for a particular population, we apply an optimization-based search routine, Powell's conjugate direction method, to systematically search the stimulus waveform space. This routine utilizes a 1-D sigmoid activation model and 2-D strength–duration curve to measure neuronal activation throughout the stimulus waveform space. We implement our search routine in both an experimental study and a simulation study to characterize potential stimulus-evoked populations and the associated selective stimulus

---

This manuscript is being prepared for publication by:  
Michelle L. Kuykendal, Stephen P. DeWeerth, Martha A. Grover\*  
\*Corresponding author e-mail address: martha.grover@chbe.gatech.edu

waveform spaces. We found that for a population of five neurons, there were seven distinct sub-populations that could be activated. The stimulus waveform space and evoked neuronal activation curves will vary with each new combination of neuronal culture and electrode array, yielding a unique selectivity space. The method presented here can be used to systematically uncover the selectivity space, focusing experiments in regions with the desired activation pattern.

## **4.2 Introduction**

Improving the selectivity of electrical stimuli for targeted neuronal activation is a critical step in the development of advanced neural prostheses. The prosthetics field is expansive, including peripheral and cortical prostheses, with applications including restoration of lost motor and sensory function in artificial limbs; cochlear prostheses for restoring audition (Loeb et al. 1983; Clark 2013); retinal prostheses for restoring vision (Fried et al. 2006; Sekirnjak et al. 2006; Jepson et al. 2011); and cortical prostheses for inducing sensory percepts and reading motor intent directly from the brain (Ryu & Shenoy 2013; Hochberg et al. 2006; Lebedev et al. 2011; Kipke et al. 2008; Guggenmos et al. 2013; Carmena et al. 2003; Fitzsimmons et al. 2007). An effective prosthesis must encode a variety of unique stimuli. For example, the hand senses surface texture, heat, pressure, and directionality of contact, all of which are encoded uniquely. If distinctive messages could be conveyed by activating various subpopulations of the accessible neuronal population, then there is a vast potential neuronal activation space available for exploitation to extend the repertoire of stimulus messages. Studies have shown that by using cortical electrodes, patients are able to detect the activation of even a single neuron

(Parker & Newsome 1998), suggesting even the smallest differences in the activated population of neurons are detectable.

Our goal is to develop a technique that facilitates the measurement of all accessible neuronal subpopulations and finds the waveforms most selective for each target group. Exploiting the spatial location and natural variation in stimulus-evoked activation probabilities assists in the preferential selection of neuronal populations. The activation probability, in response to a rectangular current-pulse, is described by a two-parameter strength–duration curve. Although a neuron will typically activate with greater probability as charge is increased, some neurons activate preferentially to a long pulse-width, while others respond preferentially to a short-pulse-width, high-amplitude pulse, as was described in Chapter 2. For any given pair of accessible neurons, there is typically a region in the stimulus waveform space where the probability of activating one neuron is greater than activating another.

Closed-loop (CL) methods are well-suited for fast searches through a large input parameter space to find an optimal stimulus waveform owing to their online feedback of measured responses for determining subsequent stimuli (Arsiero et al. 2007; Benda et al. 2007; Zrenner et al. 2010; DiMattina & Zhang 2013). Closed-loop techniques are advantageous over open-loop techniques in a multi-parameter space because CL techniques can learn from past data to rapidly locate the stimulus space that provides the most differential neuronal activation. Lewi and colleagues (2009) showed that optimization of experiments, by delivering stimuli that are most informative to uncover model parameters, can greatly improve the speed of searches in high-dimension input spaces. A model-based search routine can guide the search and mitigate the inherent

noise in the stimulus-evoked neuronal response. By utilizing CL search methods, Brocker and colleagues (2013) developed non-regular temporal stimulation patterns for DBS that improve stimulus efficacy while reducing device power requirements using a genetic algorithm. Additionally, Pais-Vieira and colleagues (2013) implemented a brain-to-brain interface in rats that altered the stimulus waveform in one cortical prosthesis based on the actions of a separate rat, and the pair of rats learned to change their behavior to benefit them both. These developments in science and technology, which were successful due to the adoption of closed-loop methodologies, are not limited to neuroscience. For example, McMullen and Jensen (2010) developed a model-based multi-dimensional optimization of a microreactor that monitors a chemical reaction where no a priori information is available on the reaction parameters. By utilizing real-time feedback of an estimate of the system state, CL techniques can improve on current technologies by increasing search efficiency to find optimal input parameters.

In this work, we have implemented a non-gradient search technique, Powell's conjugate direction method, to traverse the input parameter space. The difference in strength-duration curves among neurons creates regions in the stimulus waveform space, which offer new access to stimulus selectivity. Adopting Powell's method for optimizing stimulus parameters allows for multiple parameters to be probed simultaneously in order to find the global maximum of selectivity. Deterministic optimization methods, such as Powell's method, generally start with an initial guess, and then iteratively improve on the solution according to a directional search algorithm. Our application of Powell's method allows us to rapidly search through multiple variables to maximize the difference between activation curves. Resistance to noise is a design priority, given that neuronal

responses are inherently noisy, and Powell's method is more resistant to noise than gradient approaches since taking the derivative of noisy data is difficult.

### **4.3 Methods**

We designed a closed-loop system, as was described in Chapter 2, for optimizing stimulus pulse parameters based on a model of neuronal activation and an experimental goal. The system comprises hardware and software components that select and deliver stimuli designed to evoke a particular neuronal response. Each measured response is used to refine the model and the next stimulus is automatically chosen. The modular design, which separates data collection from both data analysis and decision-making, enables the user to select a model function and a variety of experimental goals in order to investigate a variety of questions. Each section of the system is described in more detail below.

#### 4.3.1 Cortical cell culture

Embryonic Day 18 (E18) rat cortices were enzymatically and mechanically dissociated according to (Potter & DeMarse, 2001). Cortices were digested with trypsin (0.25% w/EDTA) for 10-12 minutes, strained through a 40  $\mu\text{m}$  cell strainer to remove clumps and centrifuged to remove cellular debris. Neurons were re-suspended in culture medium [90 mL Dulbecco's Modified Eagle's Medium (Irvine Scientific 9024), 10 mL horse serum (Life Technologies 16050-122), 250  $\mu\text{L}$  GlutaMAX (200 mM; Life Technologies 35050-061), 1 mL sodium pyruvate (100 mM; Life Technologies 11360-070) and insulin (Sigma-Aldrich I5500; final concentration 2.5  $\mu\text{g}/\text{mL}$ )] and diluted to 3000 cells/ $\mu\text{L}$ . Microelectrode arrays (MEAs; Multi Channel Systems 60HDMEA30/10iR-ITO) were sterilized by soaking in 70% ethanol for 15 minutes followed by UV exposure overnight.

MEAs were treated with polyethylenimine to hydrophilize the surface, followed by three water washes and 30 minutes of drying. Laminin (10  $\mu$ L; 0.02 mg/mL; Sigma-Aldrich L2020) was applied to the MEA for 20 minutes, half of the volume was removed, and 30,000 neurons were plated into the remaining laminin atop the MEA. Cultures were protected using gas-permeable lids (Potter & DeMarse, 2001) and incubated at 35°C in 5% carbon dioxide and 95% relative humidity. The culture medium was fully replaced on the first day in vitro (DIV) and then once every four DIV afterwards.



Figure 4.1. Phase contrast micrograph of the high-density electrode array, on which healthy neurons are growing. The HD array comprises two arrays of 6 X 5 electrodes (10  $\mu$ m diameter, 30  $\mu$ m spacing). The distance from center-to-center of the two electrode arrays is 200  $\mu$ m. The left half of the array was used in these experiments.

### 4.3.2 Electrical stimulation

Extracellular electrical stimuli were used to elicit neuronal activity. Stimuli were delivered to the neurons using a STG-2004 stimulator and MEA-1060-Up-BC amplifier (Multi Channel Systems). MATLAB (Natick, MA) was used to control all hardware devices, which were synchronized by TTL pulses sent from the stimulator at the beginning of each stimulation loop. In all stimulus iterations, a trigger pulse was first delivered to the camera to begin recording so that background fluorescence levels could be measured. An enable pulse was then delivered to the amplifier, which connected the stimulus channel to a pre-programmed electrode. A single cathodic square current pulse was then delivered to a single electrode centered under the camera field of view. Cathodic pulses were chosen because they have been shown to be most effective at evoking a neuronal response (Wagenaar, 2004).

### 4.3.3 Optical imaging

As is described in Chapter 2, automated optical imaging was used to measure the stimulus-evoked neuronal response. All preparation procedures were conducted in the dark to lengthen experiments by minimizing photobleaching and phototoxicity. First, culture media was removed and neurons were loaded with Fluo-5F AM (Life Technologies F-14222), a calcium-sensitive fluorescent dye with relatively low binding affinity (2.3  $\mu\text{M}$ ) at a concentration of 9.1  $\mu\text{M}$  in in DMSO (Sigma-Aldrich D2650), Pluronic F-127 (Life Technologies P3000MP) and artificial cerebral spinal fluid (aCSF; 126 mM NaCl, 3 mM KCl, 1 mM  $\text{NaH}_2\text{PO}_4$ , 1.5 mM  $\text{MgSO}_4$ , 2 mM  $\text{CaCl}_2$ , 25 mM D-glucose) with 15 mM HEPES buffer for 30 minutes at ambient 25°C and atmospheric carbon dioxide. Before imaging, cultures were rinsed two times with aCSF to remove

free dye. Cultures were bathed in a mixture of synaptic blockers in aCSF (15 mM HEPES buffer). This included (2R)-amino-5-phosphonopentanoate (AP5; 50  $\mu$ M; Sigma-Aldrich A5282), a NMDA receptor antagonist; bicuculline methiodide (BMI; 20  $\mu$ M; Sigma-Aldrich 14343), a GABAA receptor antagonist; and 6-cyano-7-nitroquinoxaline-2,3-dione (CNQX; 20  $\mu$ M; Sigma-Aldrich C239), an AMPA receptor antagonist. This cocktail was shown to suppress neuronal communication (Bakkum et al. 2008) to ensure that the recorded neuronal activity was directly evoked by the stimulus. The culture was then kept in a heated amplifier (Multichannel systems TC02, 37C) within the imaging chamber. The stage position was calibrated with respect to the desired field of view (FOV) using the electrodes as fiducial markers. A MATLAB GUI was used to automatically position the FOV over the stimulation electrode. During an experiment neurons were illuminated using a light-emitting diode (LED; center wavelength of 500 nm) and LED current source (TLCC-01-Triple LED, relative power = 30; Prizmatix) through a 20X water-immersion objective, NA = 1.0, and a fluorescein isothiocyanate (FITC) filter cube. Evoked activity was optically recorded using a high-speed electron multiplication CCD camera (30 fps; QuantEM 512S; Photometrics), which has a 512 X 512 pixel grid covering a 400  $\mu$ m X 400  $\mu$ m area. After an experiment concluded, three aCSF washouts were performed at three minute intervals, the culture media was replaced, and the culture was returned to the incubator.

#### 4.3.4 Detecting action potentials

For each neuron, the measured intensity of 16 X 16 pixels (12.5  $\mu$ m X 12.5  $\mu$ m) surrounding the soma center was spatially averaged. The relative change in fluorescence,  $\Delta F/F$ , was calculated by subtracting the baseline (an average of four pre-stimulus frames)

from the peak (an average of four post-stimulus frames) and dividing the difference by the baseline. The standard deviation of the baseline frames was calculated in initial stimulus iterations and used as a measure of the fluorescence noise level. An action potential was said to have occurred if the  $\Delta F/F$  was greater than three times the noise level within a particular neuron. The average decay time constant of a stimulus-evoked fluorescence curve was 1.5 seconds. Because of this relatively slow signal decay, the experimental loop time was chosen to be 4.5 seconds, which is three decay constants long, to give the signal sufficient time to return to baseline.

#### 4.3.5 The sigmoid activation model

A saturating nonlinear curve was used to fit to the neuronal probability of firing an action potential in response to a varying stimulus current or pulse width. Specifically, a two-parameter sigmoid (Equation 4.1) was used to describe this 1-D activation curve for cathodic square-pulse stimuli.

$$p = \frac{1}{1 + b_2 e^{-(x-b_1)}} \quad \text{Equation 4.1}$$

The sigmoid model provides an approximation for the stimulus needed to activate a particular neuron with any given probability. The input activation parameter,  $x$ , is either the stimulus current or pulse width, and the output is the probability,  $p$ , of a neuron to fire an action potential. The two parameters describing the sigmoid are  $b_1$ , the midpoint of the sigmoid, and  $b_2$ , the slope of the curve at the midpoint. Because the sigmoid describes a probability of activation, it spans from zero to one.

#### 4.3.6 The strength–duration activation model

Neuronal activation in the 2-D strength–duration waveform space was described according to Lapicque (1907, Equation 4.2).

$$I = r \left( 1 + \frac{c}{PW} \right) \quad \text{Equation 4.2}$$

The stimulus pulse width, PW, is the input; the stimulus current, I, is the output, and the two model parameters are the rheobase, r, and the chronaxie, c. The rheobase describes the stimulus current below which a stimulus with infinite pulse width will not evoke an action potential, and the chronaxie describes the stimulus pulse width that corresponds to a stimulus current of twice the rheobase. A strength–duration curve can be defined for a particular activation probability, such that there are a set of non-intersecting probability strength–duration curves spanning the two-parameter waveform space.

#### 4.3.7 Cross sections through the strength–duration waveform space for simulation studies

When a one dimensional cross section is taken through the SD waveform space in either the horizontal, vertical or positively-sloped diagonal direction, the activation probability is modeled by a sigmoidal activation curve according to Equation 4.1. The sigmoidal curve is determined by fitting Equation 4.1 to the points where the cross section intersects with the P=0.25, 0.5 and 0.75 SD curves. However, a cross section with negative slope in the SD waveform space comprises a set of either zero, one or two sigmoidal activation curves depending on the number of times that the cross section intersects with the probabilistic SD curves (Figure 4.2A). If all values of the input parameters lying along the cross section fall below the P=0.25 probability line, then the activation model is zero for the line defining the entire cross section (Figure 4.2B). If the cross section intersects

once with the set of probability SD curves, then the activation model comprises a single sigmoid. The sigmoidal curve is, again, determined by fitting Equation 4.1 to the points where the cross section intersects with the  $P=0.25$ ,  $0.5$  and  $0.75$  SD curves (Figure 4.2C). Lastly, if the cross section intersects with the SD curves twice, once along the left-hand portion of the SD curves and once along the right-hand portion, then the activation model for the cross section comprises the addition of two sigmoids (Figure 4.2D). Each sigmoidal model is built as was described for the previous case, using Equation 4.1.

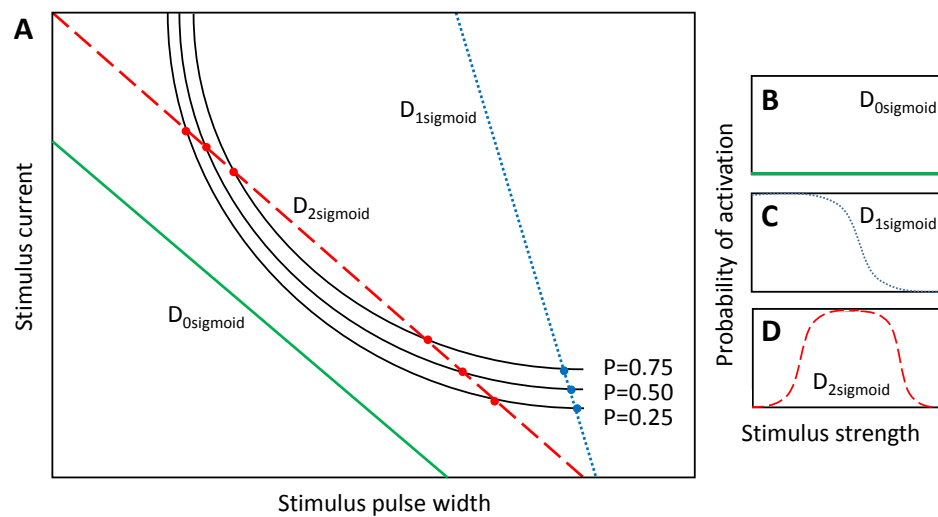


Figure 4.2. (A) Cartoon depiction of negatively-sloped cross sections through the strength–duration waveform space. (B) The solid line,  $D_{0\text{sigmoid}}$ , from (A) falls below the  $P=0.25$  probability curve producing a constant zero magnitude activation curve. (C) The dotted line,  $D_{1\text{sigmoid}}$ , from (A) intersects with the set of probability strength–duration curves only once, which is modeled with a single sigmoidal activation curve. (D) The dashed line,  $D_{2\text{sigmoid}}$ , from (A) intersects with the set of probability strength–duration curves twice, and the resulting activation curve is modeled by the addition of two sigmoids.

#### 4.3.8 Building one dimensional sigmoidal activation curves

Sigmoidal activation curves are built to model neuronal activation along a one dimensional cross section through the two-dimensional strength–duration waveform space. The closed-loop model-building search procedure begins with five open-loop stimuli that divided the stimulation space evenly and bracket the activation region. After the fifth iteration, the sigmoidal model is analytically linearized, and a linear least-squares fit of the midpoint and slope parameters is performed. All measured stimulus-evoked responses are equally weighted. The output of the linear regression is used as an initial guess for a nonlinear least squares curve fit using the MATLAB Optimization Toolbox, which generates the best-fit sigmoid parameters. The measured response is a binomial distribution describing the evoked action potential probability, which is calculated as a mean of all responses at a particular stimulus value. In order to gain information about the midpoint and slope, a probability goal is randomly chosen from the set of [0.25, 0.50, 0.75], which spans the transition region of the sigmoid. The stimulus that is predicted to produce the target firing probability is calculated analytically by inverting the sigmoid model. The probability goals span the linear portion of the transition region of the sigmoid curve, and an accurate measurement of the stimulus values at these probabilities provides an estimate of the slope of the curve at the midpoint. In the case that the next stimulus chosen was the same as the previously delivered stimulus, a uniformly random jitter was added to the stimulus up to 20% in either direction so that more data are collected over the full range of the transition region of the activation curve. After every stimulus iteration, the linear and nonlinear curve-fits were run to update the model. For each sigmoidal activation curve, a total of 50 stimuli were presented.

#### 4.3.9 Powell's conjugate direction method search routine

Powell's conjugate direction method is a non-gradient search routine for finding the maximum (or minimum) of a function. It is especially applicable to multi-dimensional searches of noisy systems since its calculations do not rely upon derivatives, which are sensitive to noise. Powell's method specifically dictates the direction of each search iteration through the input parameter space, which in this study is the strength–duration stimulus space, comprising a stimulus current and pulse-width for a rectangular pulse. An illustration of the generic search routine is depicted in Figure 4.3, which consists of a series of line searches through the input space. Each line search comprises one execution of the methods described above in which the 1-D sigmoidal activation curves are constructed for each of the neurons within the population. Along each line search, an objective function is evaluated. For this study, the objective function,  $f$ , measures the differences in sigmoidal activation curves according to Equation 4.3 such that the sum of off-target neuronal activation probabilities, for  $m$  neurons, is subtracted from the sum of target neuronal activation probabilities, for  $n$  neurons.

$$f = \sum_{i=1}^n P_i - \sum_{j=1}^m P_j$$

Equation 4.3

The sigmoidal activation curves for the target population are summed such that as each target neuron activates, and the probability of firing transitions from zero to one, the objective function increases by one. As the off-target neurons begin to activate, and their probabilities of firing transition from zero to one, the objective function decreases by one. Therefore, along each line search, once all sigmoidal activation curves have been

estimated, the on- and off-target activation curves are summed, and the maximum of the objective function is found.

The Powell search routine begins with an arbitrary point, PT0, chosen from the input space. The first search direction (D1) is a vertical search crossing through PT0, which spans the extent of the space. For this implementation, D1 is a variable-current, fixed-pulse-width search bracketed by a minimum current of 0  $\mu\text{A}$  and a maximum current of 25  $\mu\text{A}$ . The maximum of the function is found at PT1, which is a measurement of the selectivity achievable between two neurons. Point PT1 corresponds to the peak of the difference between the two neuronal activation curves, both modeled as sigmoids. Like PT1, all following points found during a search also correspond to the maximum of the objective function, which we have defined as the absolute value of the difference of sigmoid activation curves. The next search direction, D2, is perpendicular to D1 and crosses through point PT1. The search for the maximum of the selectivity curve (PT2) is repeated, but in this case, the search is a variable-pulse-width, constant-current search, which spans the entire pulse-width space. After the first two searches, the routine alternates between diagonal and horizontal searches. Search direction 3, D3, is a multi-dimensional search in both current and pulse-width that passes through points PT0 and PT2. When the maximum of this search is found at PT3, the next search commences in direction D4, which passes through PT3 and is parallel to D2. The following search is in the direction that connects points PT2 and PT4. The search routine continues until the search goal is met.

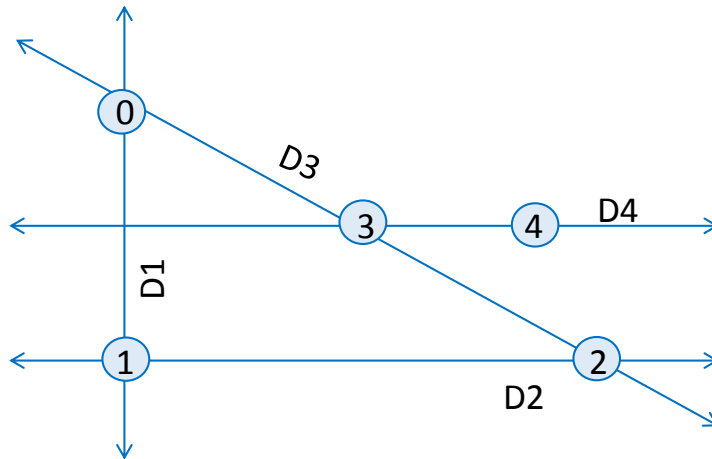


Figure 4.3. Depiction of the first four Powell's method searches. An arbitrary point (PT0) is chosen in the 2-D search space. A search is performed in the vertical direction, D1, locating the maximal selectivity at PT1. Point PT1 becomes the starting point for a search orthogonal to the first search in direction D2. The maximal selectivity of the second search is found at PT2. The third search is performed in the direction connecting points PT0 and PT2, direction D3, and resulting in a new maximum PT3. The search continues with another horizontal search parallel to D2 and intersecting PT3; a subsequent search is performed in the direction that connects the newly found point, PT4, to PT2. The algorithm iterates until the search goal reached.

#### 4.3.10 Simulations of Powell's conjugate direction method search routine

In the simulation studies, we used the experimentally derived probabilistic strength-duration curves to estimate the behavior of the Powell method for various neuronal subpopulations. To implement Powell's method, a starting point was arbitrarily chosen from the input parameter space, similarly to what was described in the experimental study above. A "true" sigmoidal activation model was then constructed for each neuron according to methods section 4.3.7, for each neuron along the first line search, in either the vertical or horizontal direction. This "true" sigmoidal activation curve was then estimated in simulation similarly to the experimental study, according to methods section 4.3.8. The closed-loop routine for building sigmoidal activation models was executed, delivering 50 simulated stimuli through the one dimensional input parameter space, and a simulated model of the activation sigmoid was defined for each neuron in the study.

## 4.4 Results

We implemented Powell's method in a model-based search routine of the multi-parameter stimulus waveform space to find the optimal waveform to selectively activate a subpopulation of accessible neurons. In the first study (Section 4.4.1), we applied our system to an experimental setting of cultured neurons to analyze the selectivity achievable between two neurons. We then extended this study by experimentally measuring strength–duration curves for a population of five cultured neurons (Section 4.4.2). The selectivity space was mapped for the five neurons and the CL search routine was used in simulation studies of the experimental data. In the simulation studies, the robustness of the Powell search method was explored for various subpopulations of neurons (Section 4.4.3).

### 4.4.1 Powell's method applied experimentally to find the most selective waveform between a pair of neurons

Five Powell's method iterations were performed to find the most selective waveform between Neurons N1 and N2. In all five line searches, activation curves were constructed using the sigmoid model of Equation 4.1. Probability measurements were collected at each stimulus point, and the sigmoid model was fit to all available data for each neuron according to the methods. The closed-loop search algorithm applied 50 stimuli to each neuron, along the line defined by the Powell search. After each iteration was performed, the difference between the activation curves for N1 and N2 was determined and a maximal selectivity point was calculated.

The search routine began from a starting point near the middle of the range of stimulus currents and pulse widths (600  $\mu\text{s}$ , 12.0  $\mu\text{A}$ ), denoted as PT0 in Figure 4A. The first search was a vertical stimulus current search from the starting point (D1, Figure 4A), with the stimulus pulse width fixed at 600  $\mu\text{s}$ . The maximum of the difference in sigmoids produced by Neurons N1 and N2 occurred at 10.7  $\mu\text{A}$ , depicted as point PT1. The second search was a perpendicular (Figure 4.4C), horizontal stimulus pulse-width search (D2) crossing through PT1. The current was fixed at 10.7  $\mu\text{A}$ , and the sigmoid search spanned the range of durations from 0 to 1000  $\mu\text{s}$ . The maximum of the difference of sigmoids for Neurons N1 and N2 was at 375  $\mu\text{s}$ , point PT2 (375  $\mu\text{s}$ , 10.7  $\mu\text{A}$ ). The third search direction connected points PT0 and PT2 along the line in Equation 4.4, where  $I$  is the current ( $\mu\text{A}$ ) and  $PW$  is the pulse width ( $\mu\text{s}$ ).

$$I = 5.77 \times 10^{-3} PW + 8.53 \quad \text{Equation 4.4}$$

The difference in sigmoids was calculated, and the maximum was measured at a pulse-width of 511  $\mu\text{s}$  and current of 11.5  $\mu\text{A}$ . The fourth search direction was then conducted parallel to the horizontal pulse-width search. The current was fixed from the previous point at 11.5  $\mu\text{A}$ , and the stimulus pulse-width was allowed to vary through the entire range from 0 to 1000  $\mu\text{s}$ . The maximum of the difference of sigmoids for Neurons N1 and N2 was measured as point PT4, at 455  $\mu\text{s}$  and 11.5  $\mu\text{A}$ . The fifth and final selectivity search was a two-parameter diagonal search connecting points 2 and 4 along the line defined in Equation 4.5. The maximum difference between sigmoids was measured at a pulse width of 524  $\mu\text{s}$  and a current of 12.1  $\mu\text{A}$ .

$$I = 10.11 \times 10^{-3} PW + 6.95$$

Equation 4.5

The two neuronal activation curves were sufficiently steep and far apart that by the second search iteration the maximum selectivity achieved was nearly unity. Had a stopping criterion been imposed on the routine, it would have stopped the search at this iteration. Although applying the Powell search to the case of two neurons is relatively straightforward, the true utility of Powell's method becomes apparent only in higher dimensions. Such a higher dimensional space would include a larger population of neurons and more stimulus parameters.

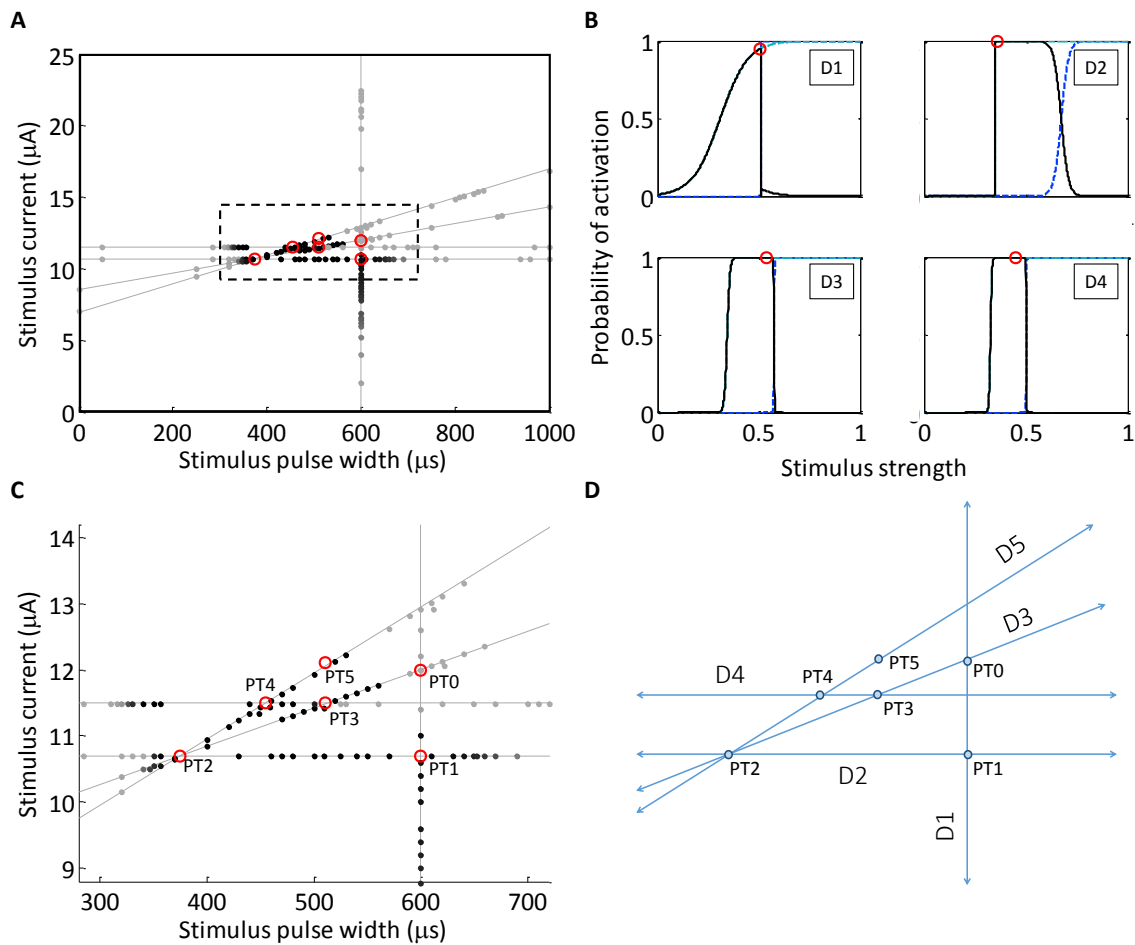


Figure 4.4. (A) Implementation of the Powell search routine in the strength–duration waveform space. The thin lines denote the five search segments. The stimuli applied along each stimulus path is color coded such that the darker the point, the greater the selectivity between the two neurons. The maxima found along the search lines are highlighted with open circles. (B) The objective function was evaluated along each line search in the Powell search routine of (A) according to Equation 4.3. The objective function for each of the first four searches is plotted in each panel, and the maximum of the objective function is denoted with an open circle, similarly to in (A). The sigmoidal activation functions for each of the two neurons, N1 and N2, are plotted with dotted lines. The output from the first four are depicted here. In all five searches, activation curves for Neurons N1 and N2, dotted lines, were measured. The difference in the activation curves between N1 and N2 is plotted in a solid black line, and a maximal selectivity point was calculated, which is depicted with open circles. (C) The implementation of the Powell search routine, magnified from the dashed box in panel (A). An arbitrary starting point was chosen near the middle of the range of stimulus currents and pulse widths (600  $\mu$ s, 12.0  $\mu$ A). (D) A cartoon depiction of the search routine, as shown in panel (C). Each of the search directions and measured peak selectivity points is highlighted.

#### 4.4.2 Experimentally measured strength-duration curves for the neuronal population

During the implementation of the search routine for Neurons N1 and N2, three additional neuronal activation curves were measured. As described previously, 50 targeted stimuli were delivered, per neuron, in each of the stimulus search directions. These stimuli were delivered in order to increase the probability measurement resolution along the transition region (0.25 – 0.75) of each neuron. At the conclusion of the Powell search routine, the algorithm had collected measurements for the each of five neuronal activation curves through the strength–duration waveform space. Each sigmoid provided estimates of the 0.25, 0.50 (midpoint, or activation threshold) and 0.75 probabilities along the experimental search directions; these points were used to construct probability strength–duration curves fit to Equation 4.2. This means that a separate strength–duration curve was calculated for each neuron at three probability levels. For other search directions through the 2-D strength–duration space, a sigmoid activation curve could be

approximated by fitting the model in Equation 4.1 to the points where the search line intersected the 0.25, 0.50, and 0.75 probability strength–duration curves. Therefore, the sets of strength–duration curves could be used to approximate the activation probability for each neuron at any point in the strength–duration waveform space.

All possible neuronal activation combinations were highlighted in the strength–duration waveform space (Figure 4.5). This selectivity map shows that regardless of the goal, Neuron N2 will always be activated using this stimulating electrode. However, there is a more complicated space between the four other activation curves because they intersect each other. This means that some neurons preferentially activate at shorter stimulus pulse widths and higher currents, while other prefer longer stimulus pulse widths and lower currents.

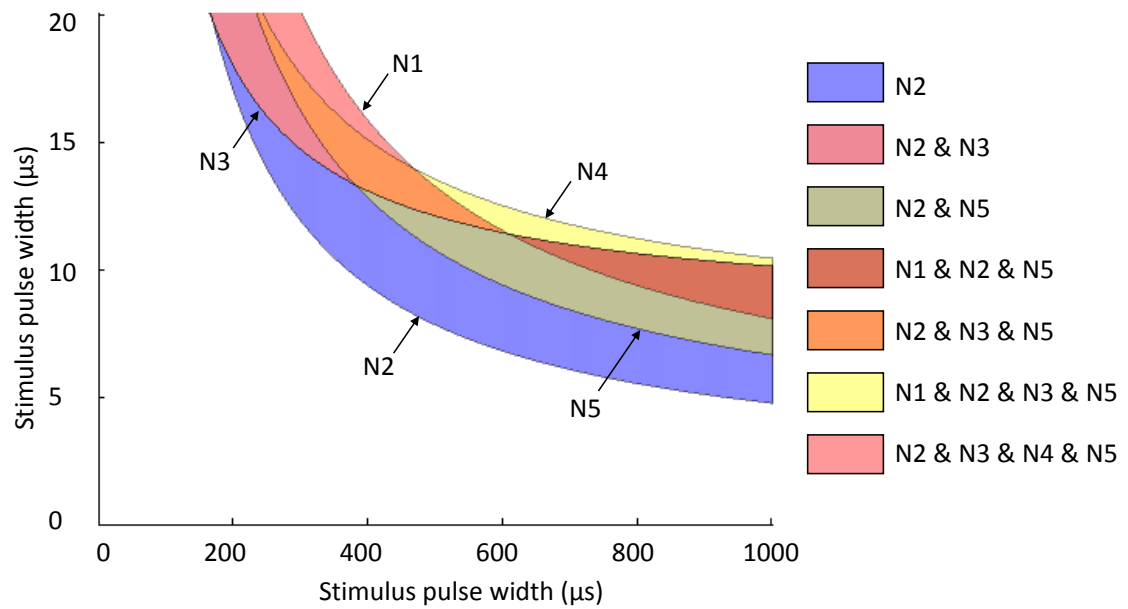


Figure 4.5. A map of selectivity regions accessible using one stimulating electrode. The strength–duration curves for five neurons are plotted, and the regions in between the curves are color coded to define the population that is activated within that waveform space.

#### 4.4.3 Powell's method applied in simulation to find the most selective waveform for a population of neurons

Simulation studies were performed in order to estimate the behavior of the Powell method for various neuronal subpopulation configurations. As a first example, we chose a target region within the population strength–duration space defined in Figure 4.5 that promotes the activation of Neurons N2, N3 and N5, while suppressing the activation of Neurons N1 and N4. The region within the stimulus waveform space that maximizes the objective function is closed (Figure 4.6A). We chose this region because we predicted that it would be the most difficult region to locate using Powell's method. The theoretical maximum of the objective function is 3, which occurs when the three target neurons are activated and the two off-target neurons are not. As the stimulus strength increases and the target neurons activate, the value of the objective function increases, but as the off-target neurons activate, the value of the function decreases. For example, if an off-target neuron activates while the 3 target neurons activate, then the objective function will evaluate to 2. However, if none of the target neurons activate along a particular line search, but both off-target neurons activate, then the objective function will evaluate to –2, which is the theoretical minimum. The objective function for each line search was defined according to Equation 4.3. For the target population N2, N3 and N5, the objective function was,

$$f = -P_{N1} + P_{N2} + P_{N3} - P_{N4} + P_{N5} \quad \text{Equation 4.6}$$

We found that there was a large variation in possible outcomes of the search routine, depending on two initial conditions: the starting point,  $PT_0$ , in the strength–

duration space, and the orientation of the first search direction, D1. For the first study (Figure 4.6A,B), we first tried using the same starting point as in the experimental study; however, we altered the first search direction, and for the second study (Figure 4.6C,D), we shifted the starting point and used the same starting direction as in the first study. In the first study, the initial search direction was a horizontal line crossing through the point PT0 (600  $\mu$ s, 12.0  $\mu$ A). On the first search, the theoretical maximum of the objective function was found. This point was located in the lower corner of the target region in the SD waveform space at 535  $\mu$ s and 12.0  $\mu$ A.

For the second study, the starting point was shifted to a region where a line search in either direction could not yield an objective function value of 3. This point was located at 700  $\mu$ s and 10.0  $\mu$ A. The first horizontal line search crossed the waveform space where target Neurons N2 and N5 activated first, however, Neuron N3 only activated after Neuron N1. The maximum of the objective function was 2. As in the experimental Powell search routine demonstrated earlier, the maximum of the objective function became the point through which the next search direction would cross. The Powell search was iterated until the theoretical maximum of 3 was found at 366  $\mu$ s and 14.8  $\mu$ A, after search D3. To confirm that the result was stable in the target region, an additional 3 searches were run after D3, and all results remained within in the target area.

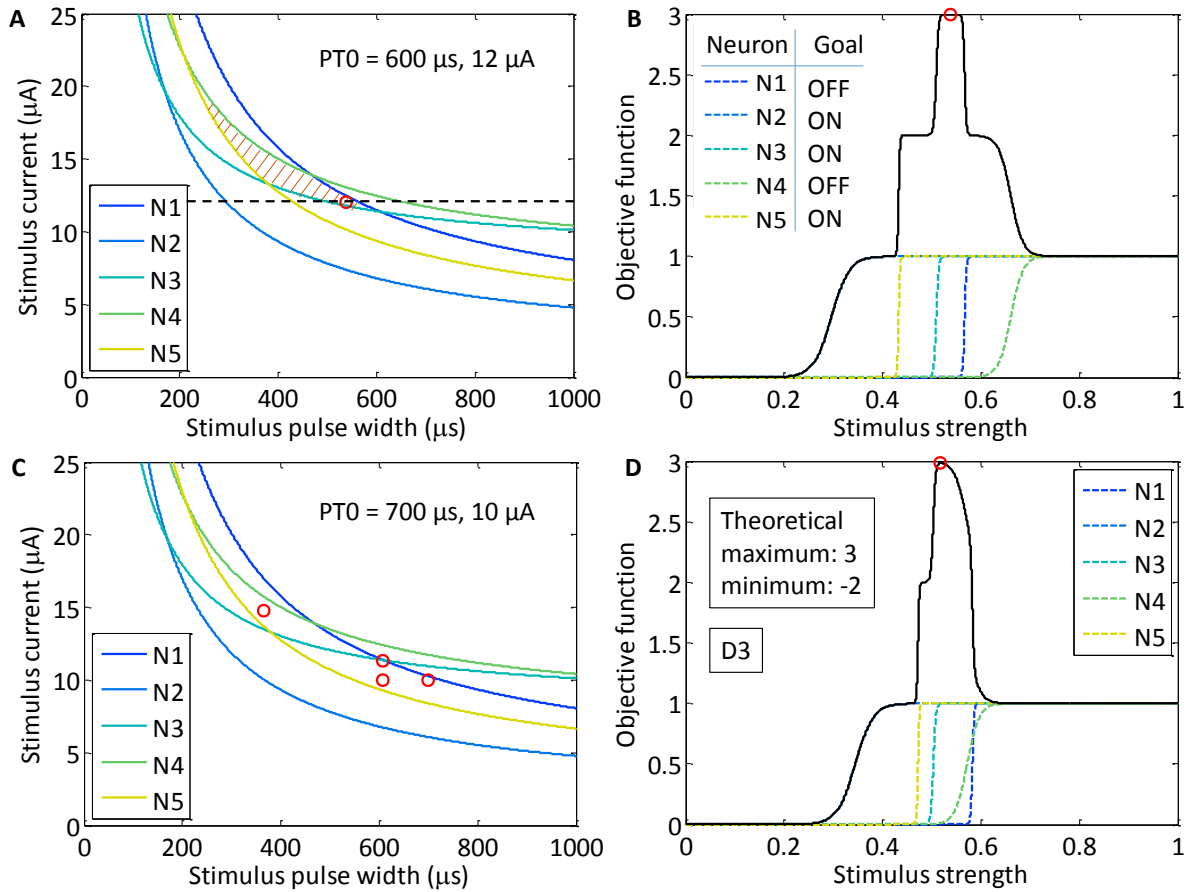


Figure 4.6. Two simulation studies were performed to find the selective region for the subpopulation of neurons including Neuron N2, N3 and N5. (A) The selective region is highlighted with stripes. For the first study, a horizontal search through the starting point,  $PT_0$  ( $600 \mu s, 12.0 \mu A$ ) yielded the theoretical maximum of the objective function (open red circle at  $535 \mu s, 12.0 \mu A$ ). (B) The objective function value is plotted along the first line search, D1. The individual neuronal activation sigmoids are plotted alongside the objective function (dotted lines). The first three target neurons activated before the off-target neurons activated. (C) The output from the second stimulation study, in which the starting point,  $PT_0$ , was shifted to  $700 \mu s$  and  $10.0 \mu A$ . (D) After the 3rd line search, the theoretical maximum was found for the objective function.

For a second target population, we chose an objective function that promotes the activation of Neurons N1, N2 and N5, while penalizing the activation of Neurons N3 and N4:  $P(N1) + P(N2) - P(N3) - P(N4) + P(N5)$ . As in the implementation of the experimental two-neuron Powell search routine, we chose to use the starting point, PT0 (600  $\mu$ s, 12.0  $\mu$ A), which was located in the middle of the strength–duration waveform space. The first search was a stimulus current search with fixed stimulus pulse-width (Figure 4.7B). The maximum of the objective function was found at PT1 (600  $\mu$ s, 10.1  $\mu$ A) and was approximately 2. Through this vertical search line, there was no region where all three target neurons were ON while the two off-target neurons were OFF. There existed, however, a stimulus region where two of the target neurons activated, but the third neuron would not activate until after one of the off-target neurons turned ON. As the stimulus value increased, the first two neurons activated, and the objective function evaluated to 2; then as an off-target neuron activated, the objective function decreased to 1; next the third target neuron activated, which brought the objective function close to 2 again, until the final off-target neuron activated and pulled the objective function back down to 1. At the highest allowed stimulus value, the function would always evaluate to 1.

The next search was simulated in the variable-pulse-width, constant-current direction. Again a sigmoid model was constructed for each neuron and the objective function was evaluated. The maximum was 3, the maximum that was theoretically possible, and was found at PT2 (807  $\mu$ s, 10.1  $\mu$ A). The third search was along the line that connected PT0 and PT2, and the maximum of selectivity was found at PT3 (870  $\mu$ s, 9.5  $\mu$ A). The fourth search was parallel to the second search and the maximum of the

function was found at PT4 (990  $\mu\text{s}$ , 9.5  $\mu\text{A}$ ). Finally, the fifth search was again in a negative slope direction and the maximum selectivity was found at PT5 (954  $\mu\text{s}$ , 9.6  $\mu\text{A}$ ).

As the search progressed, the waveform at the maximum selectivity shifted toward long-pulse-width stimuli. As is observable within the set of SD curves, at longer pulse widths, the activation of Neurons N2 and N4 converge toward a higher level, while Neurons N1, N2 and N5 all tend lower. This produces a selectivity region exhibiting larger stimulus pulse widths.

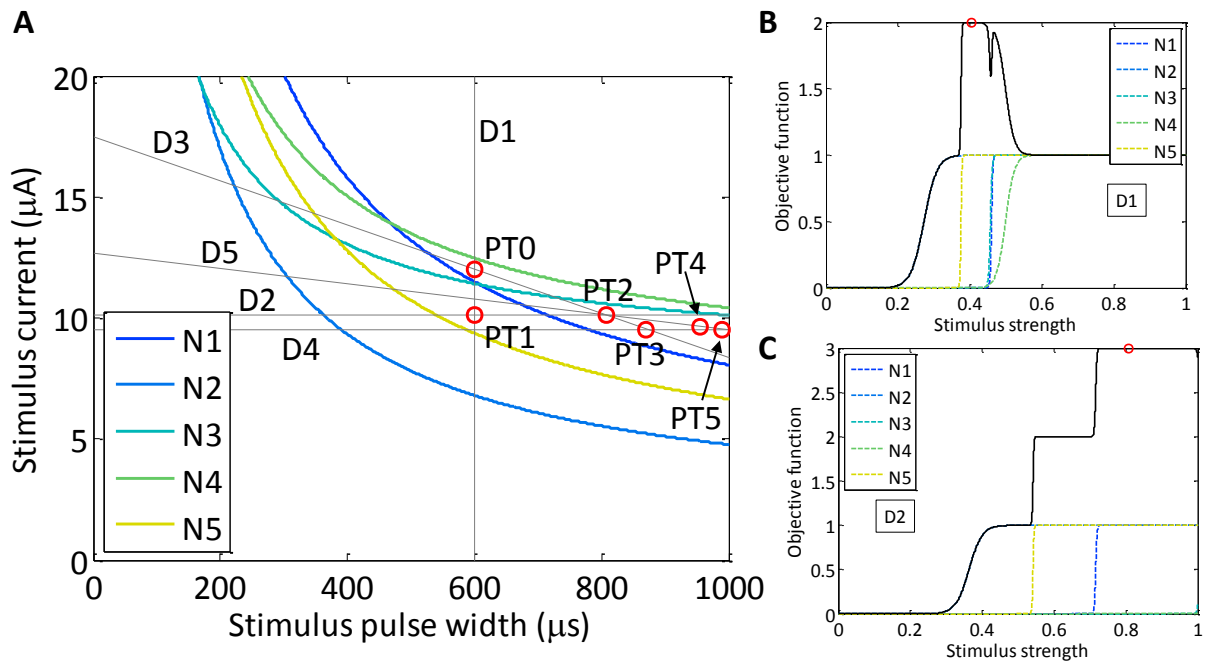


Figure 4.7. (A) The strength–duration curves from a curve-fit to Equation 4.2, are plotted for five neurons using the experimental data collected during the Powell search routine. The simulated target population of neurons was chosen, including N1, N2 and N5, and an objective function was created to promote the activation of the target neurons while penalizing the activation of the off-target neurons,  $P(N1) + P(N2) - P(N3) - P(N4) + P(N5)$ . The five searches resulting from a simulated Powell search routine are marked with faint lines, and the objective function maxima are labeled and highlighted with open circles. (B,C) The objective function along each search direction is plotted with a solid black line. The maximum of the function is found at the open circles in each plot, which correspond to the various Powell search directions.

## 4.5 Discussion

### 4.5.1 The choice of Powell's Method

Deterministic search methods, like Powell's Method, have a great strength in optimization because they converge quickly with a good initial starting point; the downside of deterministic methods is that the search can be trapped in local minima if a poor initial starting point is used. A gradient-based search method, such as gradient descent, is an undesirable method for finding the selective region between populations of neurons because there exists a plateau of maximum selectivity between neuronal strength–duration curves. Additionally, a gradient-based search routine is susceptible to instability when applied to noisy data. Other non-gradient search methods could conceivably be implemented for optimizing neuronal stimulation parameters including, Nelder-Meade, simulated annealing, or a genetic algorithm. The importance in this experiment was to demonstrate the execution of the Powell search routine. In this experimental work, the neuronal activation curves were relatively far apart in the strength–duration waveform space, resulting in a large region between the two curves where selectivity of Neuron N2 over N1 is high. For that reason, the algorithm was able to converge and find a stimulus solution where the absolute value of the difference in activation sigmoids was approximately 1, the theoretical maximum of the two-neuron objective function, after only two search iterations.

#### 4.5.2 Weighting the objective function

As the objective function complexity increases, there is an increasing likelihood that the theoretical maximum of the objective function is unachievable. For these cases, the goal is to find the stimulus that will be most selective for one subpopulation over another. For example, there is no perfect waveform space for an objective function that targets Neurons N1, N2 and N3 while not activating Neurons N4 and N5 (Figure 5). However, the objective function is still non-zero in various regions of the space. The objective function would evaluate to 2 in the region where Neurons N2 and N3 are activated ( $P1 + P2 + P3 - P4 - P5 = 0 + 1 + 1 - 0 - 0$ ) because there is a penalty for not activating Neuron N1. In the waveform space where Neurons N1, N2, N3 and N5 activate, the objective function would again evaluate to 2 ( $P1 + P2 + P3 - P4 - P5 = 1 + 1 + 1 - 0 - 1$ ). In this waveform space, all three target neurons were activated, but there was a penalty because the off-target Neuron N5 was also activated. The preference for one waveform space over another will require additional factors to be included into the objective function. For example, the objective function could emphasize the activation of on-target neurons by applying additional weight to P1, P2 and P3. This weighting would naturally prefer the second waveform space, in which all three target neurons are activated because the increase in the objective function from activating the third neuron would outweigh the penalty for activating the off-target neuron. Conversely, the objective function could minimize off-target activation by applying an increased penalty for activating off-target neurons. This increased penalty would naturally select the first waveform space, in which only Neurons N2 and N3 are activated, because the penalty for activating Neuron N5 would outweigh the benefit of activating Neuron N1.

### 4.5.3 Choosing the selectivity point after each iteration

We chose an objective function that maximized the difference of sigmoids. However, this function is susceptible to sudden shifts in the output when there is a plateau between the neuronal activation curves, because the value of the objective function changes very slightly across the plateau. For example, given a pair of neurons in which one has a very steep activation curve and the other has a shallower curve, the maximum of the difference in sigmoids will occur very close to the steep neuron's transition region. This result occurs because the steep activation curve will evaluate to nearly one very near to the transition region, while the shallower sigmoid will more slowly transition from zero to one; the maximum of the objective function will appear as far from the shallower sigmoid as possible. The resulting maximum of the objective function occurring so close to the steep neuronal activation curve may not be the ideal place to stimulate for selectivity. It may be preferable instead to stimulate closer to the midpoint of span of stimuli that produce difference in sigmoids, or selectivity points, above a predetermined fixed value. In selecting a stimulus at the midpoint of the span, the chosen stimulus will maximize the distance between the selected neurons. As a selectivity point, the midpoint will have greater robustness because any variation in the internal state of either neuron is less likely to cause the neuronal activation probability to deviate significantly. Accounting for this factor is of greater import for longer term studies or those in which synaptic blockers are not used, where drifting is more likely to occur.

## 4.6 Conclusions

In this work we demonstrated that the CL Powell search routine can be used to find the waveform region that is most selective for a subpopulation of accessible neurons. We used a model-based search method for optimizing stimulus parameters in the strength–duration space to target an arbitrary set of neurons. The success of this technique is attributable to the natural variation in strength–duration curves between neurons.

The use of a model-based CL search routine shows greatest benefit in larger dimensional spaces. Multiple stimulating electrodes are needed to maximize selectivity; each additional electrode doubles the dimensionality of the input parameter space. Future studies will examine the increase in selectivity achievable using multiple electrodes and more complex stimulus waveforms, which will result in even higher dimensional spaces. In the following chapter, I explore future medical devices, which will use many electrodes in order to encode more complex messages. The use of many stimulating electrodes will require optimization routines, similar to the work presented here, that are effective in higher dimensional spaces.

## 4.7 Supplemental data relating to Chapter 4

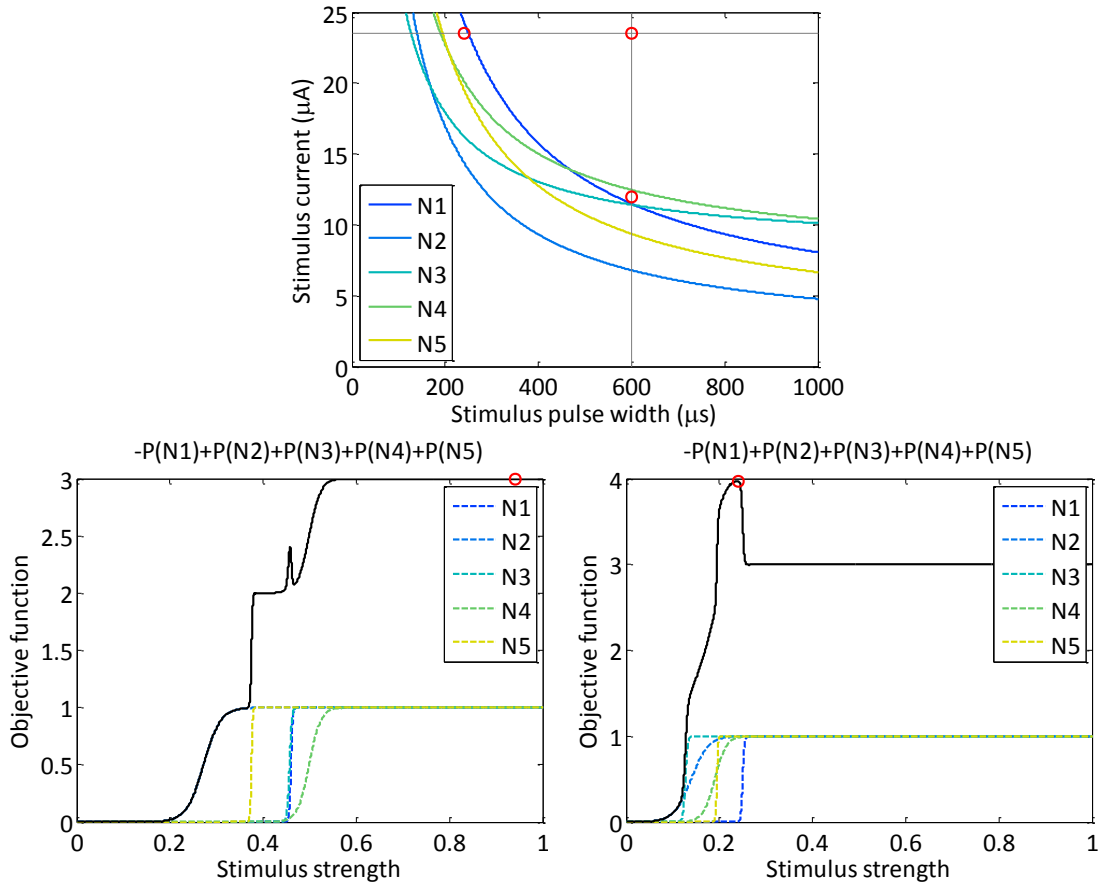


Figure 4.8. The Powell Method was implemented in a simulation study. The strength-duration curves from a curve-fit to Equation 4.2, are plotted for five neurons using the experimental data collected during the Powell search routine. A target population of neurons was selected, including N2, N3, N4 and N5 and an objective function was created to promote the activation of the target neurons while penalizing the activation of the off-target neurons. This objective function,  $-P(N1) + P(N2) + P(N3) + P(N4) + P(N5)$ , is plotted with a solid black line. In the first search (bottom, left), three target neurons were able to be activated, however, the off-target neuron was also activated. This produced a maximum output of the objective function of only 3 out of a possible 4. The maximum value that the objective function could take is four, which was found on the second search (bottom, right).

#### 4.7.1 Preliminary work in simultaneous multi-electrode stimulation

We investigated the way in which interacting stimuli activate dissociated neurons living atop the MEA. We performed our stimulation on high-density (30  $\mu\text{m}$  spacing) arrays and found that, in this experiment, stimuli add in a nonlinear fashion. Neurons were able to be activated with smaller pulses when delivered on two electrodes, although the combined charge delivered was greater than activating the neuron with a single electrode. We constructed the activation sigmoids for 300  $\mu\text{s}$  and 800  $\mu\text{s}$  stimuli delivered at various angles with respect to the electrode 1/electrode 2 stimulation field. The CL routine described earlier was used to search along these multi-electrode directions.

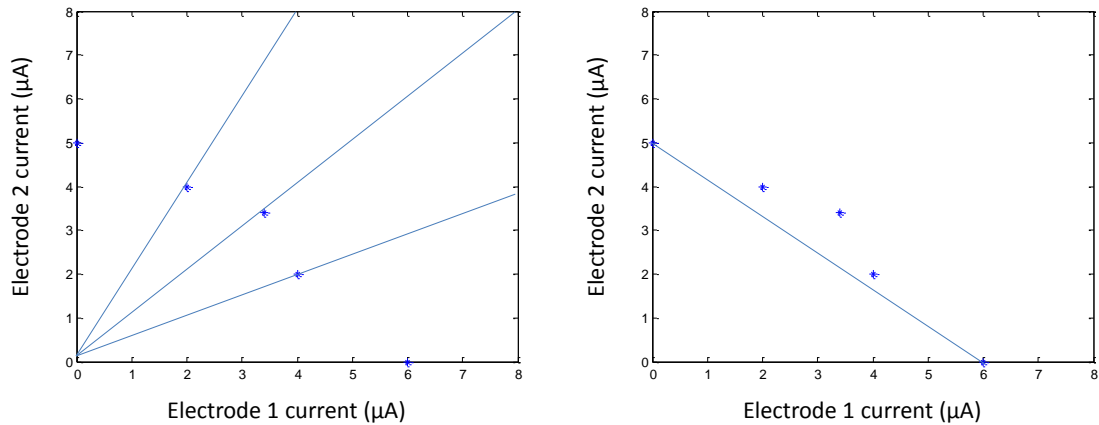


Figure 4.9. Simultaneous two electrode stimulation. Sigmoid midpoints are plotted in each panel (stars). Left: The lines illustrate the span of the searches that were performed to find the sigmoid activation curve for an 800  $\mu\text{s}$  stimulus pulse width. Additionally, searches were performed along the x-axis and y-axis, which comprised one-electrode searches. Right: A line is drawn to connect the two thresholds that were measured using a single electrode, representing the constant-total-charge path. The activation threshold for this neuron increased in total charge required during the multi-electrode stimulation searches.

This work was our first exploration of the simultaneous multi-electrode activation space; further work will better characterize this space, which we explore in the next chapter. Based on our preliminary results, we propose it is possible that some combination stimuli interact in a constructive way to activate a neuron, whereas other combination stimuli may activate in a destructive way. In the case of one neuron, the activation threshold increased in total charge along the two-electrode search directions.

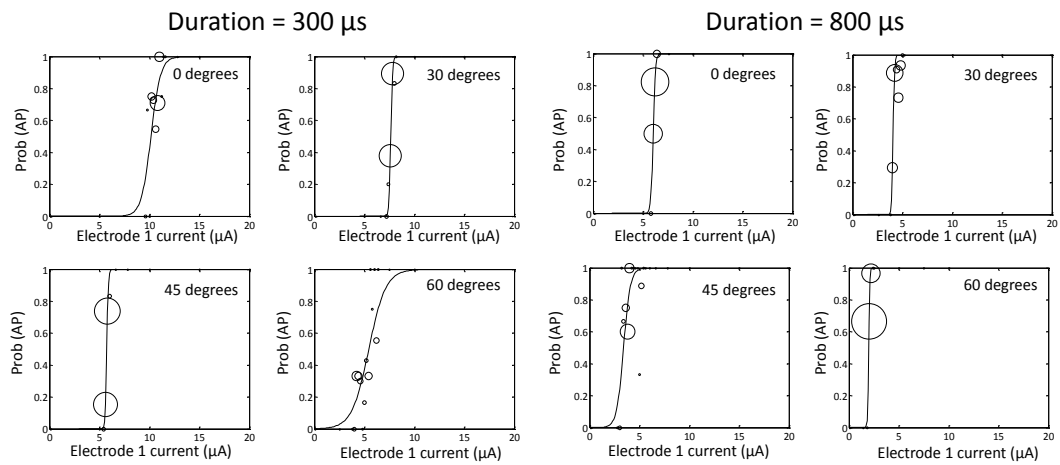


Figure 4.10. The activation curves for one neuron across four stimulation directions for two different stimulus pulse-widths.

## CHAPTER 5

### CONCLUSIONS AND FUTURE DIRECTIONS

#### 5.1 Summary

The research presented in this dissertation is an investigation of closed-loop (CL) methodology for specific targeting of single neurons and neuronal populations using extracellular electrical stimulation. This research developed techniques for optimizing stimulus parameters to rapidly characterize neuronal activation curves in the stimulus strength–duration waveform space from multiple electrodes. In order to selectively activate a neuron, the functional relationship of individual neurons to stimulating electrodes was uncovered, which created a mapping of neuronal activation probabilities within the strength–duration waveform space. In order to create a stimulation system for targeted neuronal activation, we first had to design and characterize a CL model-driven system.

In Chapter 2 of this dissertation we demonstrated that optimized closed-loop electrical stimulation is superior to open-loop (OL) techniques for measuring and characterizing neuronal activation across a large parameter space. The developed CL routine quickly found the relevant activation curve features so that they could be more thoroughly probed to increase our measurement confidence. We showed that the stimulus-evoked neuronal response is probabilistic, and by using our CL imaging system and micro-stimulation technology, we were able to stimulate a neuron with an arbitrarily selected probability. Exploiting the shape of the strength–duration curve, we

demonstrated that it is possible to activate a neuron with different probabilities by varying the aspect ratio of a constant-charge stimulus pulse.

We next showed in Chapter 3 that by utilizing the differences in activation probabilities between two neurons with intersecting strength–duration curves, a single electrode can deliver stimuli preferentially targeting one neuron of the pair. For those pairs of neurons in which the strength–duration curves do not overlap, adjacent stimulating electrodes are an additional level of control for differentially activating neurons. Knowledge of the soma location alone is insufficient to predict activation. We proposed that to improve the specificity of our stimuli, it is essential that the stimulus-evoked activity for each reachable neuron within the population is first characterized. The organization of the culture with respect to the stimulating electrode can be functionally mapped in real-time to assess the achievable selectivity.

The vast parameter space of multiple waveform parameters and multiple neurons lead us in Chapter 4 to employ a search routine for optimizing stimulus parameters, based on Powell’s Method, to rapidly find a viable waveform for neuronal population targeting. Optimized strategies are indispensable for developing techniques to selectively activate neurons because the parameter space is too large for an OL routine. CL search techniques are critical towards the advancement of next-generation clinical stimulation solutions. The techniques developed in this chapter may be used to improve the selectivity of a stimulus waveform by simultaneously stimulating on multiple electrodes.

## **5.2 Future directions**

By developing new techniques to selectively activate particular neurons within a population, devices can better control their direct effects on activated tissue, and thereby improve stimulus efficacy. The ability to target specific neuronal populations will enable researchers to probe neuronal circuitry with high precision. Selective activation to modulate neuronal activity is crucial for many science and clinical applications because selectivity allows stimuli to target a specific population. Targeted stimulation can guide the stimulus to alleviate symptoms due to disease or injury while preventing the activation of off-target populations, which can lead to side effects.

The future of selective stimulation lies in technological advancements to electrode arrays and the way in which arrays are utilized, including improvements in the delivery of an in vivo high-density array, for applications such as deep brain stimulation. Concurrently, stimulation algorithms must incorporate feedback of the evoked activity to inform the stimulus parameters. These improvements will enable devices to optimize their stimulus routines for neuronal targeting that can be implemented independent of the variability across patients.

### 5.2.1 Utilizing the electrode array

In order to selectively activate neuronal populations, the spatial distribution of electrodes within an array should be utilized. Most stimulation routines make use of a single electrode because of simplicity and ease of use. Many opportunities for improving selectivity lie in using multiple electrodes such that stimuli may be spatially and

temporally confined. An electrode array offers greater selectivity by enabling manipulation of electric field interactions, use of bipolar stimulation to create a spatially localized return path for current, and through use of extremely high-density electrode arrays to reduce the size of electrodes such that they are similar in scale to the target neuronal elements.

#### *High-density arrays and bipolar stimulation*

Technological developments in creating higher density electrode arrays will facilitate more localized delivery of stimulus pulses to individual neurons. It is essential that while the electrode area is decreased, efforts to simultaneously lower the electrode impedance by using coatings such as platinum black are employed to improve current delivery. Furthermore, improved methods for implantation of the electrode array into the tissue, minimizing tissue disruption, can help maximize stimulus efficacy. Retinal prostheses, for example, employ high-density electrode arrays with electrodes on the scale of single cells (Fried et al. 2006), which allows stimuli to be reduced in amplitude such that they activate only very local populations of neurons. Greater selectivity of stimuli to target single cells or extremely small populations increases the image resolution that is deliverable to the retina.

Another method for improving spatial selectivity of stimuli is to utilize bipolar stimulation techniques to spatially localize a stimulus to a region within the array (Nathan et al. 1991). Localizing the current path between adjacent electrodes can be implemented to target various muscle types in an intramuscular array. Guvanasen and colleagues are using spatially distributed pairs of bipolar electrodes to target particular muscle cell types

using a stretchable electrode arrays. By selectively activating fast- or slow-fatiguing muscle fibers, it can become possible to produce a more biologically natural muscle contraction.

Combining electric field manipulation with higher density arrays and local bipolar stimulus protocols could further enable the localization of stimulus currents in arbitrary configurations. For example, the electric field around a neuron of interest could be precisely controlled even along the length of the axon by creating a barrier of activated bipolar electrode pairs.

#### *Electric field interactions and multipolar stimulation*

Distributed stimulation across an array of electrodes offers the ability to deliver more focal stimuli for selective activation of a neuronal population. High-density electrode arrays offer the possibility of electric field interaction when stimulating electrodes are used in parallel, resulting in more complex stimuli than using each electrode serially. By simultaneously stimulating on multiple electrodes, future technologies could encode more messages into the nervous system. The larger range of messages would allow, for example, more robust control of a prosthetic device, improved perception for a cortical prosthesis and more efficacious deep brain stimulation.

The interaction of simultaneous stimuli delivered from adjacent electrodes alters the neuronal activation threshold. This interaction between multi-parameter stimulus waveforms creates another opportunity for increased stimulus selectivity within a population. There is no guarantee that a pair of adjacent electrodes will enable selectivity between a pair of neurons, which emphasizes the need for a method to determine the

necessary electrodes within the array for achieving a particular goal. More specifically, a fast closed-loop search routine is required because it is unknown, a priori, which electrodes provide access to which neurons.

Chaturvedi and colleagues (2012) studied the great impact that multipolar stimulation, distributed across multiple electrodes implanted within deep brain structures, can have to selectively activate neuronal populations without activating side-effect related fibers. They showed, in computational studies, that by using multiple electrodes in a current-controlled stimulation modality, they could steer the current path into more desirable configurations, which is especially helpful because not all surgically implanted electrodes are optimally aligned within the neural tissue. Additionally, developments in cochlear implant technology that utilize multipolar stimulation techniques to create a “virtual electrode,” have shown that patients can perceive a frequency other than that which is being applied to an electrode when it is simultaneously applied to neighboring electrodes, as if there were another “virtual” electrode in between the two (Wilson & Dorman 2008). This technology employs stimulus waveform shaping to increase the number of discriminable channels beyond the number of implanted electrodes.

### 5.2.2 Stimulus waveform design

Effective waveform design is integral in improving the selectivity and control of neuronal stimulation systems. Altering the stimulus amplitude (current or voltage) is the most frequently used method for waveform modification; this approach is inherently limited in its selectivity as it typically activates many axons within a region (Nowak & Bullier 1998; Tehovnik et al. 2006). Control of the stimulus amplitude is an essential element but

alone is insufficient for differential activation of neurons within a population using a single electrode. Expanding the one-dimensional approach to multi-dimensional waveforms facilitates the development of targeted stimulation technologies.

### *Irregular pulse shapes*

Numerous modeling and experimental studies have shown a difference in the efficacy of single anodic versus cathodic square current pulses (Tehovnik et al. 2006, Wagenaar et al. 2004, Rattay 1999). To further investigate single pulses, Wang and colleagues (2012) measured the effect of changing the aspect ratio of an asymmetric stimulus pulse, which is a biphasic current pulse of variable amplitude and duration on each phase such that the total charge was balance in each phase. They found that cathode-leading asymmetric pulses preferentially activated cell bodies over axons, and symmetric waveforms preferentially activated axons over cell bodies. Future advances in stimulation will require that researchers investigate the use of more complex stimulus waveforms to find particular stimulus characteristics that preferentially activate individual neurons, or populations of neurons.

### *Stimulus trains*

Many stimulation applications, such as DBS, utilize trains of regularly spaced stimuli. Grill and colleagues utilized a genetic algorithm to develop irregular pulse trains, in which the inter-pulse intervals were variable, for DBS in patients with Parkinson's Disease (Brocker et al. 2013). They found that by varying the temporal pattern of the stimulus, the efficacy of the stimulus train could be increased and the power consumption could be decreased relative to typical clinical stimulation protocols. By combining

temporal pattern manipulation with waveform design delivered on multiple electrodes, there is an even greater access granted to manipulate and target a neuronal population. These techniques for determining optimal stimuli to achieve a particular goal, such as reducing power consumption in a clinical device, could be integrated into the spatial localization provided by high-density arrays to improve selectivity simultaneously in both spatial and temporal dimensions.

#### *Experimental studies without synaptic blockers*

The work that we presented in this dissertation made use of an accessible in vitro neuronal culture test-bed to demonstrate the importance of the shape of a stimulus pulse for activating a neuron with differing probabilities. Future research may expand on this work to better understand the susceptibility of neurons to activate to particular stimulus features. Furthermore, in vitro investigations into the efficacy of particular stimuli to modulate neuronal network activity should make use of waveform design. Investigation into the downstream effects of varying pulse shapes by experimenting without the use of synaptic blockers will help define the methods that can best be implemented to modulate population activity.

Most currently available device technology, clinical devices in particular, allow for only a limited number of electrodes with which to deliver stimuli. The development of more complex stimulus pulses to encode more stimulus messages will provide advantages to device design. One way to accomplish this reduction is to exploit the variability in the neuronal response to the shape of an electrical stimulus. Differential stimuli could be delivered to a network if a waveform could be designed to multiplex a

message allowing it to differentially target a population of neurons (Sekirnjak et al. 2006; Lebedev et al. 2011; Jepson et al. 2011; Kipke et al. 2008; Fried et al. 2006; Guggenmos et al. 2013; Carmena et al. 2003; Fitzsimmons et al. 2007). Stimulation algorithms optimized to exploit the probabilistic nature of neuronal activation can offer access to selectivity that is otherwise unobtainable.

### 5.2.3 Closed-loop optimization of stimulus parameters

Closed-loop (CL) methods facilitate fast searches through a large input space to find an optimal stimulus waveform (Arsiero et al. 2007; Benda et al. 2007; Zrenner et al. 2010; DiMattina & Zhang 2013). Search routine performance may be further improved by taking advantage of the available models of neuronal activation. A model-based search routine can guide the search and mitigate the inherent noise in the stimulus-evoked neuronal response. Closed-loop techniques are advantageous over open-loop techniques in a multi-parameter space because CL techniques can learn from past data to rapidly locate the stimulus space that provides the most differential neuronal activation.

#### *Electrical recording and stimulation*

In the research presented here, we used optical imaging techniques for measuring evoked activity. Electrical recording has an advantage in clinical application over optical recording due to its extensive history of successful use. Although future technology could make use of fiber optics for delivering light for in vivo stimulation, present technology utilizes electrical stimulation and recording. Translating the system presented in this work to in vivo applications may require converting the optical recording system to an electrical recording system, such that the entire system is electrically based. Electrical

recording has seen use in CL neuronal stimulation systems previously. Zrenner and colleagues (2010) developed a CL system of electrical recording and stimulation to control the firing probability of a neuron. They electrically measured neuronal activity in a feedback loop to adjust the stimulus online. Newman and colleagues (2012) developed a closed-loop system of integrated hardware and software for controlling neuronal activity in real time, in vitro, which expanded on the closed-loop bursting control previously developed by Wagenaar and colleagues (2005). They showed that by using feedback of the electrical activity for a multi-electrode population of neurons, they could alter the aggregate stimulation frequency across electrodes to clamp the population firing rate. Additionally, Pais-Vieira and colleagues (2013) implemented a CL brain-to-brain interface in rats capable of altering the electrical stimulus waveform in one cortical prosthesis based on the actions of a separate rat, and the pair of rats learned to change their behavior to benefit them both. These developments could not have been possible without closed-loop methodologies to feedback information about changes in evoked responses to their controller.

#### *Deterministic search methods*

CL methods are essential for improving experimental techniques because they can be used to efficiently explore a multi-dimensional parameter space. Deterministic search methods, like Powell's Method, have a great strength in optimization because they converge quickly with a good initial starting point; the downside of deterministic methods is that the search can be trapped in local minima if a poor initial starting point is used. A gradient-based search method, such as gradient descent, is an undesirable method

for finding the selective region between populations of neurons because there exists a plateau of maximum selectivity between neuronal strength–duration curves.

The Powell search routine is of greatest utility for larger dimension spaces. The waveform dimension is doubled with each additional electrode added to the system, and the use of an electrode array enables selectivity, even in the one-parameter search space by using different stimulation electrodes. The Powell search method could be implemented from multiple electrode locations providing even greater access to many unique selectivity regions for differing populations of neurons. The strength of this method increases with every added stimulating electrode or waveform parameter.

#### *Conclusions about CL systems*

While CL systems enable learning about the nervous system, they are also essential for clinical applications. For example, in delivering sensory stimuli from a prosthesis back to the brain, message encoding algorithms must be developed that measure evoked activity online. Online feedback of the evoked activity will enable the controller to find the most separable stimuli. Closed-loop techniques are indispensable for guiding a stimulus to be most efficacious in a neuronal environment. Every subject and neuronal population is unique, and in order to control the activity of a particular population, it must be characterized online to measure how it is changing and evolving with each stimulus presentation. A CL routine could be developed for many different stimulation goals, including finding the most selective stimulus range to divide a population or stimulate individual neurons.

#### 5.2.4 Clinical applications for neuronal selectivity

In our experimental system, we use widefield optical imaging as a measurement tool; it is likely that in a clinical application that non-optical methods will be used to record evoked activity. The findings in this work are independent of measurement method, and so also apply to non-optical recording methods. Ultimately, any stimulation routine needs to implement a technique to probe and characterize the population response in order to design targeted stimuli that will enable more sophisticated control of the evoked response.

In the experimental application, there is variability in population size, absolute neuron position, and relative position of the cells to the micro-electrode arrays (MEA). The high variability in neuronal configurations will similarly apply to clinical applications, given natural patient-to-patient variability. It must therefore be assumed that each experimental or clinical application will have a unique response. It is the uniqueness of each application that requires that the accessible neuronal population be learned, and this accessible population be probed for response in the stimulus parameter space.

##### *Deep brain stimulation*

An example target application for selective techniques is deep brain stimulation (DBS), which is used in treating Parkinson's Disease and epilepsy. During DBS, stimuli must be designed to specifically target a baseline activity level such that the stimulus evokes sufficient activity to provide a therapeutic effect, while not excessively activating tissue leading to side effects (McIntyre et al. 2011; Freeman et al. 2010; Twyford et al. 2014; Lee et al. 2013) There is a subspace in the strength–duration waveform space in between

the two curves, and a search technique is needed to find that region. Future stimulation algorithms will make use of non-gradient search methods for finding and delivering stimuli that fall within the therapeutic subspace. Although the Powell search routine was implemented in this dissertation, other search methods could be implemented including Nelder-Meade, simulated annealing, or a genetic algorithm. These alternative search algorithms may offer advantages over Powell's method depending on the specific stimulation configuration and recording environment. Because the relevant therapeutic and side-effect curves can be described by strength-duration equations, any search through the waveform space should be model-driven to most quickly home in on the desirable subspace.

### *Optogenetic stimulation*

Next generation neural prostheses will incorporate clever techniques for garnering more control, using both stimulation techniques and stimulation technology to access a more precise and robust population of neurons. Tchumatchenko and colleagues (2013) have developed a CL system for delivering a light stimulus for optogenetic stimulation.

Closed-loop optogenetic control is an extremely powerful tool that is in its early stages and is rapidly advancing. The advantage of optical stimulation for optogenetics is that its effects are limited to neurons in the targeted genetic population. Combining the genetic specificity of optogenetics with the specificity offered by sophisticated electrode arrays offers a fine-grained control over neuronal activation.

### *Human augmentation*

Electrical stimulation is an established and essential interfacing methodology for bridging the biological-technological boundary. As more sophisticated approaches are developed to increase stimulus efficacy and specificity, doors will open to a more seamless integration of artificial devices into the human body. These approaches will allow technology to replace damaged or diseased tissue with highly functional counterparts. As Potter (2013) observed, our world is changing at an escalating pace, and technology can bridge the gap between the problems of the primitive world in which our brains have evolved with the complex problems facing our brains in the present day. Ultimately, these developments in technology will extend to a world of elective augmentation of neural function. It may sound like the science-fiction of the future, the time is rapidly approaching when having a third, functionally integrated arm may not be so far-fetched.

### **5.3 Conclusions**

Selectivity between two neurons is achievable using a single electrode. For a single stimulus parameter search, in either current or pulse-width, a CL search routine can find the stimulus waveform that will selectively activate the lower threshold neuron, even for neurons with very similar activation transition regions. This selectivity is assured, however, only for the lower threshold neuron. For this reason, it is important that the full stimulus waveform space be exploited to differentially target neurons. When the strength–duration curves of a pair of neurons cross one another, selectivity of either neuron is achievable using a single stimulating electrode. For other neuron pairs or populations, the utilization of multiple stimulating electrodes to provide spatially

distributed access to different neurons can enable selectivity. The organization of the culture with respect to the stimulating electrode can be functionally measured in real-time to assess the achievable selectivity.

The complex and probabilistic activation of neurons in response to an electrical stimulus offers opportunities to improve the ability of stimulation devices to selectively target neuronal populations. In particular, neurons activate along a strength–duration curve in the stimulus current and pulse-width waveform space. The shape of this curve cannot be inferred from soma location, and so it must be measured in real time to be characterized. Developing stimulus waveforms to access the difference in neuronal activation curves allows many unique populations of neurons to be activated. Presenting only large, on/off stimuli to neurons, as is classically done, greatly reduces the complexity of messages that may be encoded. For clinical stimulation applications, improvement in both stimulus selectivity, to access a particular population of neurons, and in stimulus efficacy, to activate the target population with high probability, is essential for designing devices with superior biological mimicry.

## **APPENDIX A: SOFTWARE DESIGN**

This appendix describes the software that was developed in this dissertation.

Source code is available on request to the author.

### **A.1 Experiment Interface**

We designed a software package to execute electrical stimulation and optical recording experiments. Software for the CL system was designed in a modular way. This enabled the target functions to be swapped out for any given experiment.

#### caExpLib

This is a library for the calcium imaging experiment.

#### expSettings

This is a library for all of the experiment settings.

### **A.2 Libraries for Hardware Interfacing**

We developed four libraries for interfacing with the pre-amplifier, automated stage, camera and stimulator.

#### meaSelectLib

This library includes functions that set electrode configurations at the Multichannel Systems 1060BC-UP pre-amplifier.

#### stageControlLib

This library includes functions that control the movement of the stage.

#### camMMLib

This library uses the Micro-Manager interface to retrieve images from the Photometrics QuantEM camera.

## STG2004Lib

This library includes functions that program and initiate stimulus and synchronization routines on the Multichannel Systems STG2004 stimulator.

### **A.3 Stage Control**

We designed a GUI for controlling the movement of the stage platform that utilizes the *stageControlLib* library previously described.



Figure A.1. GUI for controlling the automated stage movement.

## A.4 CaGUI\_Select

We designed a GUI to control the stimulator connectivity to an arbitrary set of electrodes, which utilizes the *meaSelectLib* library previously described.

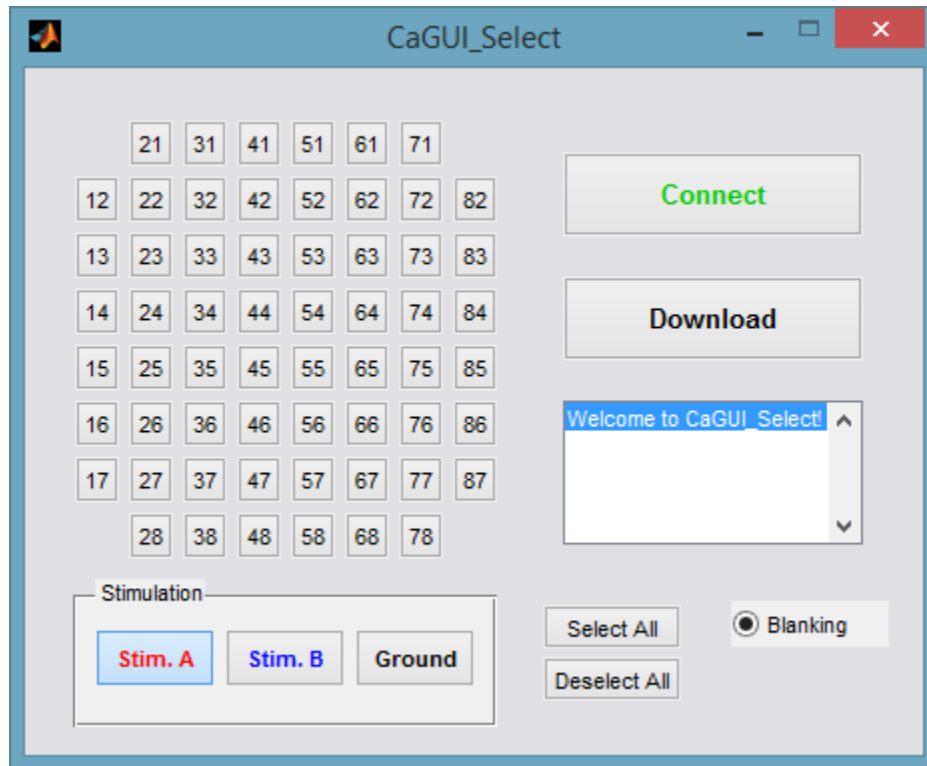


Figure A.2. GUI for controlling the stimulation channels.

## **A.5 Locating Cell Somata**

The automated process for locating cell bodies is outlined in. A single raw image is shown from a series along with the evoked difference image, the processed image gradient and the cells overlaid on the gradient image. In order to first define the population of neurons an automated strategy was employed to locate all cell somata in which activity was evoked in response to a relatively large stimulus. A relatively large current amplitude, which varied depending on the electrode impedance, was chosen to evoke as much activity as possible without creating voltages at the electrode that would electrolyze water or current densities that could be harmful to those neurons located nearest to the electrode. The first step in the image processing routine was to average the four post-stimulus peak frames and four pre-stimulus baseline frames, as was described above. The averaged baseline frame was subtracted from the averaged peak frame to create a difference image. A smoothing Gaussian filter with a large standard deviation was applied to measure the general activity throughout the image, and this activity was subtracted from the difference image. This technique was used to eliminate the fluorescence signal originating from neurites that span the culture because each axon and dendrite contributes to the image fluorescence, making detection of cell soma boundaries more difficult. A sharp Gaussian filter was then applied to smooth the image, and a gradient image was calculated to highlight soma boundaries. A circular Hough filter was applied to the gradient image, which looks for circle centroids belonging to cell borders, over a range of diameters (adapted from Peng (2005)). “Gradient pixels” were found as pixels having gradients surpassing a threshold, which designated the border between soma fluorescence and background. Gradient pixels then “voted” on possible soma

centers; each pixel located at a given radius from a gradient pixel was counted as a potential soma center for that particular radius. The votes were weighted by the gradient of the pixels that contributed each vote. All of the possible votes for the image area were tallied in the “accumulation array,” to which a threshold was applied to find the most common votes, or circle centers. Five standard deviations of the image intensity was used as a measure of the noise and as a threshold for the voting accumulation array.

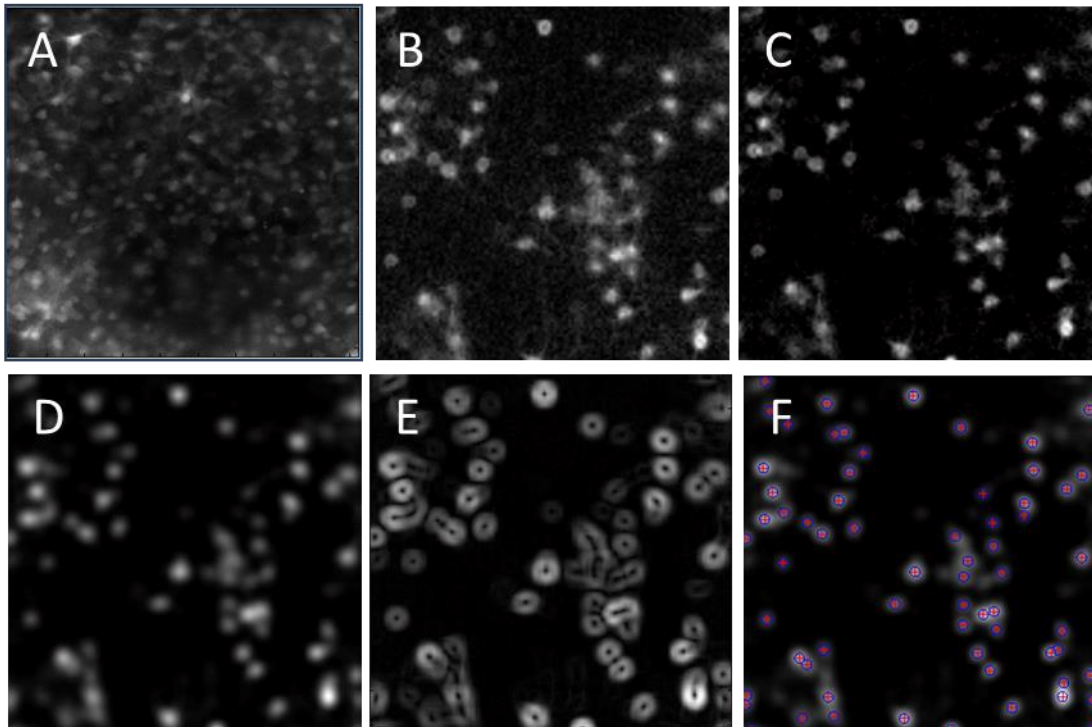


Figure A.3. Automated image processing for locating cell somata. (A) A raw single post-stimulus frame (512 X 512 pixels) is displayed from a series of frames (30 fps). (B) Image subtraction is performed to highlight the fluorescence difference post-stimulus from pre-stimulus. (C) The background is subtracted, and a gradient of the difference image is used to highlight the somata boundaries. (D) A circular Hough filter is applied to the gradient image to locate neuronal somata. Grid of 16 X 16 pixels (shown with dark squares) mark the soma centers. Scale bar: 100  $\mu\text{m}$ .

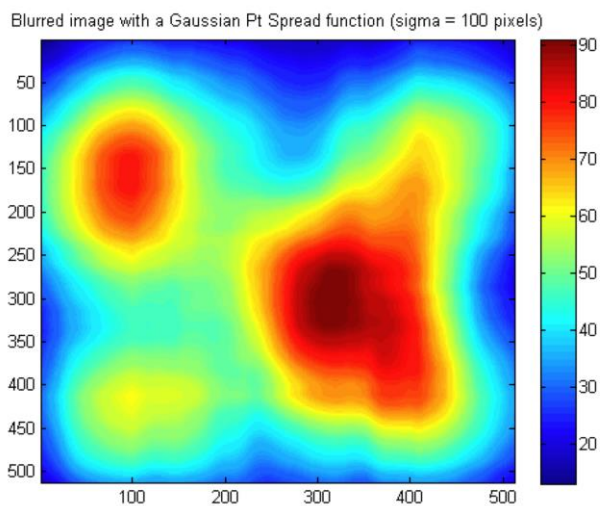


Figure A.4. A heat map representation of the background activity that was subtracted in the previous figure.

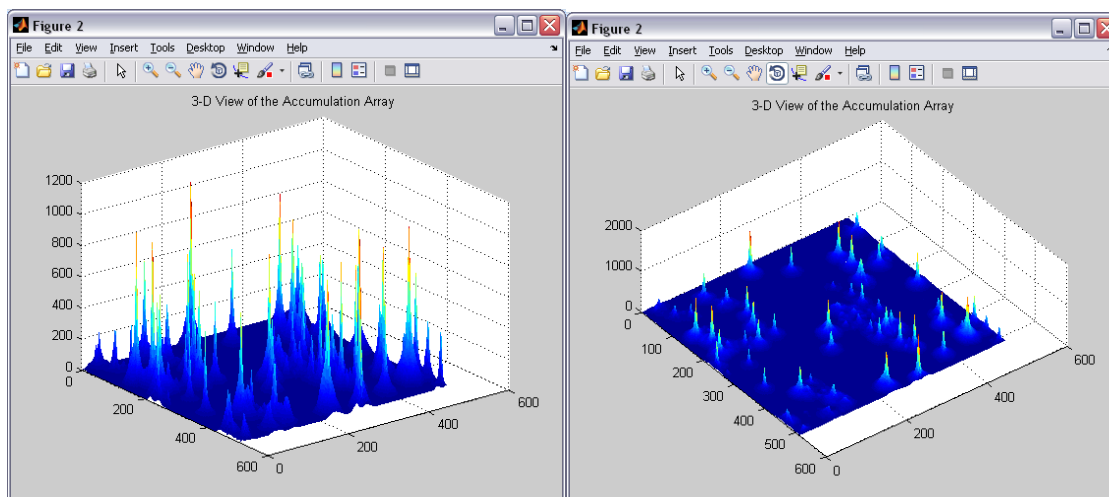


Figure A.5. Two views of the Hough voting accumulation array.

## A.6 Movalyze: GUI for Processing Image Series'

The image processing routines described above were integrated into a GUI for easy user access to evaluate stimulus-evoked activity.

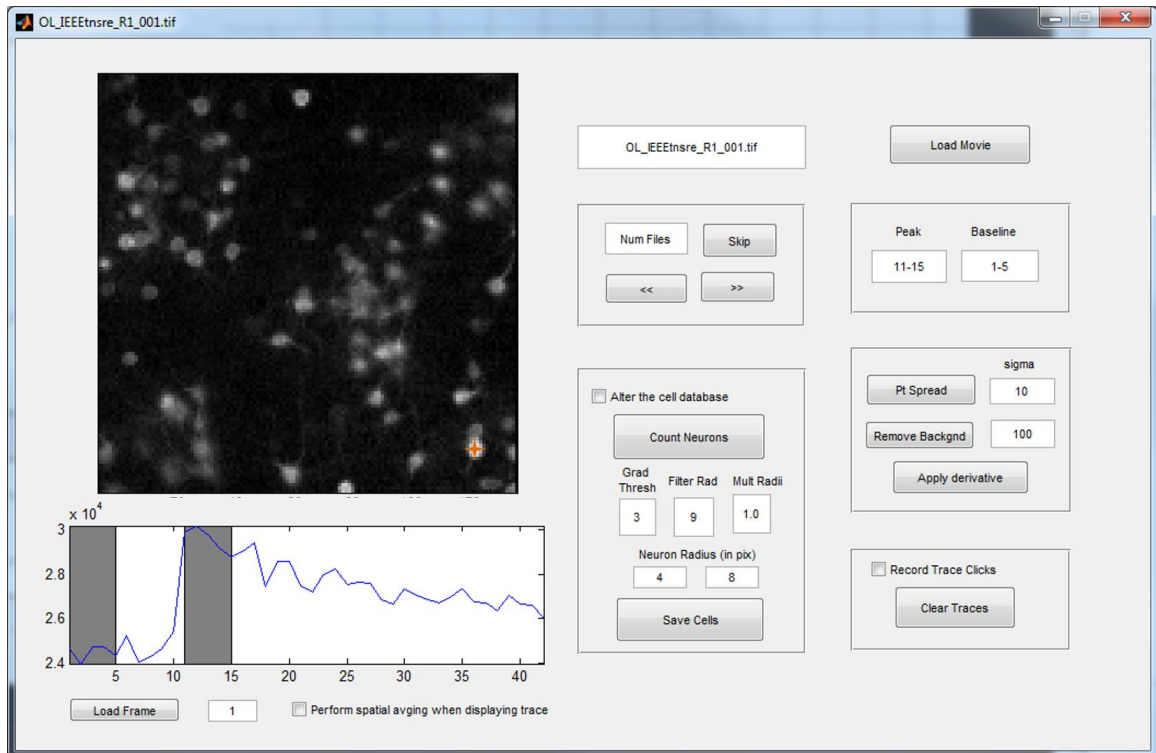


Figure A.6. The movalyze GUI to evaluate the stimulus-evoked activity.

## APPENDIX B: PROTOCOLS

This appendix describes the various chemical, biological and software protocols that were used in this dissertation.

### B.1 Dye Loading

Automated optical imaging was used to measure the stimulus-evoked neuronal response. All preparation procedures were conducted in the dark to lengthen experiments by minimizing photobleaching and phototoxicity. First, culture media was removed and neurons were loaded with Fluo-5F AM (Life Technologies F-14222), a calcium-sensitive fluorescent dye with relatively low binding affinity at a concentration of 9.1  $\mu\text{M}$  in DMSO (Sigma-Aldrich D2650), Pluronic F-127 (Life Technologies P3000MP) and artificial cerebral spinal fluid (aCSF; 126 mM NaCl, 3 mM KCl, 1 mM  $\text{NaH}_2\text{PO}_4$ , 1.5 mM  $\text{MgSO}_4$ , 2 mM  $\text{CaCl}_2$ , 25 mM D-glucose) with 15 mM HEPES buffer for 30 minutes at ambient 25°C and atmospheric carbon dioxide. Before imaging, cultures were rinsed two times with aCSF to remove free dye.

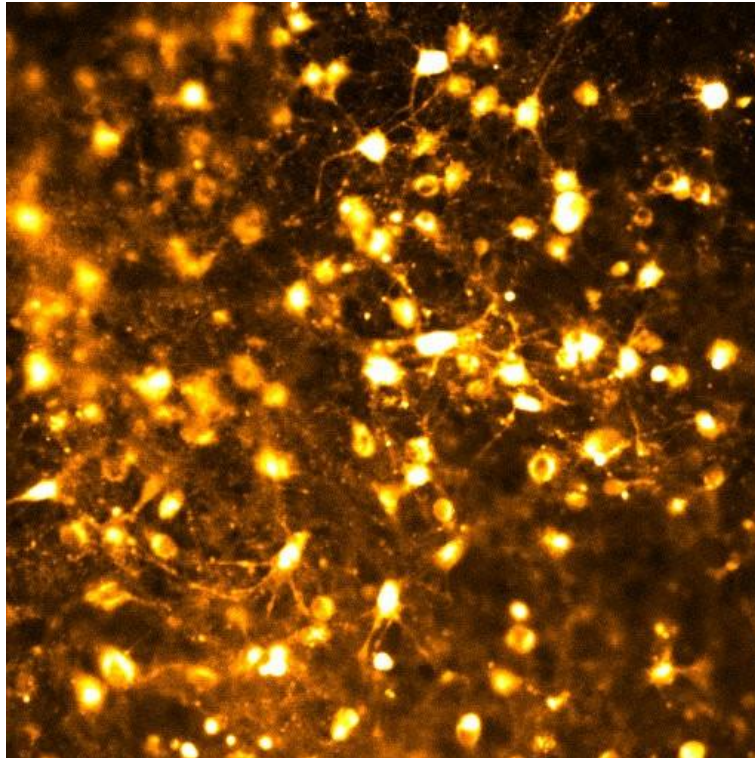


Figure B.1. Integrated spontaneous activity.

## **B.2 Blocker Loading**

Cultures were bathed in a mixture of synaptic blockers in aCSF (15 mM HEPES buffer). This included (2R)-amino-5-phosphonopentanoate (AP5; 50  $\mu$ M; Sigma-Aldrich A5282), a NMDA receptor antagonist; bicuculline methiodide (BMI; 20  $\mu$ M; Sigma-Aldrich 14343), a GABAA receptor antagonist; and 6-cyano-7-nitroquinoxaline-2,3-dione (CNQX; 20  $\mu$ M; Sigma-Aldrich C239), an AMPA receptor antagonist. This mixture was shown to suppress neuronal communication (Bakkum et al. 2008) to ensure that the recorded neuronal activity was directly evoked by the stimulus.

### B.3 Stimulus Pulse

Extracellular electrical stimuli were used to elicit neuronal activity. Stimuli were delivered to the neurons using a STG-2004 stimulator and MEA-1060-Up-BC amplifier (Multi Channel Systems). MATLAB (Natick, MA) was used to control all hardware devices, which were synchronized by TTL pulses sent from the stimulator at the beginning of each stimulation loop. In all stimulus iterations, a trigger pulse was first delivered to the camera to begin recording so that background fluorescence levels could be measured. An enable pulse was then delivered to the amplifier, which connected the stimulus channel to a pre-programmed electrode. A single cathodic square current pulse was then delivered to a single electrode centered under the camera field of view. Cathodic pulses were chosen because they have been shown to be most effective at evoking a neuronal response (Wagenaar et al. 2004).

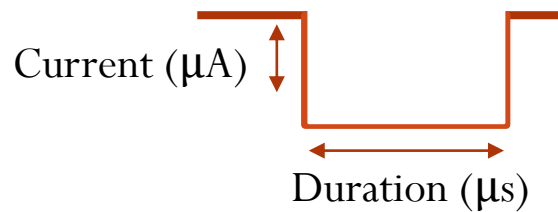


Figure B.2. A cartoon depiction of a rectangular cathodic stimulus pulse.

#### **B.4 Cell Culture Medium**

Culture medium [90 mL Dulbecco's Modified Eagle's Medium (Irvine Scientific 9024), 10 mL horse serum (Life Technologies 16050-122), 250  $\mu$ L GlutaMAX (200 mM; Life Technologies 35050-061), 1 mL sodium pyruvate (100 mM; Life Technologies 11360-070) and insulin (Sigma-Aldrich I5500; final concentration 2.5  $\mu$ g/mL)]

#### **B.5 Neuronal Dissociation**

Embryonic Day 18 (E18) rat cortices were enzymatically and mechanically dissociated according to Potter & DeMarse (2001). Cortices were digested with trypsin (0.25% w/EDTA) for 10-12 minutes, strained through a 40  $\mu$ m cell strainer to remove clumps and centrifuged to remove cellular debris. Neurons were re-suspended in culture medium [90 mL Dulbecco's Modified Eagle's Medium (Irvine Scientific 9024), 10 mL horse serum (Life Technologies 16050-122), 250  $\mu$ L GlutaMAX (200 mM; Life Technologies 35050-061), 1 mL sodium pyruvate (100 mM; Life Technologies 11360-070) and insulin (Sigma-Aldrich I5500; final concentration 2.5  $\mu$ g/mL)] and diluted to 3000 cells/ $\mu$ L. Microelectrode arrays (MEAs; Multi Channel Systems 60MEA200/30iR-Ti) were sterilized by soaking in 70% ethanol for 15 minutes followed by UV exposure overnight. MEAs were treated with polyethylenimine to hydrophilize the surface, followed by three water washes and 30 minutes of drying. Laminin (10  $\mu$ L; 0.02 mg/mL; Sigma-Aldrich L2020) was applied to the MEA for 20 minutes, half of the volume was removed, and 30,000 neurons were plated into the remaining laminin atop the MEA. Cultures were protected using gas-permeable lids (Potter & DeMarse, 2001) and incubated at 35°C in 5% carbon dioxide and 95% relative humidity. The culture medium was fully replaced on the first DIV and then once every four DIV afterwards.

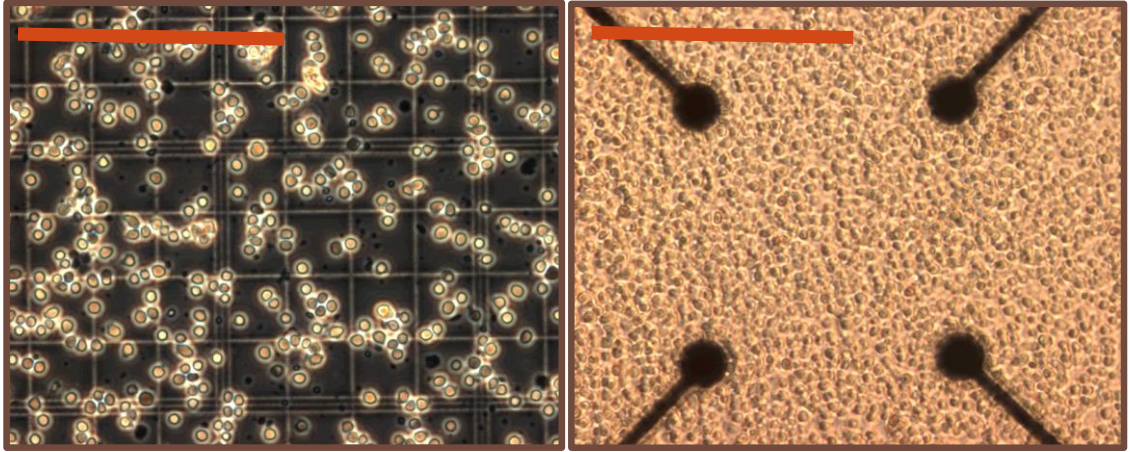


Figure B.3. Phase contrast image of dissociated neurons atop a hemacytometer for counting. Axons and dendrites have been removed from the majority of the cells, returning them to a spherical configuration. Right: Phase contrast image of the neuronal culture after plating the dissociated neurons atop a MEA. Scale bars are 200  $\mu\text{m}$ .

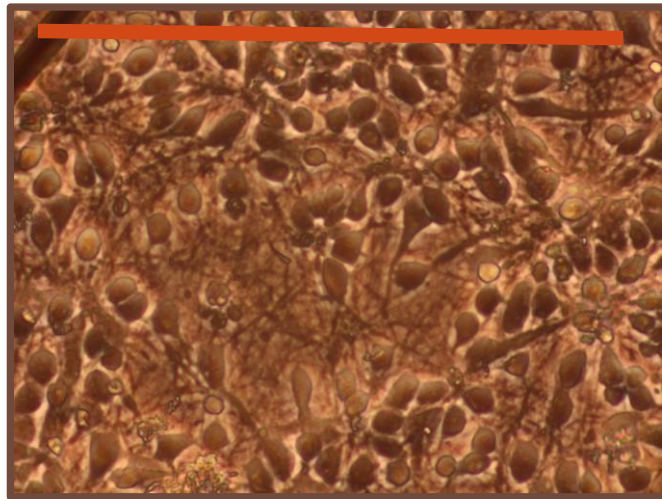


Figure B.4. Dissociated neuronal culture. A phase contrast micrograph of a dissociated rat cortical culture at 14 days in vitro (DIV) illustrates the extent to which the culture has developed. Neurites (axons and dendrites) can be seen in the space between the somata. Scale bar: 100  $\mu\text{m}$ .

## B.6 Cell Culture Confinement

A stencil for cell plating is created using a thin sheet (10 – 20 mil) of PDMS, and the opening is made with a blunt-needle punch. By confining the growth of our cortical cultures to an area spanning only one field of view in our camera, we will know that all evoked cellular signals will be recorded in every experiment.

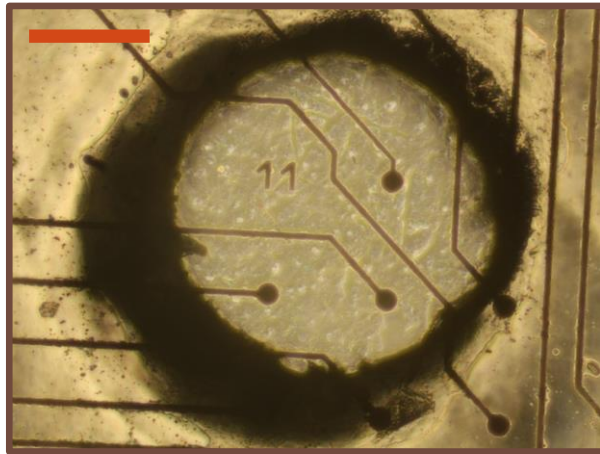


Figure B.5. Phase contrast image of a PDMS stencil atop a MEA. Scale bar is 200  $\mu\text{m}$ .

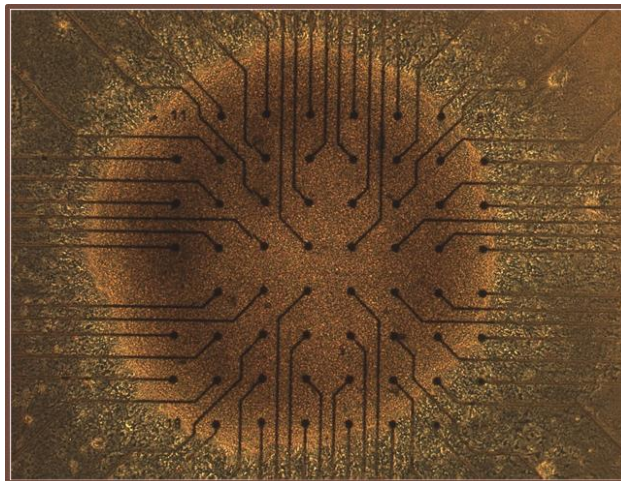


Figure B.6. Neurons were plated at an extremely high density (15  $\mu\text{L}$  at 50k cells/  $\mu\text{L}$ ) atop an MEA using a 1.5mm diameter PDMS stencil to observe the potential spread of neurons over the lifetime of the culture. Seen here is the healthy culture after two weeks of growth. Processes have grown beyond the cell circle, but no cell bodies have migrated.

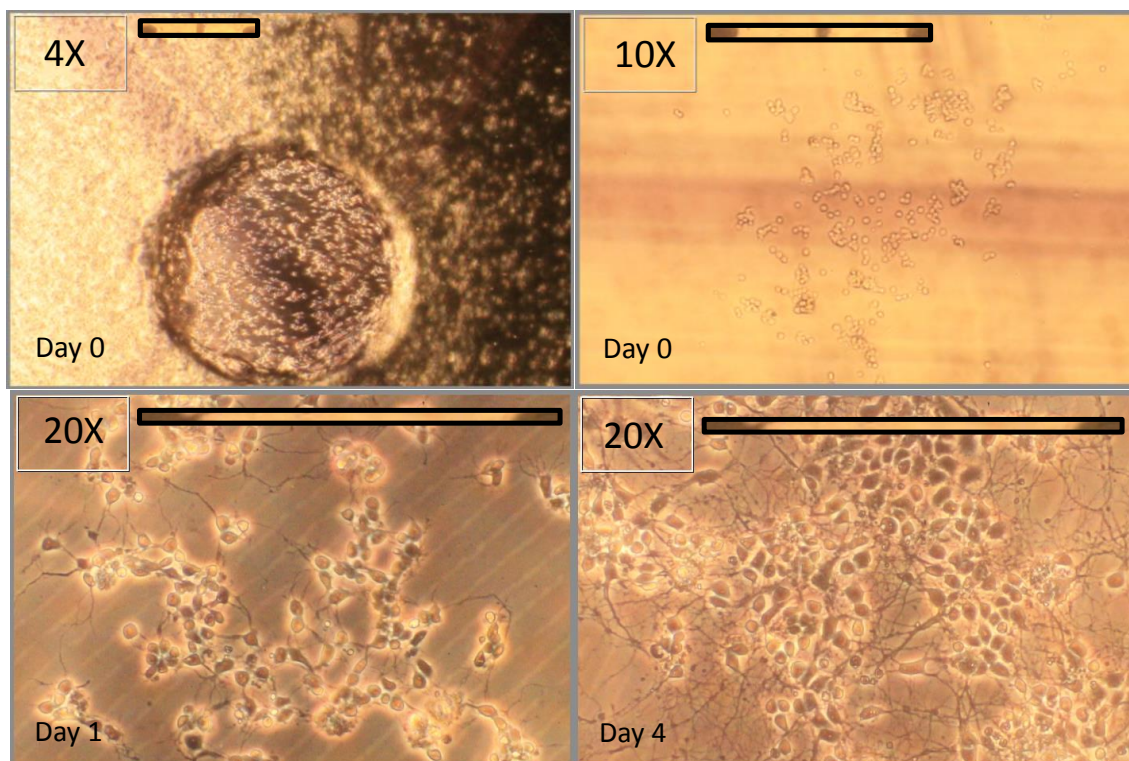


Figure B.7. The next generation of PDMS stencils was developed using a spin coating technique for higher precision control of the stencil thickness and opening. Shown above is the stencil overlaid on a polystyrene culturing dish and neurons are plated on top of the combination. Then the stencil is removed and only the neuronal culture remains where the PDMS opening resided. After 1 DIV the neurons began to differentiate. After 4 DIV extensive processes have developed within the culture. The population density has increased as a result of glia division.

## REFERENCES

- Arsiero, M., Luscher, H. R., & Giugliano, M. (2007). Real-time closed-loop electrophysiology: towards new frontiers in in vitro investigations in the neurosciences. *Arch Ital Biol*, *145*(3-4), 193–209.
- Bakkum, D. J., Chao, Z. C., & Potter, S. M. (2008). Long-term activity-dependent plasticity of action potential propagation delay and amplitude in cortical networks. *PLoS One*, *3*(5), e2088.
- Basser, P. J., & Roth, B. J. (2000). New currents in electrical stimulation. *Annu. Rev. Biomed. Eng.* *2*:377-97.
- Benda, J., Gollisch, T., Machens, C. K., & Herz, A. V. (2007). From response to stimulus: adaptive sampling in sensory physiology. *Current Opinion in Neurobiology*, *17*(4), 430–6.
- Boinagrov, D., Loudin, J., & Palanker, D. (2010). Strength-duration relationship for extracellular neural stimulation: numerical and analytical models. *Journal of Neurophysiology*, *104*(4), 2236–48.
- Boinagrov, D., Pangratz-Fuehrer, S., Suh, B., Mathieson, K., Naik, N., & Palanker, D. (2012). Upper threshold of extracellular neural stimulation. *Journal of Neurophysiology*, *108*(12), 3233–8.
- Bölinger, D., & Gollisch, T. (2012). Closed-loop measurements of iso-response stimuli reveal dynamic nonlinear stimulus integration in the retina. *Neuron*, *73*(2), 333–46.
- Borchers, S., Himmelbach, M., Logothetis, N., & Karnath, H. O. (2012). Direct electrical stimulation of human cortex - the gold standard for mapping brain functions? *Nature Reviews. Neuroscience*, *13*(1), 63–70.
- Bostock, H. (1983). The strength-duration relationship for excitation of myelinated nerve: computed dependence on membrane parameters. *J Physiol*, *341*, 59–74.
- Brocker, D. T., Swan, B. D., Turner, D. A., Gross, R. E., Tatter, S. B., Koop, M. M., & Grill, W. M. (2013). Improved efficacy of temporally non-regular deep brain stimulation in Parkinson's disease. *Experimental Neurology*, *239*, 60–7.
- Bruce, I. C., White, M. W., Irlicht, L. S., O'Leary, S. J., Dynes, S., Javel, E., & Clark, G. M. (1999). A stochastic model of the electrically stimulated auditory nerve: single-pulse response. *IEEE Transactions on Bio-Medical Engineering*, *46*(6), 617–29.

- Buonomano, D. V., & Maass, W. (2009). State-dependent computations: spatiotemporal processing in cortical networks. *Nature Reviews. Neuroscience*, *10*(2), 113–25.
- Butson, C. R., & McIntyre, C. C. (2006). Role of electrode design on the volume of tissue activated during deep brain stimulation. *Journal of Neural Engineering*, *3*(1), 1–8.
- Butson, C. R., & McIntyre, C. C. (2008). Current steering to control the volume of tissue activated during deep brain stimulation. *Brain Stimulation*, *1*(1), 7–15.
- Carmena, J. M., Lebedev, M. A., Crist, R. E., O’Doherty, J. E., Santucci, D. M., Dimitrov, D. F., & Nicolelis, M. L. (2003). Learning to control a brain-machine interface for reaching and grasping by primates. *PLoS Biology*, *1*(2), E42.
- Chabardes, S., Fraix, V., Ardouin, C., Koudsie, A., & Limousin, P. D. (2003). Five-Year Follow-up of Bilateral Stimulation of the Subthalamic Nucleus in Advanced Parkinson’s Disease, *The New England Journal of Medicine*. 1925–1934.
- Chaturvedi, A., Foutz, T. J., & McIntyre, C. C. (2012). Current steering to activate targeted neural pathways during deep brain stimulation of the subthalamic region. *Brain Stimulation*, *5*(3), 369–77.
- Chamorro, P., Muñiz, C., Levi, R., Arroyo, D., Rodríguez, F. B., & Varona, P. (2012). Generalization of the dynamic clamp concept in neurophysiology and behavior. *PloS One*, *7*(7), e40887.
- Clark, G. M. (2013). The multichannel cochlear implant for severe-to-profound hearing loss. *Nature Medicine*, *19*(10), 1236–9.
- Clark, K. L., Armstrong, K. M., & Moore, T. (2011). Probing neural circuitry and function with electrical microstimulation. *Proceedings. Biological Sciences / The Royal Society*, *278*(1709), 1121–30.
- Cleary, D. R., Raslan, A. M., Rubin, J. E., Bahgat, D., Viswanathan, A., Heinricher, M. M., & Hutchison, W. D. (2000). Microstimulation-Induced Inhibition of Neuronal Firing in Human Globus Pallidus, *J Neurophysiol* *84*:570-574, 2000.
- Cohen, M. R., & Newsome, W. T. (2004). What electrical microstimulation has revealed about the neural basis of cognition. *Current Opinion in Neurobiology*, *14*(2), 169–77.
- Cox, D. R. (1959). The regression analysis of binary sequences. *Journal of the Royal Statistical Society*, *20*(2), 215–242.
- DiMattina, C., & Zhang, K. (2013). Adaptive stimulus optimization for sensory systems neuroscience. *Frontiers in Neural Circuits*, *7*(June), 101.

- Edelstein, A., Amodaj, N., Hoover, K., Vale, R., & Stuurman, N. (2010). Computer control of microscopes using  $\mu$ Manager. *Current Protocols in Molecular Biology*, 14, Unit14.20.
- Fitzsimmons, N., Drake, W., Hanson, T. L., Lebedev, M., & Nicolelis, M. L. (2007). Primate reaching cued by multichannel spatiotemporal cortical microstimulation. *The Journal of Neuroscience*, 27(21), 5593–602.
- Foutz, T. J., & McIntyre, C. C. (2010). Evaluation of novel stimulus waveforms for deep brain stimulation. *Journal of Neural Engineering*, 7(6), 066008.
- Fozzard, H. A., & Schoenberg, M. (1972). Strength--duration curves in cardiac Purkinje fibres: effects of liminal length and charge distribution. *J. Physiol.*, 226(3), 593–618.
- Freeman, D. K., Eddington, D. K., Rizzo, J. F., & Fried, S. I. (2010). Selective activation of neuronal targets with sinusoidal electric stimulation. *Journal of Neurophysiology*, 104(5), 2778–91.
- Fried, S. I., Hsueh, H. a, & Werblin, F. S. (2006). A method for generating precise temporal patterns of retinal spiking using prosthetic stimulation. *Journal of Neurophysiology*, 95(2), 970–8.
- Fritsch, G., & Hitzig, E. (1870). Ueber die elektrische Erregbarkeit des Gros- shirns. *Archiv fur Anatomie, Physiologie und wissenschaftliche Medizin*. 37, 300–339.
- Guggenmos, D. J., Azin, M., Barbay, S., Mahnken, J. D., Dunham, C., Mohseni, P., & Nudo, R. J. (2013). Restoration of function after brain damage using a neural prosthesis. *Proceedings of the National Academy of Sciences of the United States of America*, 110(52), 21177–82.
- Gustafsson B, & Jankowska E. Direct and indirect activation of nerve cells by electrical pulses applied extracellularly. *J Physiol* 1976;258:33–61.
- Hatsopoulos, & Donoghue. (2009). The Science of Neural Interface Systems. *Annu Rev Neurosci*, 249–266.
- Histed, M. H., Bonin, V., & Reid, R. C. (2009). Direct activation of sparse, distributed populations of cortical neurons by electrical microstimulation. *Neuron*, 63(4), 508–22.
- Hochberg, L., Serruya, M., Friehs, G., Mukand, J., Saleh, M., Caplan, A., & Donoghue, J. (2006). Neuronal ensemble control of prosthetic devices by a human with tetraplegia. , *Nature*, 442 pp164–171.

- Holsheimer, J., Dijkstra, E. A., Demeulemeester, H., & Nuttin, B. (2000). Chronaxie calculated from current-duration and voltage-duration data. *J Neurosci Methods*, 97(1), 45–50.
- Jankowska, E., & Roberts, W. J. (1972). Synaptic actions of single interneurons mediating reciprocal Ia inhibition of motoneurons. *J. Physiol.*, 222(3), 623–642.
- Jensen, A. L., & Durand, D. M. (2007). Suppression of axonal conduction by sinusoidal stimulation in rat hippocampus in vitro. *Journal of Neural Engineering*, 4(2), 1–16.
- Jensen, R. J., Ziv, O. R., Rizzo, J. F., Scribner, D., & Johnson, L. (2009). Spatiotemporal aspects of pulsed electrical stimuli on the responses of rabbit retinal ganglion cells. *Experimental Eye Research*, 89(6), 972–9.
- Jepson, L. H., Gunning, P. H. D. E., Mathieson, K., Dąbrowski, W., & Litke, A. M. (2011). Spatially Patterned Electrical Stimulation of the Retina for Improved Specificity, *Proceedings of the 5th International IEEE EMBS Conference on Neural Engineering*, 495–498.
- Katona, G., Szalay, G., Maák, P., Kaszás, A., Veress, M., Hillier, D., & Rózsa, B. (2012). Fast two-photon in vivo imaging with three-dimensional random-access scanning in large tissue volumes. *Nature Methods*, 9(2), 201–8.
- Kipke, D. R., Shain, W., Buzsáki, G., Fetz, E., Henderson, J. M., Hetke, J. F., & Schalk, G. (2008). Advanced neurotechnologies for chronic neural interfaces: new horizons and clinical opportunities. *The Journal of Neuroscience*. 28(46), 11830–8.
- Konrad, P., & Shanks, T. (2010). Implantable brain computer interface: challenges to neurotechnology translation. *Neurobiology of Disease*, 38(3), 369–75.
- Koralek, A. C., Jin, X., Long, J. D., Costa, R. M., & Carmena, J. M. (2012). Corticostriatal plasticity is necessary for learning intentional neuroprosthetic skills. *Nature*, 483(7389), 331–5.
- Kringelbach, M. L., Jenkinson, N., Owen, S. L. F., & Aziz, T. Z. (2007). Translational principles of deep brain stimulation. *Nature Reviews. Neuroscience*, 8(8), 623–35.
- Lapicque, L. (2007). Quantitative investigations of electrical nerve excitation treated as polarization. 1907. *Biological Cybernetics*, 97(5-6), 341–9.
- Lebedev, M., Tate, A. J., Hanson, T. L., Li, Z., O’Doherty, J. E., Winans, J. & Nicolelis, M. L. (2011). Future developments in brain-machine interface research. *Clinics*, (66 1), 25–32.
- Lebedev, M., & Nicolelis, M. L. (2006). Brain-machine interfaces: past, present and future. *Trends Neurosci*, 29(9), 536–546.

- Lee, S. W., Eddington, D. K., & Fried, S. I. (2013). Responses to pulsatile subretinal electric stimulation: effects of amplitude and duration. *Journal of Neurophysiology*, *109*(7), 1954–68.
- Levy, R. M. (2003). Deep brain stimulation for the treatment of intractable pain. *Neurosurgery Clinics of North America*, *14*(3), 389.
- Lewi, J., Butera, R., & Paninski, L. (2009). Sequential optimal design of neurophysiology experiments. *Neural Computation*, *21*(3), 619–87.
- Loeb, G. E., Byers, C. L., Rebscher, S. J., Casey, D. E., Fong, M. M., Schindler, R. & Merzenich, M. M. (1983). Design and fabrication of an experimental cochlear prosthesis. *Medical & Biological Engineering & Computing*, *21*(3), 241–54.
- Logothetis, N. K., Augath, M., Murayama, Y., Rauch, A., Sultan, F., Goense, J. & Merkle, H. (2010). The effects of electrical microstimulation on cortical signal propagation. *Nature Neuroscience*, *13*(10), 1283–91.
- Machens, C. K., Gollisch, T., Kolesnikova, O., & Herz, A. V. M. (2005). Testing the efficiency of sensory coding with optimal stimulus ensembles. *Neuron*, *47*(3), 447–56.
- Mandonnet, E., Winkler, P., & Duffau, H. (2010). Direct electrical stimulation as an input gate into brain functional networks: principles, advantages and limitations. *Acta Neurochirurgica*, *152*(2), 185–93.
- McIntyre, C. C., & Grill, W. M. (2000). Selective microstimulation of central nervous system neurons. *Annals of Biomedical Engineering*, *28*(3), 219–33.
- McIntyre, C. C., & Grill, W. M. (2002). Extracellular stimulation of central neurons: Influence of stimulus waveform and frequency on neuronal output. *J. Neurophys.*, *88*, 1592–1604.
- McIntyre, C. C., Grill, W. M., Sherman, D. L., & Thakor, N. V. (2004). Cellular effects of deep brain stimulation: model-based analysis of activation and inhibition. *Journal of Neurophysiology*, *91*(4), 1457–69.
- McIntyre, C. C., Grill, W. M., Walker, H. C., Watts, R. L., Schrandt, C. J., Huang, H., & Lemay, M. A. (2011). Extracellular Stimulation of Central Neurons : Influence of Stimulus Waveform and Frequency on Neuronal Output, *J Neurophysiol* *88*:1592-1604, 2002.
- Mcmullen, J. P., & Jensen, K. F. (2010). An Automated Microfluidic System for Online Optimization in Chemical Synthesis, *Organic Process Research & Development*, *14*, 1169–1176.

- Mogyoros, I., Kiernan, M. C., & Burke, D. (1996). Strength-duration properties of human peripheral nerve. *Brain : A Journal of Neurology*, *119 Pt 2*, 439–47.
- Nathan, S. S., Thakor, N. V., Lesser, R. P., & Gordon, B. (1991). Finite Element Analysis Of Field Distributions In The Cerebral Cortex Generated By Electrical Stimulation. *Proceedings of the IEEE Engineering in Medicine and Biology Society* *13*: 515–516.
- Newman, J. P., Zeller-Townson, R., Fong, M.-F., Arcot Desai, S., Gross, R. E., & Potter, S. M. (2012). Closed-Loop, Multichannel Experimentation Using the Open-Source NeuroRighter Electrophysiology Platform. *Frontiers in Neural Circuits*, *6*, 98.
- Nicolelis, M. A. L., Dimitrov, D., Carmena, J. M., Crist, R., Lehew, G., Kralik, J. D., & Wise, S. P. (2003). Chronic, multisite, multielectrode recordings in macaque monkeys. *Proceedings of the National Academy of Sciences of the United States of America*, *100(19)*, 11041–6.
- Nowak, L. G., & Bullier, J. (1998). Axons, but not cell bodies, are activated by electrical stimulation in cortical gray matter. *Experimental Brain Research*, *118(4)*, 477–488.
- O'Connor, K. N., Petkov, C. I., & Sutter, M. L. (2005). Adaptive stimulus optimization for auditory cortical neurons. *Journal of Neurophysiology*, *94(6)*, 4051–67.
- Pais-Vieira, M., Lebedev, M., Kunicki, C., Wang, J., & Nicolelis, M. L. (2013). A Brain-to-Brain Interface for Real-Time Sharing of Sensorimotor Information. *Scientific Reports*, *3*, 1–10.
- Parker, A. J., & Newsome, W. T. (1998). Sense and the single neuron: Probing the Physiology of Perception. *Annual Review of Neuroscience*, *21*: 227-27.
- Peng, T. (2005). Detect circles with various radii in grayscale image via Hough Transform. MATLAB Central File Exchange. Retrieved from <http://www.mathworks.com/matlabcentral/fileexchange/9168>.
- Perlmutter, J. S., & Mink, J. W. (2006). Deep brain stimulation. *Annual Review of Neuroscience*, *29*, 229–57.
- Potter, S. M., & DeMarse, T. B. (2001). A new approach to neural cell culture for long-term studies. *J. Neurosci. Methods*, *110*, 17–24.
- Potter, S. M., Wagenaar, D. A., & Demarse, T. B. (2006). Closing the loop : Stimulation feedback systems for embodied MEA cultures. *Advances in Network Electrophysiology*, 215-242.
- Potter, S.M. (2013). Better minds: Cognitive enhancement in the 21<sup>st</sup> century. *Evolution haute couture: Art and science in the post-biological age*. 304-319.

- Ranck, J. B. (1975). Which elements are excited in electrical stimulation of mammalian central nervous system: A review, *Brain Research*, 98.
- Rattay, F. (1999). The basic mechanism for the electrical stimulation of the nervous system. *Neuroscience*, 89(2), 335–346.
- Rattay, F., Paredes, L. P., & Leao, R. N. (2012). Strength-duration relationship for intra-versus extracellular stimulation with microelectrodes. *Neuroscience*, 214, 1–13.
- Richardson, A. G., McIntyre, C. C., & Grill, W. M. (2000). Modelling the effects of electric fields on nerve fibres: influence of the myelin sheath. *Medical and Biological Engineering and Computing*, 38(4), 438–446.
- Rolston, J. D., & Gross, R. E. (2008). The clinical utility of methods to determine spatial extent and volume of tissue activated by deep brain stimulation. *Clin Neurophysiol*, 119(9), 1947–1950.
- Rutishauser, U., Kotowicz, A., & Laurent, G. (2013). A method for closed-loop presentation of sensory stimuli conditional on the internal brain-state of awake animals. *Journal of Neuroscience Methods*, 215(1), 139–55.
- Ryu, S., & Shenoy, K. (2013). Human cortical prostheses: lost in translation? *Neurosurg Focus*, 27(1), 1–21.
- Schiff, S. J. (2010). Towards model-based control of Parkinson's disease. *Philosophical Transactions. Series A, Mathematical, Physical, and Engineering Sciences*, 368(1918), 2269–308.
- Schwartz, A. B. (2004). Cortical neural prosthetics. *Annual Review of Neuroscience*, 27, 487–507.
- Sekirnjak, C., Hottowy, P., Sher, A., Dabrowski, W., Litke, a M., & Chichilnisky, E. J. (2006). Electrical stimulation of mammalian retinal ganglion cells with multielectrode arrays. *Journal of Neurophysiology*, 95(6), 3311–3327.
- Tchumatchenko, T., Newman, J. P., Fong, M., & Potter, S. M. (2013). Delivery of continuously-varying stimuli using channelrhodopsin-2. *Frontiers in Neural Circuits*, 7, 184.
- Tehovnik, E. J. (1996). Electrical stimulation of neural tissue to evoke behavioral responses. *Journal of Neuroscience Methods*, 65(1), 1–17.
- Tehovnik, E. J., & Slocum, W. M. (2013). Two-photon imaging and the activation of cortical neurons. *Neuroscience*, 245, 12–25.

- Tehovnik, E. J., Tolia, S., Sultan, F., Slocum, W. M., & Logothetis, N. K. (2006). Direct and indirect activation of cortical neurons by electrical microstimulation. *Journal of Neurophysiology*, 96(2), 512–21.
- Tolia, A. S., Sultan, F., Augath, M., Oeltermann, A., Tehovnik, E. J., Schiller, P. H., & Logothetis, N. K. (2005). Mapping cortical activity elicited with electrical microstimulation using fMRI in the macaque. *Neuron*, 48(6), 901–11.
- Tsai, D., Morley, J. W., Suaning, G. J., & Lovell, N. H. (2009). Direct activation and temporal response properties of rabbit retinal ganglion cells following subretinal stimulation. *Journal of Neurophysiology*, 102(5), 2982–93.
- Twyford, P., Cai, C., & Fried, S. (2014). Differential responses to high-frequency electrical stimulation in ON and OFF retinal ganglion cells. *Journal of Neural Engineering*, 11(2), 025001.
- Wagenaar, D. A., Pine, J., & Potter, S. M. (2004). Effective parameters for stimulation of dissociated cultures using multi-electrode arrays. *Journal of Neuroscience Methods*, 138(1-2), 27–37.
- Wagenaar, D. A., Madhavan, R., Pine, J., & Potter, S. M. (2005). Controlling bursting in cortical cultures with closed-loop multi-electrode stimulation. *The Journal of Neuroscience*, 25, 680–688.
- Wagenaar, D. A., Pine, J., & Potter, S. M. (2006). Searching for plasticity in dissociated cortical cultures on multi-electrode arrays. *Journal of Negative Results in Biomedicine*, 5 (16), 1–19.
- Wang, Q., Millard, D. C., Zheng, H. J. V., & Stanley, G. B. (2012). Erratum: Voltage-sensitive dye imaging reveals improved topographic activation of cortex in response to manipulation of thalamic microstimulation parameters. *Journal of Neural Engineering*, 9(5), 059601.
- Weiss G. Sur la possibilite de rendre comparables entre eux les appareils servant a l'excitation électrique. *Arch Ital Biol* 1901;35:413-446.
- Wilke, R. G. H., Moghadam, G. K., Lovell, N. H., Suaning, G. J., & Dokos, S. (2011). Electric crosstalk impairs spatial resolution of multi-electrode arrays in retinal implants. *Journal of Neural Engineering*, 8(4), 046016.
- Wilson, B. S., & Dorman, M. F. (2008). Cochlear implants: Current designs and future possibilities. *Journal of Rehabilitation Research & Development*. 45 (695-730).
- Yasuda, R., Sabatini, B. L., & Svoboda, K. (2003). Plasticity of calcium channels in dendritic spines. *Nature Neuroscience*, 6(9), 948–55.

- Yazdan-Shahmorad, A., Kipke, D. R., & Lehmkuhle, M. J. (2011). Polarity of cortical electrical stimulation differentially affects neuronal activity of deep and superficial layers of rat motor cortex. *Brain Stimulation*, 4(4), 228–41.
- Yeomans, J. S., Maidment, N. T., & Bunney, B. S. (1988). Excitability properties of medial forebrain bundle axons of A9 and A10 dopamine cells. *Brain Research*, 450(1-2), 86–93.
- Yizhar, O., Fenno, L. E., Davidson, T. J., Mogri, M., & Deisseroth, K. (2011). Optogenetics in neural systems. *Neuron*, 71(1), 9–34.
- Zrenner, C., Eytan, D., Wallach, A., Thier, P., & Marom, S. (2010). A generic framework for real-time multi-channel neuronal signal analysis, telemetry control, and sub-millisecond latency feedback generation. *Frontiers in Neuroscience*, 173.